AN ABSTRACT OF THE DISSERTATION OF

Alabbas Al-Aukaily for the degree of Doctor of Philosophy in Civil Engineering presented on May 15, 2017.

Title: Response Sensitivity Formulations for Geometrically Nonlinear Finite Element Analysis

Abstract approved: _____

Michael H. Scott

Significant amounts of uncertainty owing to both modeling decisions and inherent randomness are present in simulating the material and geometric nonlinear response of structural systems to extreme loading. Computing the sensitivity of structural response with respect to model parameters indicates which parameters have the largest affect on the response, which can in some cases be more important to an engineer than only the deterministic response. Considering the large number of parameters in a structural model, accurate and efficient response sensitivity computations, or gradients of the structural response, are required for nonlinear structural reliability, optimization, and system identification analyses. Response sensitivity for geometric nonlinear finite element analysis are presented including a geometrically-nonlinear displacement based-beam column element formulation, the displacement control nonlinear static solution method, and the corotational trans-

formation of space frame finite elements. The direct differentiation method (DDM) is used to derive the response sensitivity equations for the aforementioned formulations. The response sensitivity equations for geometric nonlinear displacement-based beam-column element are formulated in the deformed configuration using Lagrangian strain. The derivation of the sensitivity equations for the displacement control solution method is performed according to an incremental-iterative solution strategy. The sensitivity equations of space frame formulations require the derivative of the system triads in the deformed configuration according to the corotational theory and the numerical algorithms for its implementation in a finite element setting.

The derived equations are implemented in the OpenSees software framework. To verify the accuracy of the derived equations, standalone sensitivity analysis is performed by comparing the response sensitivity results obtained by the DDM with those obtained by the finite difference method (FDM). The standalone sensitivity analysis is performed for different element, material, and section models. Furthermore, the response sensitivity equations are utilized to perform reliability and ranking of importance measures for complex steel and reinforced concrete structures.

Response Sensitivity Formulations for Geometrically Nonlinear Finite Element Analysis

by

Alabbas Al-Aukaily

A DISSERTATION

submitted to

Oregon State University

in partial fulfillment of
the requirements for the
degree of

Doctor of Philosophy

Presented May 15, 2017
Commencement June 2017

Doctor of Philosophy dissertation of Alabbas Al-Aukaily presented on May 15, 2017.

APPROVED:

Major Professor, representing Civil Engineering

Head of the School of Civil and Construction Engineering

Dean of the Graduate School

I understand that my dissertation will become part of the permanent collection of Oregon State University libraries. My signature below authorizes release of my dissertation to any reader upon request.

Alabbas Al-Aukaily, Author

ACKNOWLEDGEMENTS

I would like to thank Prof Michael Scott, my research advisor, for his support and his guidance in this work. Without his support I would not be able to understand and solve my research problems. He has been very patient in helping me develop my skills in OpenSees. I would also like to thank Professor Christopher Higgins, Professor Andre Barbosa, Professor Judy Liu, and Professor Jennifer Field for serving as my committee members. I also would like to thank Prof Chris Bell, the head of the graduate office at the civil engineering department and Ms. Marigold, the International student advisor, for their tremendous support to Iraqi students. Special thanks to the higher committee for education development in Iraq (HCED) for their support. HCED is the first educational committee in Iraq that helps Iraqi students to get admitted to highly ranked universities all over the world. Special thank to both Dr. Zohair Hammadi and Dr. Abed Alhakim for their hard work to make HCED a very competitive department.

I wish to find suitable words to describe my gratitude to my mom for her love, encouragement, supplication and the money she spent on my education. I also wish to thank my wife Shahad Shafaee for her encouragement and her patience during all of the past six years. Even while working so hard on her master's degree and taking care of our kids, she made our house a good study environment. I also want to thank my kids Yousef and Ali for understanding my situation and for taking good care of their baby sister Hyah while I was busy studying. I would also

like to thank my brother Ali Fadil for his help during my educational journey. He helped me a lot during my undergraduate study and paid a lot of money to cover my tuition fees. I am so proud and happy to have him in my life.

TABLE OF CONTENTS

TABLE OF CONTENTS (Continued)

TABLE OF CONTENTS (Continued)

LIST OF FIGURES

LIST OF FIGURES (Continued)

LIST OF FIGURES (Continued)

LIST OF TABLES

LIST OF APPENDIX FIGURES

LIST OF APPENDIX TABLES

Response Sensitivity Formulations for Geometrically Nonlinear Finite Element Analysis

1 Introduction

1.1 Structural Response Sensitivity

Structural response sensitivity analysis measures the change in structural response to changes in system properties [35]. Sensitivity analysis helps identifying the most important parameters that affect structural response for different structural limit states. The most common applications that require response sensitivity are such as optimization, system identification, and reliability analysis. For instance, sensitivity analysis can be used to minimize the structural cost, and it also helps to minimize the difference between the measured and numerical response for system identification purposes [3].

Sensitivity analysis can be computed explicitly for linear analysis and implicitly for nonlinear analysis using several approaches such as the finite difference method (FDM), adjoint system method (ASM), complex perturbation method (CPM), and direct differentiation method (DDM). The FDM is the simplest method but it requires repeating the structural analysis at least once for each uncertain parameter. The accuracy of the FDM depends on the magnitude of the parameter perturbation . If the perturbed value is too small, then roundoff errors will be introduced, while if the perturbed value is too large, inaccurate estimates of sensitivity may

occur. The ASM is more accurate than the FDM especially for linear and non-linear analyses of elastic systems but is not suitable for path dependent problems [35, 69].

The CPM is also an accurate method but like the FDM requires full re-analysis for each parameter of the finite element model. In the CPM, all parameters and response quantities in a finite element analysis are represented using complex numbers and all finite element computations are carried out using complex arithmetic. The imaginary component of a parameter is set equal to a perturbation. Then the finite element analysis is performed and response sensitivities are obtained from the imaginary components of the response [34].

The DDM on the other hand, in which the governing equations of structural equilibrium, compatibility, and constitutive are differentiated exactly, is more accurate and efficient than FDM and CPM. The DDM computes the response sensitivity within the finite element analysis. To apply DDM, the finite element algorithms have to be extended to include the response sensitivity equations for material, section, and element models as well as for solution algorithms.

The application that has been used in this dissertation is reliability analysis, and hence a brief introduction on reliability analysis is presented next.

1.2 Reliability Analysis

The study of structural reliability is concerned with the calculation and estimation of the probability of violating the ultimate or safety limit state for the structural

system at any stage during its life. A limit state, G(U), is a boundary between failure and safe performance of the structure. The probability of structural failure is defined in terms of the reliability index, β, is the shortest distance from the origin of the reduced random variable space to the design point (u^*) which lies on the failure surface (G(U)=0) as shown in Fig. 1.1. Greater β represents greater safety, or lower failure probability. The main methods of calculating the reliability index are: first order second-moment method (FOSM), first order reliability method (FORM), and second order reliability method (SORM). First order second-moment reliability method is sufficient for linear structural reliability analysis where limit state function is linearized about the mean values of its variables. However, FOSM is not suitable for nonlinear reliability analysis. For nonlinear reliability analysis, FORM and SORM can be used where the limit state function is linearized about the failure point using Tylor series expansion. In this dissertation FORM is used in performing reliability analysis where first order Tylor series expansion is used to linearize the limit state function as shown in Fig. 1.1. The sensitivity of the limit state function is

$$\frac{\partial G}{\partial h} = \frac{\partial G}{\partial \mathbf{U}} \frac{\partial \mathbf{U}}{\partial h} \tag{1.1}$$

where $\frac{\partial U}{\partial h}$ represents the response sensitivity vector with respect to parameter h which maps to random variables in standard space. The derivative of the limit state function $\frac{\partial G}{\partial U}$ is readily available since G is a linear function of the response quantities U.

1.3 Finite Element Formulations

Most often, in the analysis of structural frames, linear-elastic analysis is sufficient to capture performance of civil structures under service and operational loads. However, civil structures may exhibit permanent (nonlinear) deformations under extreme loads such as earthquake, blast, or tsunami. The main types of nonlinearity the structure may exhibit under extreme loads are material and geometric nonlinearity. Material nonlinearity, which is also called material plasticity, is a permanent deformation that occurs when the applied load exceeds material yielding strength, e.g., strain hardening of steel and crushing of concrete. Geometric nonlinear behavior is the change in geometry as the structure deforms due to large displacement [15]. Many plasticity models are available to simulate the stress-strain relationship of steel material such as elastic-perfectly plastic, isotropic, and kinematic strain hardening models. The most comonly used models for concrte material are: Mander [41] and Kent-Park models [33]. For geometric nonlinear analysis, there are three formulations available in the finite element analysis, Corotational formulation, total Lagrangian formulation, and updated Lagrangian formulation. In the total Lagrangian formulation, the structural deformations are calculated based on the undeformed configuration. In the updated Lagrangian formulation, the structural deformations are calculated based on the last deformed configuration. The corotational formulation removes the rigid-body mode which allows to separate material nonlinearity due to large deformation inside the basic system from geometric nonlinearity due to large displacement outside the basic system.

Many studies have shown the advantage of using the corotational formulation over the Lagrangian formulations such as [68] and [71]. Section force-deformation can be obtained by integrating the constitutive stress strain material models. Then element forces can be obtained by integrating section forces or deformations along the structural member. In finite element analysis, element formulations are based on either principal of virtual force or principal of virtual displacement. According to the the principle of virtual work, two types of element formulations are available in the finite element analysis: force-based beam-column element and displacement based beam-column element. Three coordinate systems are used to calculate element response: global, local, and basic systems. The global coordinate system at the element level coincides with that at the structural level. The local coordinate system coincides with the longitudinal and transverse axes of the element. The basic coordinate system is the local coordinate system after removing redundant forces and rigid body modes. In the basic system, geometric nonlinearity due to large displacements is formulated outside the basic system, whereas material nonlinearity and geometric nonlinearity due to large deformations are formulated inside the basic system. The model hierarchy that describes the relationships and transitions between forces and deformations at different levels is shown in Fig. 1.2.

The focus of this dissertation is on deriving the response sensitivity equations for geometric-nonlinear finite element formulations including displacement-based beam-column element, displacement control solution method, and corotational transformation of space frame elements. Therefore, brief descriptions of the aforementioned finite element formulations are presented next.

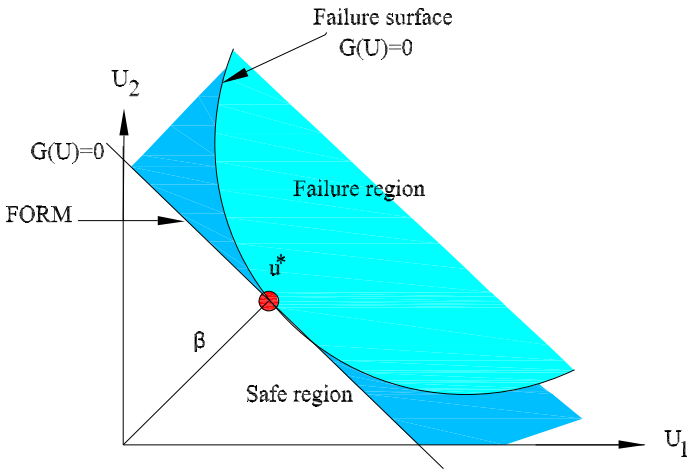

Figure 1.1: Nonlinear limit state function in two dimensional transformed basic variable space.

1.3.1 Displacement-Based Beam-Column Elements

The formulation of displacement-based beam-column element is based on the principle of virtual displacement method and Bernoulli assumptions in which plane section before deformation remains plane after deformation. The formulation is also based on assumptions of constant axial deformation and linear curvature. Geometric linear and geometric nonlinear displacement-based beam-column elements are the most types of this formulation that are commonly used in the finite element analysis. The geometric linear displacement-based element formulation is based on small deformations assumption. Engineering strain is used to calculate section deformations and consequently it does not account for geometric deformations. However, geometric nonlinear response can be captured by increasing the

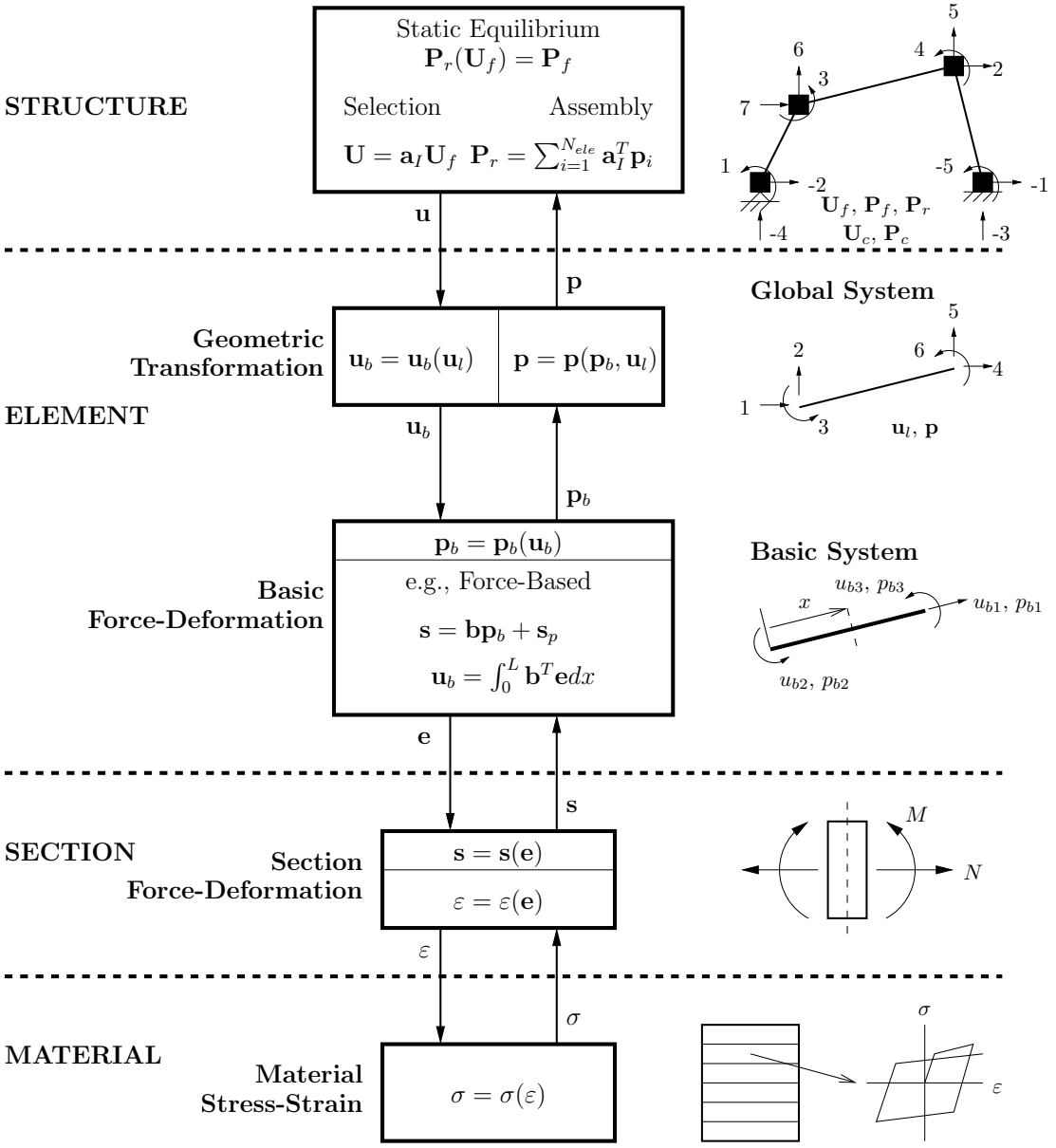

Figure 1.2: Modeling hierarchy for nonlinear frame analysis

number of elements and using large displacement analysis. The geometric nonlinear displacement-based element formulation is based on moderate deformations assumption within the basic system. The formulation of the geometric nonlinear displacement based beam-column element is obtained in the deformed configuration using Lagrangian strain to determine section deformation [15].

1.3.2 Load Control and Displacement Control Methods

There are many solution strategies for static nonlinear analysis such as load control method, displacement control method, arc length method. Most of these solutions are based on Newton-Raphson iteration algorithm. In the load control method (LC), the analysis is performed by applying the load incrementally and the structural responses are calculated accordingly. Load control solution scheme fails to capture the softening behavior when structure loses its load carrying capacity. Alternatives to the LC method have been developed where the applied load is treated as an additional variable in the finite element solution. In these approaches, a constraint equation is imposed on the structural response in order to solve for the applied load at each equilibrium iteration in a load step. Displacement control (DC) is one such method where the displacement at a single degree-of-freedom (DOF) is held constant during equilibrium iterations and the structural responses are calculated accordingly. The main advantage of using the DC over the LC can be summarized by its ability to capture the softening and snap through behaviors that can be done by controlling the displacement increments.

1.3.3 Geometric Nonlinearity: Corotational Formulation

Geometric nonlinear behaviour can be captured using either a total Lagrangian, an updated Lagrangian, or a corotational formulation. Many studies have shown the advantage of using the corotational formulation over the Lagrangian formulation such as [68, 71]. One of the main advantages of the corotational formulation is its independence of the local system while deriving the internal forces and stiffness matrices. In a two- dimensional (2D) corotational system, an exact transformation of displacements and forces can be obtained in two steps (basic to local and local to global). However, the transformation in three-dimensional (3D) frame element is more complex than 2D corotational formulation. This is because finite rotations in three dimensional analysis do not comply with the rules of vector operations and the results depend on the order in which rotations are applied. In order to overcome the problem of violating vector properties, Crisfield algorithm [19] is used to obtain the triads of the deformed configuration in the formulation of large displacements of space frame elements.

1.4 Objective and Scope

The main objective of this dissertation is to derive the response sensitivity equations for geometric nonlinear finite element formulations including geometric nonlinear displacement-based beam-column element, displacement control solution method, corotational transformation of a space frame element. Direct differentiation method (DDM) is used to derive the sensitivity equations within the algo-

rithms of the aforementioned finite element formulations. The derived equations are implemented in OpenSees (Open system for earthquake engineering simulation). To validate the sensitivity equations, a comparison between the DDM and finite difference methods (FDMs) is performed using standalone sensitivity analysis for different element, material and section models.

The first objective, presented in chapter two, is to derive and implement response sensitivity equations for geometric nonlinear based-beam column element formulation. The derivative of Lagrangian strain is the main step that leads to the formulation of the response sensitivity of the aforementioned element.

The second objective, which is presented in chapter three, is to develop displacement control (DC) solution method by deriving the sensitivity equations within the algorithm of the DC. By activating sensitivity analysis for DC, the response sensitivity gradients including sensitivity of the load factor can be recorded for the entire response including softening and snap-through behaviors.

The third objective is to extend the corotational formulation of space frame by including sensitivity equations in its formulation. The derivation requires following Crisfield algorithm [19] in which the triads of the deformed configuration are obtained. The formulation of the response sensitivity of the corotational transformation of space frame is presented in chapter four. The conclusion is presented in chapter five.

2 Response Sensitivity for Geometrically Nonlinear Displacement-Based Beam-Column Elements

Accurate and efficient response gradients are required in structural reliability, optimization and system identification when geometric nonlinearity is simulated for the structural response. The direct differentiation method (DDM) is used to obtain the response sensitivity of the displacement-based beam-column element formulation considering moderate deformations within the basic system. The derived sensitivity equations are implemented in the OpenSees software framework. To validate the sensitivity equations, a comparison between the DDM and finite difference methods (FDMs) is performed through standalone sensitivity analysis for simple example structures. Finite element reliability analysis of a steel frame structure shows that using geometrically nonlinear displacement-based elements affects the probability of failure, relative to that obtained with a geometrically linear element, but not the importance ranking of the uncertain model parameters.

2.1 Introduction

Structural response sensitivity analysis measures the change in structural response to changes in system properties [35]. Sensitivity analysis helps structural engineers better understand the relationship between design variables and structural

response under service and extreme loads. Response sensitivity, or the first derivative of the structural response, is also an important component to gradient-based algorithms where structural response is to be optimized in order to satisfy a performance objective under a variety of constraints. These algorithms are utilized in applications such as reliability, optimization, and system identification.

For nonlinear finite element analysis of structural systems, there are several approaches to obtain the response sensitivity with respect to model parameters: the finite difference method (FDM), the complex perturbation method (CPM), the adjoint system method (ASM), and the direct differentiation method (DDM). The FDM offers a simple way to approximate the structural response sensitivity. However, it is computationally intensive because it requires re-evaluating the entire time history of structural response with perturbed parameters. The accuracy of the sensitivity depends on the magnitude of each parameter perturbation. If the perturbation is too small, then roundoff errors will be introduced; while if the perturbation is too large, inaccurate estimates of sensitivity may occur.

The DDM is an attractive alternative to the FDMs. In the DDM, the analytical response sensitivity equations are derived and implemented within the finite element response algorithm. The DDM computes sensitivity using the same solver as the ordinary response while the simulation proceeds rather than by complete re-analysis for each parameter. Many researchers have contributed to the development of the DDM.

Essential components of the DDM for solid mechanics were laid out by [35] with subsequent work on composites processing, fire attack, fluid-structure inter-

action, and second order derivatives [10, 29, 74, 9]. The focus of this work is on frame elements with material and geometric nonlinearity, for which there has been a significant amount of research. DDM response sensitivity equations have been developed for material nonlinear response with both displacement and force-based element formulations [72, 58]. A mathematically equivalent approach for the DDM sensitivity of force-based frame elements was developed by [14]. Later extensions included geometric parameters such as nodal coordinates and cross-section dimensions in the derivation of DDM response sensitivity equations for both displacement and force-based formulations [31]. The effects of constitutive models on DDM computations were investigated by [6] and [2], who found that models with smooth state transitions lead to improved estimates of sensitivity for applications in structural reliability analysis. With respect to geometric nonlinearity, DDM response sensitivity has been developed for large displacements via the corotational transformation [57] and for geometrically nonlinear force-based frame elements [54].

The objective of this paper is to develop the response sensitivity of geometrically nonlinear displacement-based frame finite elements. Although force-based elements have been shown to simulate material and geometric nonlinearity better than displacement-based elements, their implementation, along with the corresponding DDM, can be complex and their state determination intense in the presence of significant material nonlinearity [39]. The implementation of geometrically nonlinear displacement-based elements is relatively straightforward and more stable in state determination. Herein, the DDM is used to obtain the response

sensitivity for the geometric nonlinear displacement based beam-column element formulation and the derived equations are implemented in the OpenSees software framework. Numerical examples verify the efficiency and the accuracy of the DDM over FDMs. The reliability analysis of a steel frame shows the importance of uncertain material and geometric parameters relative to other uncertain structural properties and assesses the effects of geometric nonlinear response in estimating structural reliability.

2.2 The Application of Response Sensitivities in Finite Element Reliability Analysis

In reliability analysis, a performance or limit state function, g, defines the boundary between safe and failure conditions for a structural system. Performance is typically defined by a response quantity, e.g., a displacement or force, not exceeding a limiting value. Negative values of g indicate the system does not satisfy the limit state. For the case of a single performance function, the probability of failure, P_f, is defined as

$$P_f = \int ..... \int_{g \leq 0} f(\mathbf{h})\ d\mathbf{h} \tag{2.1}$$

where $f(\mathbf{h})$ is the joint probability density function for the random variables collected in the vector $\mathbf{h}$. Analytical solutions to Eq. (3.2) are generally not available; however, numerical methods such as FORM and SORM provide approximate solutions. FORM approximates the failure surface as a hyperplane in the standard

normal space of random variables, defined by the transformation $\mathbf{Y} = \mathbf{Y}(\mathbf{h})$. The design point, $\mathbf{Y}^*$, represents the realization of the random variables that corresponds to the most probable point (MPP) of failure [45, 40, 50]

The gradient of the performance function, obtained by the chain rule of differentiation, is required in order to find the design point

$$\frac{\partial g}{\partial \mathbf{Y}} = \frac{\partial g}{\partial \mathbf{U}_f} \frac{\partial \mathbf{U}_f}{\partial \mathbf{h}} \frac{\partial \mathbf{h}}{\partial \mathbf{Y}} \tag{2.2}$$

where $\partial g/\partial \mathbf{U}_f$ is easily obtained for the common case where g is a simple algebraic function of the nodal displacement vector $\mathbf{U}_f$. The gradient of the nodal displacements and the Jacobian of the probability transformation are represented by $\partial \mathbf{U}_f/\partial \mathbf{h}$ and $\partial \mathbf{h}/\partial \mathbf{Y}$, respectively. After finding the design point, e.g., using the HLRF algorithm, the reliability index, $\beta = \|\mathbf{Y}^*\|_2$, which measures the distance from the origin to the design point in standard normal space, is determined and the probability of failure can be estimated by

$$P_f = \Phi(-\beta) \tag{2.3}$$

where Φ is the standard normal cumulative distribution function.

In addition to the probability of system failure, FORM provides a ranking of the random variables according to their influence on failure at the design point. An importance ranking, $\boldsymbol{\gamma}$, that accounts for statistical correlation of the random

variables was proposed by [30]

$$\boldsymbol{\gamma} = \boldsymbol{\alpha}\mathbf{J}_{\mathbf{Y}^*,\mathbf{h}^*}\sqrt{\text{diag}\left(\mathbf{J}^{-1}_{\mathbf{Y}^*,\mathbf{h}^*}\mathbf{J}^{-T}_{\mathbf{Y}^*,\mathbf{h}^*}\right)} \tag{2.4}$$

where $\mathbf{J}_{\mathbf{Y}^*,\mathbf{h}^*}$ is the Jacobian of the transformation between standard and normal spaces evaluated at the design point and $\boldsymbol{\alpha} = -\partial g/\partial \mathbf{Y}$ is the sensitivity vector from Eq. (2.2). In the case that the random variables are uncorrelated, $\mathbf{J}_{\mathbf{Y}^*,\mathbf{h}^*} = \mathbf{I}$ and $\boldsymbol{\gamma}$ reduces to $\boldsymbol{\alpha}$. The search for the design point and the computation of the importance ranking vector both require $\partial \mathbf{U}_f/\partial \mathbf{h}$, the gradient of the nodal response with respect to the random variables, whose computation is discussed in the next section.

2.3 Top-Level Response Sensitivity Equations

To compute the gradient of the nodal displacements by the DDM, the governing equations of the discrete structural response are differentiated with respect to $\mathbf{h}$, the random variables that map to the material, geometric, and load parameters of the structural model. For nonlinear static analysis, the parameterized system of nodal equilibrium equations is

$$\mathbf{P}_r(\mathbf{U}_f(\mathbf{h}), \mathbf{h}) = \mathbf{P}_f(\mathbf{h}) \tag{2.5}$$

where the vector $\mathbf{P}_r$ represents the internal resisting forces of the structure. This vector depends explicitly on $\mathbf{h}$ and implicitly on $\mathbf{h}$ via the nodal response vector

$\mathbf{U}_f$. The vector $\mathbf{P}_f$ represents the external loads applied to the structure. To formulate the structural sensitivity equations for a single parameter, h, from the vector $\mathbf{h}$, Eq. (2.5) is differentiated using the chain rule

$$\mathbf{K}_T \frac{\partial \mathbf{U}_f}{\partial h} + \left. \frac{\partial \mathbf{P}_r}{\partial h} \right|_{\mathbf{U}_f} = \frac{\partial \mathbf{P}_f}{\partial h} \tag{2.6}$$

where $\mathbf{K}_T = \partial \mathbf{P}_r / \partial \mathbf{U}_f$ represents the tangent stiffness of the structure. Assembly of the right hand side is required to obtain the response sensitivity for each parameter in the vector $\mathbf{h}$. The vector $\partial \mathbf{P}_f / \partial h$ represents the derivative of the external forces, which is nonzero only when the parameter h corresponds to an external load. The derivative $\partial \mathbf{P}_r / \partial h|_{\mathbf{U}_f}$ represents the derivative of the resisting force vector under the condition of fixed displacements and it is assembled from element contributions by standard finite element procedures. Extension of the nodal response sensitivity equations to nonlinear dynamic analysis is straightforward and independent of the element formulation for material and geometric nonlinearity [26], an example of which is shown in the following section.

2.4 Gradient Computations for Geometric Nonlinear Displacement-Based Elements

Many frame finite element formulations use a natural, or basic, system of forces and deformations that is free of rigid body modes. This approach is advantageous because it separates geometric nonlinearity due to large displacements outside the

basic system from material nonlinearity and geometric nonlinearity due to large deformations inside the basic system. The simply-supported basic system shown in Fig. 2.1 uses three basic forces: one axial force, q_1, and the bending moment at each end of the element, q_2 and q_3. The corresponding deformations are the extension of the element, v_1, and the tangents to the deflected shape, v_2 and v_3, at each end of the element.

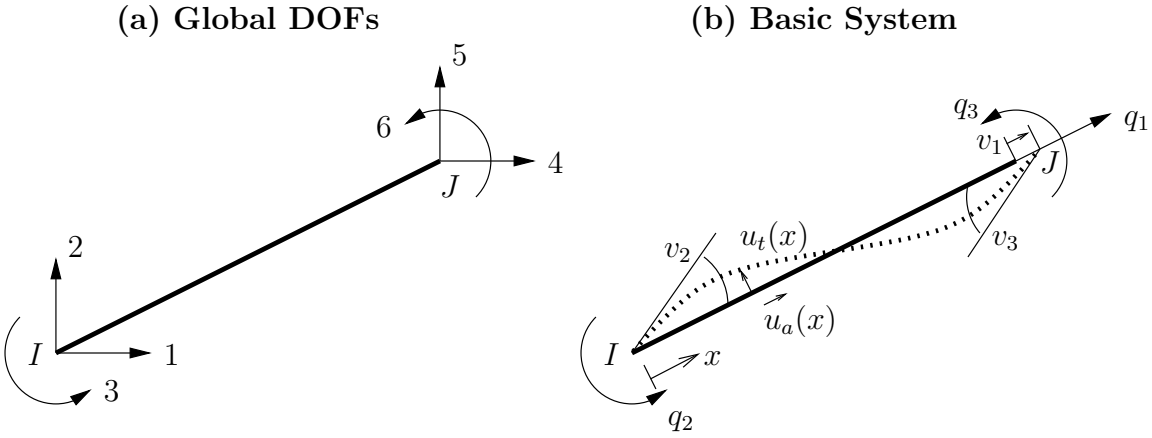

Figure 2.1: Two-dimensional frame finite elements: (a) global DOFs for displacements and forces; and (b) basic system of forces and deformations.

A displacement-based Euler-Bernoulli formulation is used herein with the assumption of moderate rotation for geometric nonlinearity [32] in the basic system. With this assumption, the axial deformation along the beam is

$$\varepsilon_a(x) = \frac{\partial u_a(x)}{\partial x} + \frac{1}{2}\left(\frac{\partial u_t(x)}{\partial x}\right)^2 \tag{2.7}$$

while the curvature is determined from the second derivative of the transverse

displacement field

$$\kappa(x) = \frac{\partial^2 u_t(x)}{\partial x^2} \tag{2.8}$$

The axial deformation and curvature are collected in the section deformation vector, $\mathbf{e}(x) = [\varepsilon_a(x)\ \kappa(x)]^T$. The corresponding axial force, $N(x)$, and bending moment, $M(x)$, are collected in the section force vector $\mathbf{s}(x) = [N(x)\, M(x)]^T$ which is computed through a fiber model or stress resultant plasticity model that account for nonlinear constitutive response. The section stiffness matrix, $\mathbf{k}_s$, is the partial derivative of the section forces with respect to section deformations

$$\mathbf{k}_s = \frac{\partial \mathbf{s}}{\partial \mathbf{e}} = \begin{bmatrix} \frac{\partial N}{\partial \varepsilon_a} & \frac{\partial N}{\partial \kappa} \\ \frac{\partial M}{\partial \varepsilon_a} & \frac{\partial M}{\partial \kappa} \end{bmatrix} \tag{2.9}$$

To interpolate the axial deformation, a linear function that satisfies the boundary conditions of the basic system is assumed

$$u_a(x) = \left(\frac{x}{L}\right) v_1 \tag{2.10}$$

Similarly, for the transverse deflection, cubic Hermitian polynomials are assumed

$$u_t(x) = L\left(\left(\frac{x}{L}\right)^3 - 2\left(\frac{x}{L}\right)^2 + \left(\frac{x}{L}\right)\right) v_2 + L\left(\left(\frac{x}{L}\right)^3 - \left(\frac{x}{L}\right)^2\right) v_3 \tag{2.11}$$

The section deformations are interpolated from the element deformations using

the spatial derivatives of the shape functions according to Eqs. (2.7) and (2.8)

$$\mathbf{e}(x) = \begin{bmatrix} u_a'(x) + \frac{1}{2}(u_t'(x))^2 \\ u_t''(x) \end{bmatrix} = \mathbf{B}(x)\mathbf{u}_b + \begin{bmatrix} \frac{1}{2}\left(\mathbf{C}(x)\mathbf{u}_b\right)^2 \\ 0 \end{bmatrix} \tag{2.12}$$

where the strain-displacement matrix is

$$\mathbf{B}(x) = \frac{1}{L}\begin{bmatrix} 1 & 0 & 0 \\ 0 & 6(\frac{x}{L}) - 4 & 6(\frac{x}{L}) - 2 \end{bmatrix} \tag{2.13}$$

and the slope-displacement matrix is

$$\mathbf{C}(x) = \begin{bmatrix} 0 & 3\left(\frac{x}{L}\right)^2 - 4\left(\frac{x}{L}\right) + 1 & 3\left(\frac{x}{L}\right)^2 - 2\left(\frac{x}{L}\right) \end{bmatrix} \tag{2.14}$$

Using the principle of virtual displacements, equilibrium between basic forces and section forces along the element is

$$\mathbf{p}_b = \int_0^L \mathbf{B}^T(x)\mathbf{s}(x)dx + \int_0^L \mathbf{C}^T(x)\mathbf{C}(x)\mathbf{u}_b N(x)dx \tag{2.15}$$

For computer implementation, Eq. (2.15) is evaluated by numerical integration

$$\mathbf{p}_b = \sum_{i=1}^{N_p} \mathbf{B}_i^T \mathbf{s}_i w_i + \sum_{i=1}^{N_p} \mathbf{C}_i^T \mathbf{C}_i \mathbf{u}_b N_i w_i \tag{2.16}$$

where N_p is the number of integration points with along the element with locations x_i and associated weights w_i. For notational convenience, response quantities are abbreviated as $f_i \equiv f(x_i)$ in Eq. (2.16) and in subsequent equations. The stiffness

matrix, $\mathbf{k}_b$, of the basic system is the partial derivative of the basic forces with respect to element deformations

$$\mathbf{k}_b = \frac{\partial \mathbf{p}_b}{\partial \mathbf{u}_b} = \sum_{i=1}^{N_p} \mathbf{B}_i^T \mathbf{k}_{si} \left(\mathbf{B}_i + (\mathbf{C}_i \mathbf{u}_b) \begin{bmatrix} \mathbf{C}_i \\ \mathbf{0} \end{bmatrix} \right) w_i + \sum_{i=1}^{N_p} \mathbf{C}_i^T \mathbf{k}_{s1i} \left((\mathbf{C}_i \mathbf{u}_b) \mathbf{B}_i + (\mathbf{C}_i \mathbf{u}_b)^2 \begin{bmatrix} \mathbf{C}_i \\ \mathbf{0} \end{bmatrix} \right) w_i + \sum_{i=1}^{N_p} \mathbf{C}_i^T \mathbf{C}_i N_i w_i \tag{2.17}$$

where $\mathbf{k}_{s1}$ is the first row of the section stiffness matrix defined in Eq. (2.9). Both the basic stiffness matrix and basic force vector of Eq. (2.16) are assembled in to the governing equations of nonlinear structural response by standard finite element procedures.

2.4.1 Element Response Sensitivity

The element response sensitivity is formulated in terms of the derivatives of section and basic forces with respect to h. The complete derivative of basic forces is

$$\frac{\partial \mathbf{p}_b}{\partial h} = \mathbf{k}_b \frac{\partial \mathbf{u}_b}{\partial h} + \left. \frac{\partial \mathbf{p}_b}{\partial h} \right|_{\mathbf{u}_b} \tag{2.18}$$

where $\partial \mathbf{p}_b / \partial h|_{\mathbf{u}_b}$ is the derivative of the basic forces under the condition of fixed element deformations, $\mathbf{k}_b$ is the basic stiffness matrix, and $\partial \mathbf{u}_b / \partial h$ is the derivative of the element deformations. Similarly, the derivative of section forces is

$$\frac{\partial \mathbf{s}}{\partial h} = \mathbf{k}_s \frac{\partial \mathbf{e}}{\partial h} + \left. \frac{\partial \mathbf{s}}{\partial h} \right|_{\mathbf{e}} \tag{2.19}$$

where $\partial \mathbf{s}/\partial h|_{\mathbf{e}}$ is computed from the section response, $\mathbf{k}_s$ is the section stiffness matrix, and $\partial \mathbf{e}/\partial h$ is the derivative of section deformations. Owing to the geometrically nonlinear term in Eq. (2.16), it is convenient to extract the derivative of the axial force from Eq. (2.19)

$$\frac{\partial N}{\partial h} = \mathbf{k}_{s1} \frac{\partial \mathbf{e}}{\partial h} + \left. \frac{\partial N}{\partial h} \right|_{\mathbf{e}} \tag{2.20}$$

where $\partial N/\partial h|_{\mathbf{e}}$ is the conditional derivative of axial force.

Before utilizing the derivatives defined in Eq. (2.18) through Eq. (2.20), the element basic force defined in Eq. (2.16) is differentiated with respect to h, which represents any parameter of the section constitutive model, cross-section geometry, or coordinates of the element nodes

$$\frac{\partial \mathbf{p}_b}{\partial h} = \sum_{i=1}^{N_p} \left(\mathbf{B}_i^T \frac{\partial \mathbf{s}_i}{\partial h} + \mathbf{C}_i^T \mathbf{C}_i \mathbf{u}_b \frac{\partial N_i}{\partial h} \right) w_i + \sum_{i=1}^{N_p} \left(\frac{\partial \mathbf{B}_i^T}{\partial h} \mathbf{s}_i + \left(\frac{\partial \mathbf{C}_i^T}{\partial h} \mathbf{C}_i + \mathbf{C}_i^T \frac{\partial \mathbf{C}_i}{\partial h} \right) \mathbf{u}_b N_i \right) w_i + \sum_{i=1}^{N_p} \mathbf{C}_i^T \mathbf{C}_i \frac{\partial \mathbf{u}_b}{\partial h} N_i w_i + \sum_{i=1}^{N_p} \left(\mathbf{B}_i^T \mathbf{s}_i + \mathbf{C}_i^T \mathbf{C}_i \mathbf{u}_b N_i \right) \frac{\partial w_i}{\partial h} \tag{2.21}$$

where similar terms have been grouped in summations. Inserting the derivatives of basic and section forces defined in Eq. (2.18) through Eq. (2.20) in to Eq. (2.21) gives

$$\begin{aligned} \mathbf{k}_b \frac{\partial \mathbf{u}_b}{\partial h} + \left. \frac{\partial \mathbf{p}_b}{\partial h} \right|_{\mathbf{u}_b} = {} & \sum_{i=1}^{N_p} \left(\mathbf{B}_i^T \left(\mathbf{k}_{si} \frac{\partial \mathbf{e}_i}{\partial h} + \left. \frac{\partial \mathbf{s}_i}{\partial h} \right|_{\mathbf{e}} \right) + \mathbf{C}_i^T \mathbf{C}_i \mathbf{u}_b \left(\mathbf{k}_{s1i} \frac{\partial \mathbf{e}_i}{\partial h} + \left. \frac{\partial N_i}{\partial h} \right|_{\mathbf{e}} \right) \right) w_i + \sum_{i=1}^{N_p} \left(\frac{\partial \mathbf{B}_i^T}{\partial h} \mathbf{s}_i + \left(\frac{\partial \mathbf{C}_i^T}{\partial h} \mathbf{C}_i + \mathbf{C}_i^T \frac{\partial \mathbf{C}_i}{\partial h} \right) \mathbf{u}_b N_i \right) w_i \\ & + \sum_{i=1}^{N_p} \mathbf{C}_i^T \mathbf{C}_i \frac{\partial \mathbf{u}_b}{\partial h} N_i w_i + \sum_{i=1}^{N_p} \left(\mathbf{B}_i^T \mathbf{s}_i + \mathbf{C}_i^T \mathbf{C}_i \mathbf{u}_b N_i \right) \frac{\partial w_i}{\partial h} \end{aligned} \tag{2.22}$$

This system has more unknowns than equations available to solve for the con-

ditional derivative of basic forces, $\partial \mathbf{p}_b / \partial h|_{\mathbf{u}_b}$. To reduce the number of unknowns, the derivative of section deformations, defined in Eq. (2.12), is differentiated with respect to h

$$\frac{\partial \mathbf{e}_i}{\partial h} = \mathbf{B}_i \frac{\partial \mathbf{u}_b}{\partial h} + \frac{\partial \mathbf{B}_i}{\partial h}\mathbf{u}_b + \mathbf{C}_i \mathbf{u}_b \begin{bmatrix} \mathbf{C}_i \frac{\partial \mathbf{u}_b}{\partial h} + \frac{\partial \mathbf{C}_i}{\partial h}\mathbf{u}_b \\ 0 \end{bmatrix} \tag{2.23}$$

then inserted in to Eq. (2.22). Utilizing the basic stiffness matrix defined in Eq. (2.17), terms involving $\partial \mathbf{e}/\partial h$ and $\partial \mathbf{u}_b/\partial h$ cancel from Eq. (2.22) after algebraic manipulation. The conditional derivative of basic forces is then

$$\begin{aligned} \left.\frac{\partial \mathbf{p}_b}{\partial h}\right|_{\mathbf{u}_b} = & \sum_{i=1}^{N_p} \left(\mathbf{B}_i^T \left.\frac{\partial \mathbf{s}_i}{\partial h}\right|_{\mathbf{e}} + \mathbf{C}_i^T \mathbf{C}_i \mathbf{u}_b \left.\frac{\partial N_i}{\partial h}\right|_{\mathbf{e}} \right) w_i + \sum_{i=1}^{N_p} \left(\frac{\partial \mathbf{B}_i^T}{\partial h}\mathbf{s}_i + \left(\frac{\partial \mathbf{C}_i^T}{\partial h}\mathbf{C}_i + \mathbf{C}_i^T \frac{\partial \mathbf{C}_i}{\partial h} \right) \mathbf{u}_b N_i \right) w_i \\ & + \sum_{i=1}^{N_p} \left(\mathbf{B}_i^T \mathbf{k}_{si} + \mathbf{C}_i^T \mathbf{C}_i \mathbf{u}_b \mathbf{k}_{s1i} \right) \left(\frac{\partial \mathbf{B}_i}{\partial h}\mathbf{u}_b + \mathbf{C}_i \mathbf{u}_b \begin{bmatrix} \frac{\partial \mathbf{C}_i}{\partial h}\mathbf{u}_b \\ 0 \end{bmatrix} \right) w_i + \sum_{i=1}^{N_p} \left(\mathbf{B}_i^T \mathbf{s}_i + \mathbf{C}_i^T \mathbf{C}_i \mathbf{u}_b N_i \right) \frac{\partial w_i}{\partial h} \end{aligned} \tag{2.24}$$

The sensitivity of the strain-displacement and slope-displacement matrices, $\partial \mathbf{B}_i/\partial h$ and $\partial \mathbf{C}_i/\partial h$, respectively, are nonzero only when h represents an uncertain nodal coordinate at the element ends. In addition to uncertain nodal coordinates, the term $\partial w_i/\partial h$, may also be non-zero when h corresponds to a prescribed integration weight [60].

In the event that h does not map to an uncertain nodal coordinate or prescribed

integration weight, Eq. (2.24) simplifies to

$$\left.\frac{\partial \mathbf{p}_b}{\partial h}\right|_{\mathbf{u}_b} = \sum_{i=1}^{N_p} \mathbf{B}_i^T \left.\frac{\partial \mathbf{s}_i}{\partial h}\right|_{\mathbf{e}} w_i + \sum_{i=1}^{N_p} \mathbf{C}_i^T \mathbf{C}_i \mathbf{u}_b \left.\frac{\partial N_i}{\partial h}\right|_{\mathbf{e}} w_i \tag{2.25}$$

while the derivative of section deformations, Eq. (2.23), reduces to

$$\frac{\partial \mathbf{e}_i}{\partial h} = \mathbf{B}_i \frac{\partial \mathbf{u}_b}{\partial h} + \mathbf{C}_i \mathbf{u}_b \begin{bmatrix} \mathbf{C}_i \frac{\partial \mathbf{u}_b}{\partial h} \\ 0 \end{bmatrix} \tag{2.26}$$

Regardless of the type of parameter, the conditional derivative of basic forces is computed by Eq. (2.24) or Eq. (2.25) for assembly in to the right-hand side of Eq. (2.6). After solution for the nodal response sensitivity, the derivative of section deformations is computed from Eq. (2.23) or Eq. (2.26) so that constitutive models can be updated for path-dependent response sensitivity. Further details of the two phase sensitivity calculations are found in [72]. The sensitivity equations have been implemented in the OpenSees finite element software framework [43, 61] and are verified and applied to reliability analysis in the following examples.

2.5 Numerical Examples

The following numerical examples verify the sensitivity formulation for the geometrically nonlinear displacement-based element and demonstrate its application in a gradient-based structural reliability analysis. Standalone sensitivity analysis for single member models verify the DDM in the first two examples followed by a

FORM analysis of a steel frame in the third example.

2.5.1 Simply Supported Beam Subjected to Uniform Distributed Load

The focus of this example is the axial force developed in the statically indeterminate, linear-elastic, prismatic beam shown in Fig. 2.2 subjected to a uniform distributed load, w. The beam length is L=10 m, the cross-section dimensions are b=0.1 m and d=0.2 m, and the elastic modulus is E=200 MPa. The intensity of the distributed load increases from zero to its peak value of 0.5 kN/m. The member is discretized into five geometrically nonlinear displacement-based elements that utilize the corotational geometric transformation [18]. Three Gauss-Legendre integration points are used along each element.

The relationship between distributed load and midspan axial force (recorded at the second integration point of the middle element) is shown in Fig. 2.3. The sensitivity of the midspan axial force with respect to section depth, d, and member length, L, is shown in Fig. 2.4. The sensitivity of the axial force shown in this figure is determined via Eq. (2.19) after computing $\partial \mathbf{e}/\partial h$ in the second phase of sensitivity computations. The finite difference approximations using 0.1 and 0.001 times the nominal parameter values show convergence to the DDM result, thereby validating the implementation of the section force sensitivity.

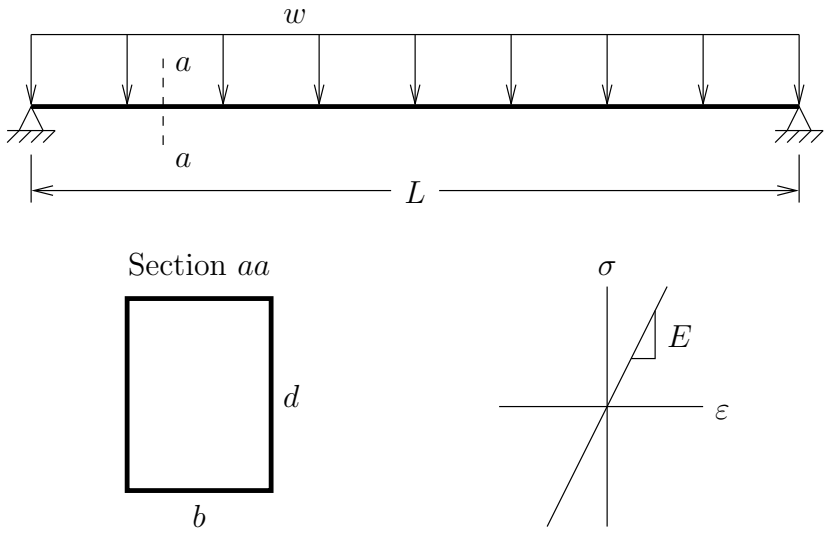

Figure 2.2: Indeterminate beam subjected to uniform distributed load.

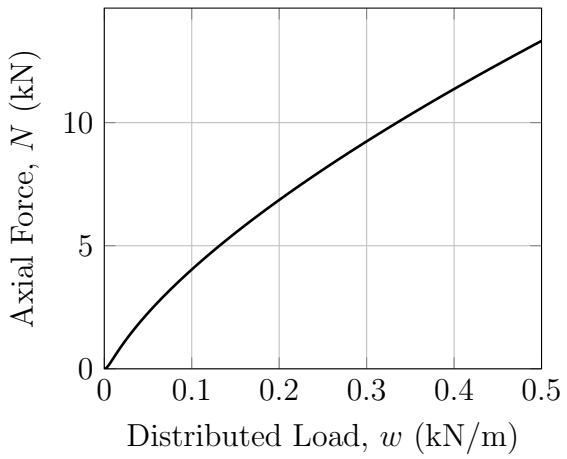

Figure 2.3: Axial force, N, at midspan beam subjected to increasing uniform distributed load.

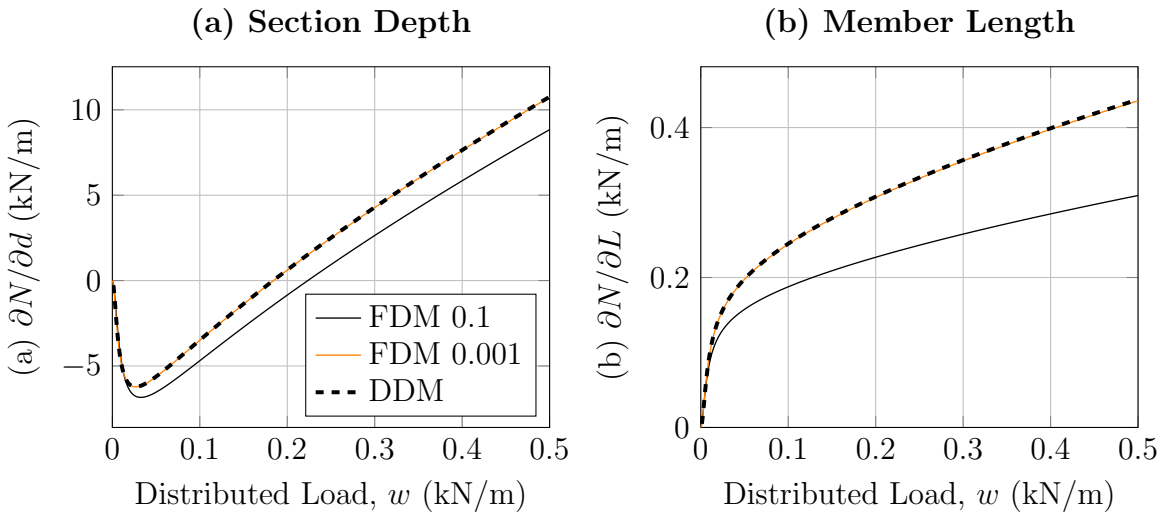

Figure 2.4: Sensitivity of midspan axial force, N, to: (a) cross-section depth, d, and (b) member length, L.

2.5.2 Simply Supported Beam Subjected to Eccentric Axial Load

The prismatic, elasto-plastic beam shown in Fig. 2.5 is subjected to an eccentric axial load. The beam section is W12x96 with elastic modulus E=200,000 MPa, kinematic strain hardening ratio α=0.05, and yield stress f_y=420 MPa. The rotation, U, at the right support is recorded as a cyclic axial load, $P(t) = 2.5(EI/L^2)\sin(t)$, is applied, where L=10 m is the length of the beam and I is the second moment of the cross-section area. The load eccentricity, e, is equal to twice the member depth.

The member is discretized in to five geometrically nonlinear displacement-based elements along its length and the corotational transformation describes the relationship between basic and local element forces. Three Gauss-Legendre integration points are used in each element. The load-rotation response for the beam is shown

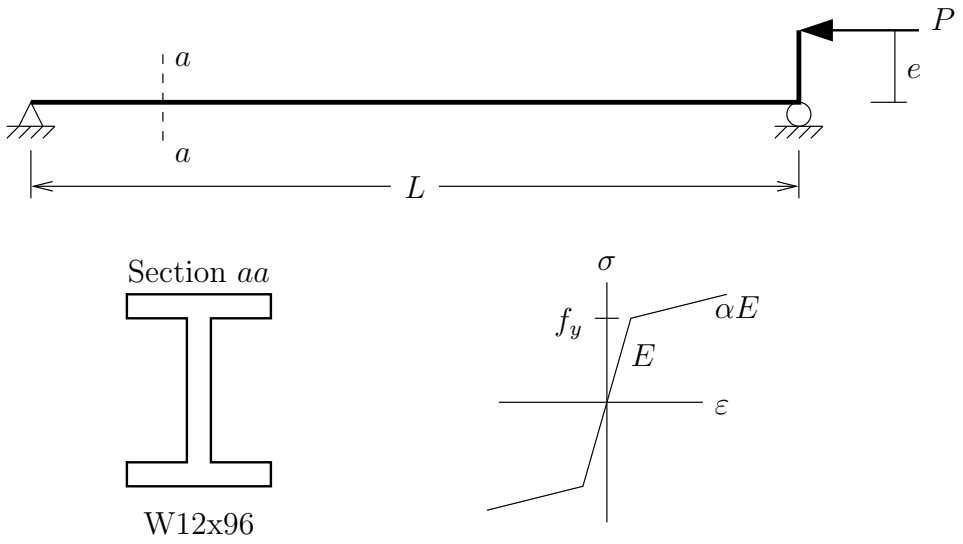

Figure 2.5: Simply supported beam subjected to an eccentric axial load.

in Fig. 2.6 where it is noted that the rotation increases rapidly after the onset of yielding along the member then yields under load reversal.

Comparisons of the DDM and FDM sensitivity of the load-rotation response with respect to the elastic modulus, E, and yield stress, f_y, of the material, cross-section depth, d, and member length, L, are shown in Fig. 2.7. Each section-level parameter maps to all sections along the member while the length parameter maps to the X-coordinate of the roller support. The finite difference parameter perturbations in Fig. 2.7 correspond to 0.1 and 0.001 times the nominal parameter value. As the parameter perturbation for the finite difference computation decreases, the results converge to the DDM sensitivity, thereby verifying the DDM equations and their implementation for the nodal response sensitivity.

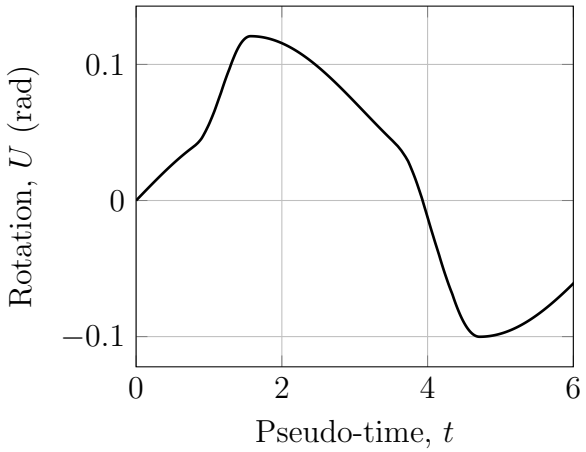

Figure 2.6: Normalized load-rotation response for the simply-supported beam.

2.5.3 Reliability Analysis of Steel Frame

With slender column members and high gravity loads, the frame developed by [21] has been studied by several researchers in the development of geometrically nonlinear frame finite element formulations [11, 20]. A reliability analysis of the steel frame shown in Fig. 2.8 is performed in this example in order to demonstrate the application of the element response sensitivity equations in a gradient-based application. Each member is a W8x31 wide flange steel section with elastic modulus, E=200,000 MPa, yield stress, f_y=250 MPa. The stress-strain response is assumed bilinear with strain hardening ratio α=0.02. Three geometrically nonlinear displacement-based elements with four Gauss-Legendre integration points is used to simulate the response of each member during the pushover analysis. For comparison, the analysis will be repeated using three geometrically linear displacement-based elements per member and one force-based CBDI element per

member [48, 20, 55]. The corotational formulation captures large displacement response in all cases.

All material and geometric parameters are considered uncertain. The elastic modulus E of each member is a lognormal random variable with mean value 200,000 MPa and coefficient of variation (cov) 5% and correlation coefficient 0.6 with the elastic modulus of the other members. The yield strength f_y of each member is a lognormal random variable with mean 250 MPa and 10% cov and correlation coefficient 0.6 with f_y of the other members. The strain hardening ratio α of each member is a lognormal random variable with mean 0.02 and 10% cov and correlation coefficient 0.6 with α of the other members. The section depth, d, and flange width, b_f, of each member are uncorrelated normal random variables with 2% cov. To account for geometric imperfections, the horizontal coordinates of the roof nodes, X_2 and X_3, are also assumed to be uncorrelated normal random variables with standard deviations equal to 10 mm. The gravity loads applied to the columns are assumed to be correlated normal random variables with 15% coefficient of variation and correlation coefficient 0.5.

Rather than quantifying the reliability of this steel frame, the focus of this example is to highlight the differences in reliability index and importance measures when using the geometrically nonlinear displacement-based frame element formulation compared to the standard geometrically linear formulation and force-based CBDI formulations. A similar approach to quantifying the uncertainty of the underlying numerical methods, rather than that of the underlying system behavior, was taken by [5].

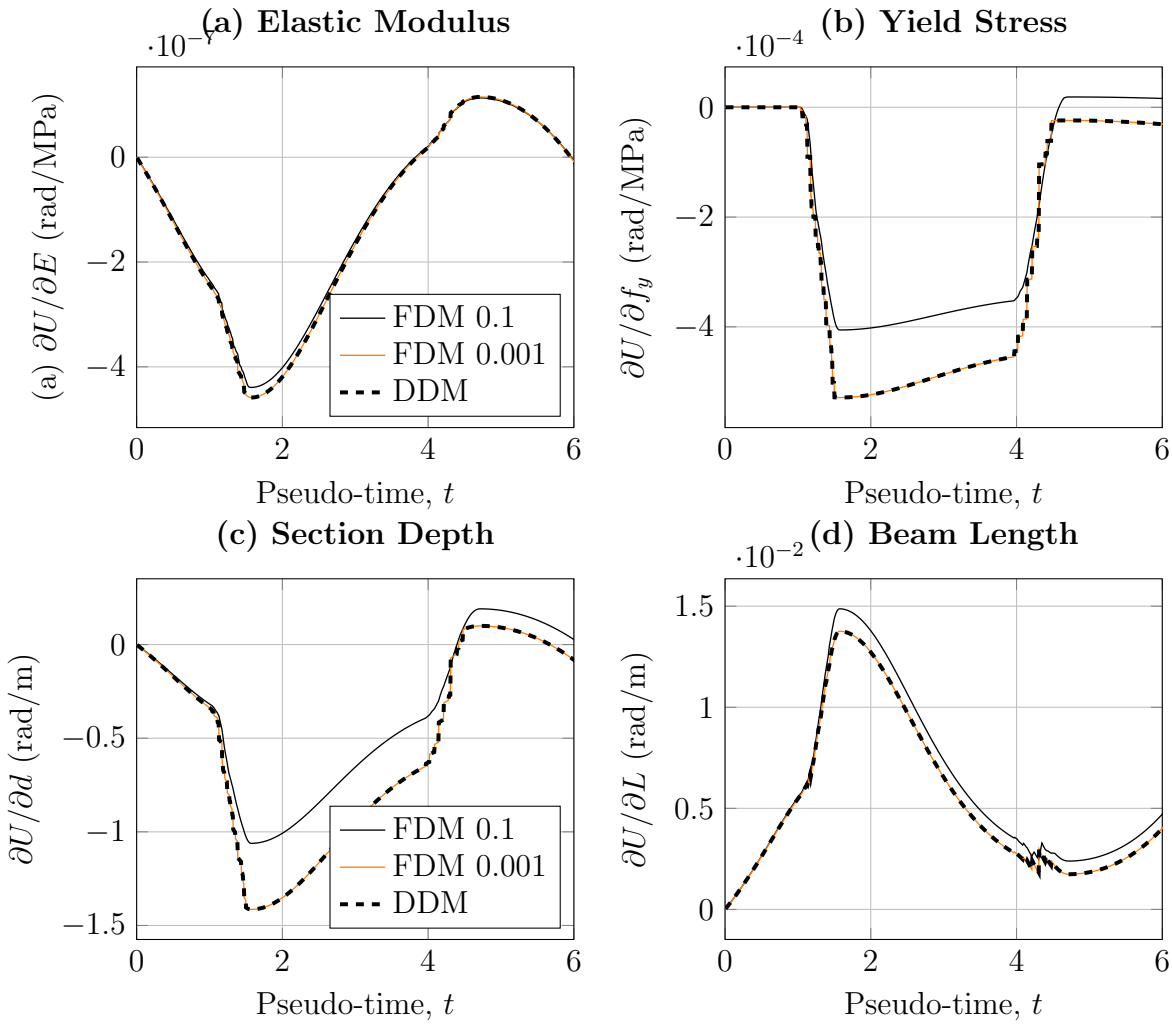

Figure 2.7: Sensitivity of load-rotation response with respect to material properties, section depth, and beam length.

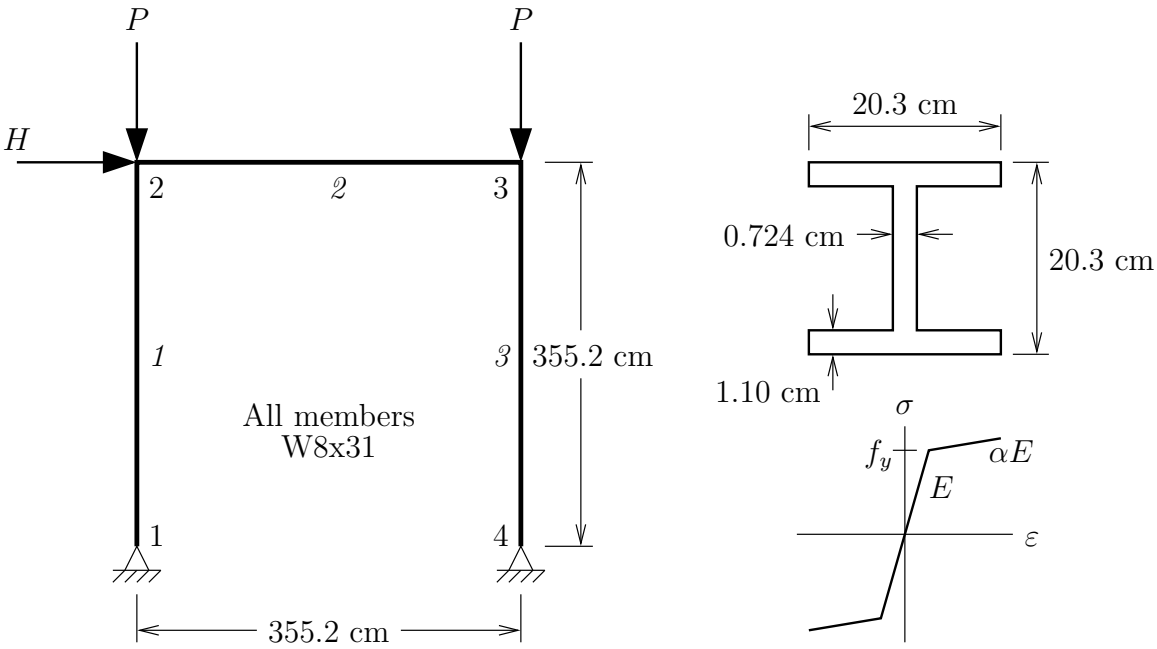

Figure 2.8: Steel frame structure: node and member numbers, loads, cross-section dimensions, and material stress-strain behavior.

2.5.3.1 Mean Response Sensitivity

The mean load-displacement response of the frame for two values of gravity load is shown in Fig. 2.9. The response using a single geometrically linear displacement-based element is presented in order to examine the significance of moderate rotations within the basic system. As expected, the simulated lateral stiffness and strength of the frame is reduced when accounting for geometric nonlinearity and the effect becomes more significant as the gravity load increases from $0.2P_y$ to $0.4P_y$. The force-based CBDI element shows a lower yield load due to the satisfaction of strong equilibrium in the element formulation.

The sensitivity of the frame load-displacement response with respect to the

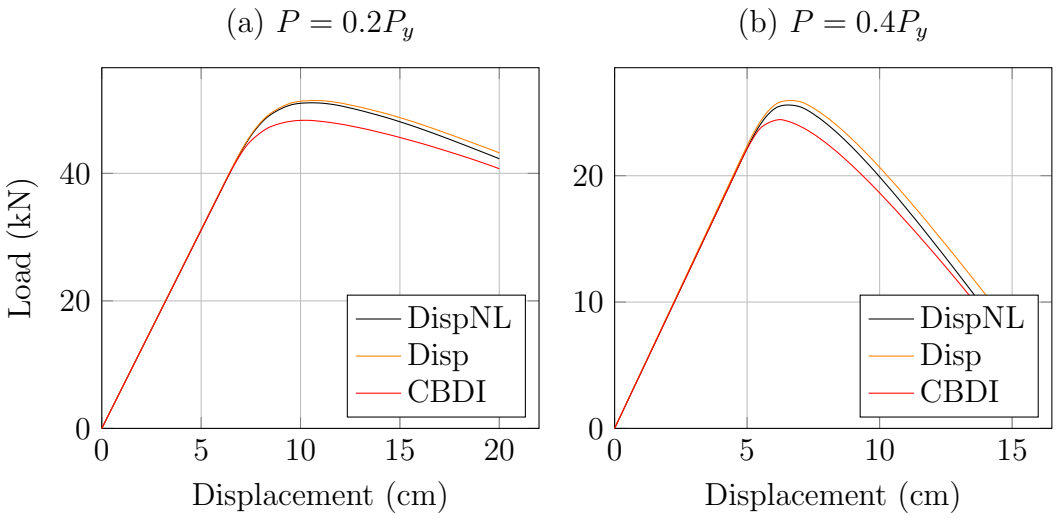

Figure 2.9: Mean load-displacement response of the steel frame structure for two values of gravity loads: (a) $P = 0.2P_y$ and (b) $P = 0.4P_y$. DispNL = geometrically nonlinear, Disp = geometrically linear displacement-based formulation.

yield stress of member 1, as computed by the DDM for each of the three element formulations, is shown in Fig. 2.10. As expected, the sensitivity of the lateral displacement is zero up to the onset of yielding in member 1. The sensitivity for the two displacement-based formulations is approximately the same as the frame reaches its ultimate lateral load capacity, then starts to diverge in the post-peak response. Although the response obtained for the three formulations is similar, the sensitivity of the frame load-displacement response is generally of greater magnitude when using the force-based CBDI formulation.

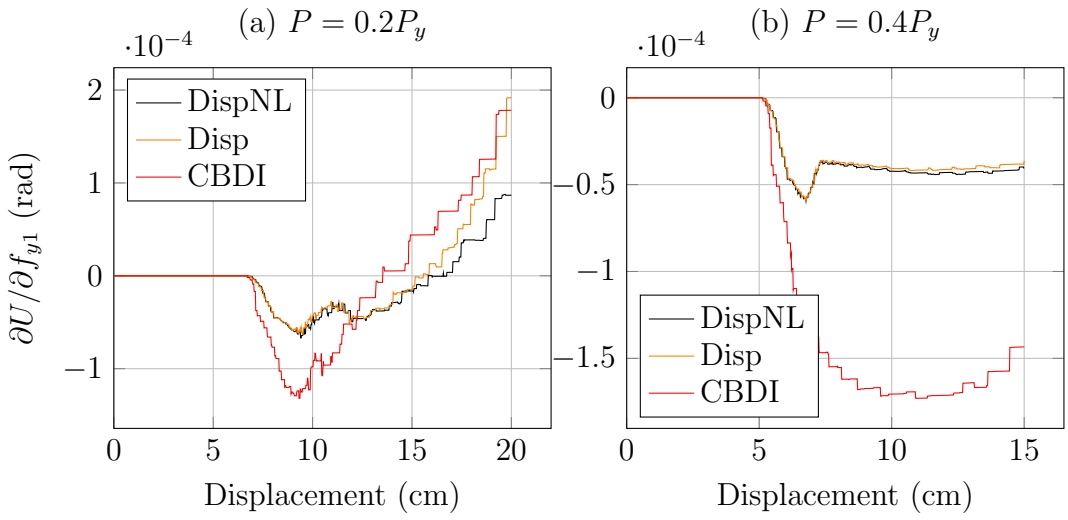

Figure 2.10: Sensitivity of the rotation at the base of column 1 with respect to column 1 material yield stress, f_y, in the steel frame structure: (a) $P = 0.2P_y$ and (b) $P = 0.4P_y$. DispNL = geometrically nonlinear, Disp = geometrically linear displacement-based formulation, CBDI = geometrically nonlinear force-based formulation.

2.5.3.2 Reliability Analysis

Using the aforementioned statistical properties for the cross-section dimensions and material properties of the frame and gravity loads, a first-order reliability (FORM) analysis is performed for each level of gravity load. For the lighter gravity load of $P = 0.2P_y$, the performance function places a limit on U_{f2}, the horizontal displacement of node 2

$$g = 10\text{cm} - U_{f2} \quad \text{for } P = 0.2P_y \tag{2.27}$$

Using the iHLRF algorithm, the FORM analysis converges to a reliability index of β=0.257 for the geometrically nonlinear displacement-based element formulation and to a higher reliability index of β=0.363 for the standard displacement-based formulation. A negative reliability index of $\beta = -0.0557$ was found for the force-based CBDI element, indicating that the mean realization of the random variables lies in the failure domain for this model. The load-displacement response associated with the values of the random variables at the design point is shown in Fig. 2.11 (a) for each element formulation. The design point response is similar between the element formulations.

The reliability analysis is repeated for the case of higher gravity load, $P = 0.4P_y$. with the performance function

$$g = 6\text{cm} - U_{f2} \quad \text{for } P = 0.4P_y \tag{2.28}$$

In this case, the FORM analysis converges to a reliability index of β=0.0089 for the geometrically nonlinear displacement-based element formulation and to β=0.0597 for its geometrically linear counterpart, while the reliability index for the force-based CBDI formulation was $\beta = -0.216$. The load-displacement response at the design point for each formulation is shown in Fig. 2.11 (b).

In addition to the variance of the reliability index among the three element formulations, Fig. 2.12 shows that the importance measures for the 16 random variables shows differences among the formulations. The yield strength of the column members, 1 and 3, along with the gravity loads rank highest in importance

for the $P = 0.2P_y$ case. The importance of the gravity loads increases for the case of $P = 0.4P_y$, as shown in Fig. 2.12 (b) with a relative decrease in importance of the material properties and cross-section dimensions. In both cases, as expected for the applied loading, the importance measures of the column section properties, f_y, E, d, and b, rank slightly higher relative to those of the girder member.

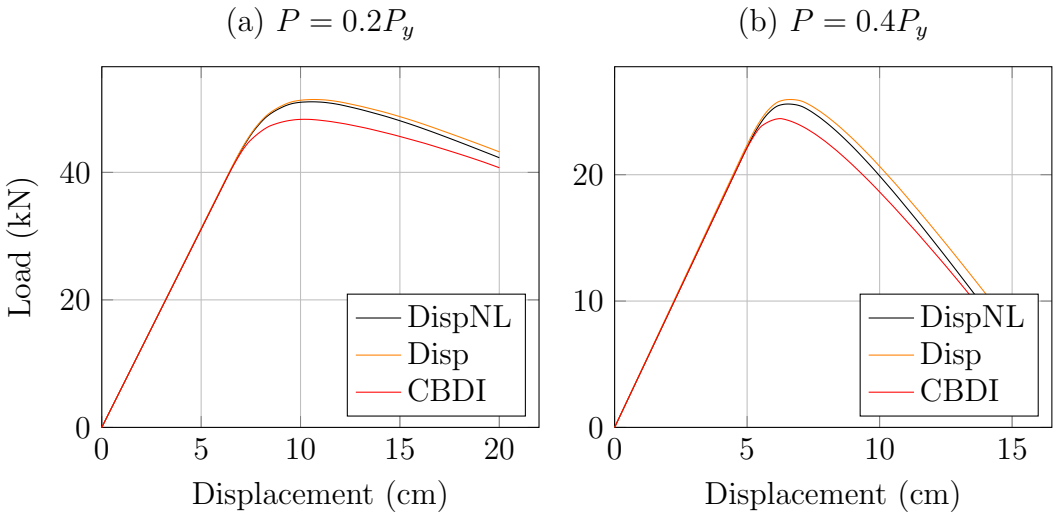

Figure 2.11: MPP load-displacement response of the steel frame structure for two values of gravity loads: (a) $P = 0.2P_y$ and (b) $P = 0.4P_y$.

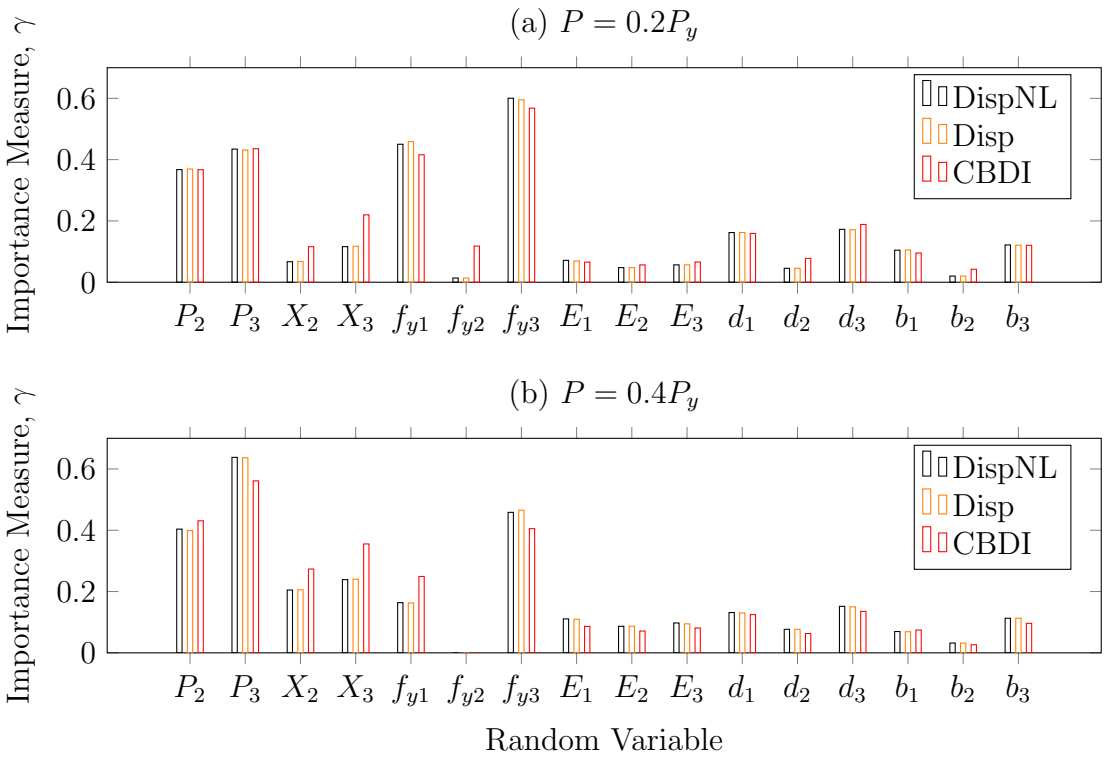

Figure 2.12: Importance measures for all random variables in steel frame analysis for two levels of gravity loads: (a) $P = 0.2P_y$ and (b) $P = 0.4P_y$.

2.6 Conclusion

The exact response sensitivity of geometrically nonlinear displacement-based frame finite elements was developed for uncertain material, cross-section dimension, nodal coordinate, and load parameters by the direct differentiation method. The inclusion of moderate rotations within the element basic system leads to additional terms in the conditional derivative of basic forces. The response sensitivity equations have been implemented in the OpenSees finite element software framework. Examples of standalone sensitivity analysis verify the DDM implementation for

the geometrically nonlinear formulation. Finite element reliability analysis of a steel frame shows that a lower reliability index is obtained compared to the standard geometrically linear formulation; however, the importance measures differ only slightly with axial loads having higher importance with the geometrically nonlinear formulation. These results indicate that modeling decisions are important for estimating the probability of failure, but not necessarily the importance ranking when comparing geometrically linear and nonlinear displacement-based formulations.

Acknowledgments

This research was made possible through the support of the Higher Committee for Education Development (HCED) in Iraq. Any opinions, findings, and conclusions or recommendations expressed in this material are those of the authors and do not necessarily reflect the views of the HCED.

3 Sensitivity Analysis for Displacement-Controlled Finite Element Analyses

Displacement-controlled finite element analyses are typically employed to simulate the nonlinear static response of structural systems where a loss of load carrying capacity due to localized material failure and/or geometric nonlinearity is expected. To utilize applications such as reliability, optimization, and system identification for structural systems where the peak load capacity is a random variable or where the performance function is defined in terms of the applied load, accurate and efficient gradients of the displacement-controlled response are required. The direct differentiation method (DDM) is applied to the displacement control method in order to compute response sensitivity with respect to the applied load, which is treated as a variable within each pseudo-time step. The resulting sensitivity gives the change in structural load carrying capacity with respect to changes in uncertain parameters. To verify the derived sensitivity equations, comparisons between the DDM and the finite difference method (FDM) are performed through standalone sensitivity analyses of structural systems with material and geometric nonlinearity. Reliability analyses of a steel frame show the importance measures obtained when the performance function is defined in terms of the structural resistance to applied loads in a displacement-controlled analysis are similar to those obtained in a load-controlled analysis where the performance function is defined in terms of

the structural displacements.

3.1 Introduction

The load control method (LC) is commonly used in nonlinear finite analysis as a straightforward means to determine the load-displacement response of a structural system, e.g., for pushover analysis in earthquake engineering. However, the LC approach gives coarse response near limit points and also suffers from convergence difficulties when the tangent stiffness matrix becomes ill-conditioned due to the loss of load-carrying capacity. To overcome these convergence problems, alternatives to the LC method have been developed where the applied load is treated as an additional variable in the finite element solution. In these approaches, a constraint equation is imposed on the structural response in order to solve for the applied load at each equilibrium iteration in a load step. Displacement control is one such method where the displacement at a single degree-of-freedom (DOF) is held constant during equilibrium iteration [8, 52, 16]. Similarly, the arc length method constrains the solution to advance by a specified distance in the hyperspace defined by the structural response at the last time step [16, 46, 25, 44, 22]. These and other incremental-iterative strategies were posed in a common framework by [13], who used a variety of benchmark problems to demonstrate the advantages and disadvantages of each approach.

Among the incremental-iterative strategies examined by [13], the displacement control (DC) approach performs well when there is no snap-back behavior in the

structural response [73, 63, 42]. This makes the DC method suited for practical applications such as pushover analysis of engineered structures under extreme loads where a loss of load carrying capacity is possible due to localized material failure and/or geometric nonlinearity. It is often of interest to find the sensitivity of the structural response with respect to modeling parameters for uncertainty quantification or for gradient-based algorithms where the response derivative is required in order to find an optimal design point.

Response sensitivity measures the change in structural response with respect to changes in the system properties [35] and in doing so, it shows the effects of modeling parameters on the response as well as the relative importance of the parameters when used in conjunction with their statistical variance. Various methods based on perturbed response and analytical differentiation and are available to compute structural response sensitivity. The finite difference method (FDM) computes sensitivity through repeated analyses with perturbed parameter values. Although the FDM is subject to round off errors [12], it is easy to implement and can be applied to any type of analysis (static, dynamic, path-dependent, etc.). A second perturbation-based approach, the complex perturbation method (CPM), uses perturbations of the complex component of parameter values. Although the CPM is highly accurate compared to the FDM [34], it requires complex arithmetic to be carried out through the entire finite element analysis. Despite their heavy computational expense, the FDM and CPM provide useful means of verifying analytical sensitivity methods.

There are two methods to compute analytical sensitivities: the adjoint structure

method (ASM) and the direct differentiation method (DDM). The ASM uses an approach based on Lagrange multipliers, but is limited to path-independent structural response making it impractical for cyclic loading. The DDM is applicable to any type of analysis and constitutive response and it computes sensitivities at the same precision as the structural response. In addition, the DDM does not require full re-analysis for every parameter. The disadvantage of the DDM is it requires extensive derivation and implementation verification for each element formulation and constitutive model; however, this is a one-time expense.

The DDM has been applied successfully to frame finite elements including the displacement-based, force-based, and mixed variational formulations for material nonlinearity [59, 14, 7], as well as the corotational formulation for large displacement analysis of frames [56]. Multiphysics finite element analysis applications to which the DDM has been applied include fire attack [29] and fluid-structure interaction [74]. In addition to individual element formulations, the DDM can be applied to higher level modules of finite element analyses, e.g., multi-point constraint handling by the penalty, transformation, and Lagrange multiplier methods [28] and Newmark time integration for nonlinear dynamic response [26]. The DDM has also been applied in order to compute second order derivatives of finite element response [9].

The objective of this paper is to use the DDM to develop response sensitivity equations for nonlinear static finite element analyses that use the displacement control method to advance through pseudo-time. After an overview of the displacement control method within the incremental-iterative framework developed

by [13], the derivation of DDM response sensitivity equations is presented. Standalone sensitivity examples verify the DDM implementation for structural systems that lose load-carrying capacity due to geometric and material nonlinearity. First order reliability analysis of a steel frame quantifies uncertain response for a performance function defined in terms of the structural load carrying capacity in a displacement-controlled pushover analysis.

3.2 Displacement Control Method

comprehensive overview of the displacement control method can be found in [13], and other continuation methods for nonlinear static analysis within an incremental-iterative framework. This framework is briefly described here because the derivative of the governing incremental-iterative equations will form the basis for DDM response sensitivity computations.

Structural equilibrium is expressed as a balance of the internal resisting forces with the external applied loads, both of which depend on an uncertain parameter, h, of the structural model

$$\mathbf{P}_r\left(\mathbf{U}_f(t,h),h\right) = \mathbf{P}_f(t,h) \tag{3.1}$$

where $\mathbf{P}_r$ is the vector of internal resisting forces that are a nonlinear function of the nodal displacements, $\mathbf{U}_f$. The resisting forces depend explicitly on h and implicitly on h through the nodal displacements. The external force vector is

represented by $\mathbf{P}_f$, which depends on the parameter h only if it corresponds to the external loads.

The external load applied to a structure is expressed as a summation over multiple load patterns

$$\{\mathbf{P}_f(t,h)\} = \sum_{l=1}^{n} \lambda_l(t,h)\{\mathbf{P}_{ref}(h)\}_l \tag{3.2}$$

where $\lambda(t)$ represents a time-variant scalar load factor applied to the l^{th} reference load vector, $\mathbf{P}_{ref}$, of the analysis. Eq. (3.2) allows for separate load patterns to be applied to a structural model, e.g., constant gravity loads along with time-varying lateral loads.

In the displacement control method, an analyst-specified displacement increment is imposed at a single degree of freedom (DOF) and held constant over each load step. In turn, the load factor is treated as a variable that is computed during equilibrium iteration within the time step. As described by [13], the first iteration of a load step is treated separately from the subsequent iterations.

3.2.1 First Iteration

At the first iteration of the i^{th} time step, the tangent displacement vector, $\{\mathbf{U}_{fT}\}_i^1$, is computed from the stiffness matrix at the start of the time step and the reference load pattern

$$[\mathbf{K}_T]_i^0\{\mathbf{U}_{fT}\}_i^1 = \{\mathbf{P}_{ref}\} \qquad \{\mathbf{U}_{fT}\}_i^1 = \left([\mathbf{K}_T]_i^0\right)^{-1}\{\mathbf{P}_{ref}\} \tag{3.3}$$

where $[\mathbf{K}_T]_i^0 = \partial\{\mathbf{P}_r\}_i^0/\partial\{\mathbf{U}_f\}$ is the tangent stiffness matrix of the structure. The superscripts on each term indicate the iteration number within the time step. The initial load increment $\Delta\lambda_i^1$ is obtained by solving a constraint equation that makes the tangent displacement at the controlled DOF equal to the analyst-specified displacement increment, ΔU_c

$$\Delta\lambda_i^1 \left(\{\mathbf{g}\}^T\{\mathbf{U}_{fT}\}_i^1\right) = \Delta U_c \qquad \Delta\lambda_i^1 = \frac{\Delta U_c}{\{\mathbf{g}\}^T\{\mathbf{U}_{fT}\}_i^1} \tag{3.4}$$

where the vector $\{\mathbf{g}\}$ contains all zeroes except for a one in the row corresponding to the controlled DOF. The incremental displacement vector $\{\Delta\mathbf{U}_f\}_i^1$ at the first iteration is then obtained by scaling the tangent displacements by the initial increment of the load factor

$$\{\Delta\mathbf{U}_f\}_i^1 = \Delta\lambda_i^1\{\mathbf{U}_{fT}\}_i^1 \tag{3.5}$$

The load factor and displacement vector are then updated from their values at the conclusion of the previous load step

$$\lambda_i^1 = \lambda_{i-1} + \Delta\lambda_i^1 \tag{3.6}$$

$$\{\mathbf{U}_f\}_i^1 = \{\mathbf{U}_f\}_{i-1} + \{\Delta\mathbf{U}_f\}_i^1 \tag{3.7}$$

At this point, the resisting force vector, $\{\mathbf{P}_r\}$, is evaluated and the convergence criterion is checked to determine if equilibrium according to Eq. (3.1) is satisfied.

For nonlinear response, equilibrium is generally not satisfied, leading to additional iterations for which the state determination differs as described next.

3.2.2 Subsequent Iterations

As the search for equilibrium continues, the increment in nodal displacements is found by solving the following linear system of equations at each iteration

$$[\mathbf{K}_T]_i^{j-1}\{\Delta\mathbf{U}_f\}_i^j = \lambda_i^j\{\mathbf{P}_{ref}\} - \{\mathbf{P}_r\}_i^{j-1} \tag{3.8}$$

where $\{\mathbf{P}_r\}_i^{j-1}$ is the resisting force vector at the previous iteration and λ_i^j is the unknown load factor, which is accumulated from the previous iteration

$$\lambda_i^j = \lambda_i^{j-1} + \Delta\lambda_i^j \tag{3.9}$$

where $\Delta\lambda_i^j$ is the unknown load factor increment to be determined. To solve for the load factor increment, Eq. (3.9) is combined with Eq. (3.8), giving the following system of equations

$$[\mathbf{K}_T]_i^{j-1}\{\Delta\mathbf{U}_f\}_i^j = \{\mathbf{R}_f\}_i^{j-1} + \Delta\lambda_i^j\mathbf{P}_{ref} \tag{3.10}$$

where $\{\mathbf{R}_f\}_i^{j-1}$ is the residual force vector of the previous iteration

$$\{\mathbf{R}_f\}_i^{j-1} = \lambda_i^{j-1}\{\mathbf{P}_{ref}\} - \{\mathbf{P}_r\}_i^{j-1} \tag{3.11}$$

The displacement increment vector, $\{\Delta \mathbf{U}_f\}_i^j$, can be obtained by solving Eq. (3.10)

$$\{\Delta \mathbf{U}_f\}_i^j = \{\Delta \mathbf{U}_{fR}\}_i^j + \Delta\lambda_i^j \{\mathbf{U}_{fT}\}_i^j \tag{3.12}$$

where $\{\Delta \mathbf{U}_{fR}\}_i^j$ is the residual displacement vector, i.e., the displacement increment based on the residual force vector

$$[\mathbf{K}_T]_i^{j-1}\{\Delta \mathbf{U}_{fR}\}_i^j = \{\mathbf{R}_f\}_i^{j-1} \qquad \{\Delta \mathbf{U}_{fR}\}_i^j = \left([\mathbf{K}_T]_i^{j-1}\right)^{-1}\{\mathbf{R}_f\}_i^{j-1} \tag{3.13}$$

and $\{\mathbf{U}_{fT}\}_i^j$ is the tangent displacement vector based on the reference load pattern

$$[\mathbf{K}_T]_i^{j-1}\{\mathbf{U}_{fT}\}_i^j = \{\mathbf{P}_{ref}\} \qquad \{\mathbf{U}_{fT}\}_i^j = \left([\mathbf{K}_T]_i^{j-1}\right)^{-1}\{\mathbf{P}_{ref}\} \tag{3.14}$$

Note that the same left-hand side matrix is used to find both the residual and tangent displacements. The incremental load factor, $\Delta\lambda_i^j$, is obtained by solving a constraint equation that ensures the change in displacement at the controlled DOF is zero, as this displacement was imposed entirely in the first iteration

$$\Delta\lambda_i^j \left(\{\mathbf{g}\}^T\{\mathbf{U}_{fT}\}_i^j\right) + \{\mathbf{g}\}^T\{\Delta \mathbf{U}_{fR}\}_i^j = 0 \qquad \Delta\lambda_i^j = \frac{-\{\mathbf{g}\}^T\{\Delta \mathbf{U}_{fR}\}_i^j}{\{\mathbf{g}\}^T\{\mathbf{U}_{fT}\}_i^j} \tag{3.15}$$

After updating the load factor via Eq. (3.9), the displacement increment is computed according to Eq. (3.12), leading to the update of the total nodal displacement vector

$$\{\mathbf{U}_f\}_i^j = \{\mathbf{U}_f\}_i^{j-1} + \{\Delta \mathbf{U}_f\}_i^j \tag{3.16}$$

With the updated nodal displacements, the convergence criterion can be evaluated to check for equilibrium between the applied loads and the resisting force vector. If the criterion is not satisfied, the search for equilibrium proceeds to the next iteration, repeating the process described by way of Eqs. (3.8) and (3.16)through.

A simple illustration of the iterations for one time step using the displacement control method is shown in Fig. 3.1. During the iteration process, the displacement increment, ΔU_c, is held constant and the load factor is calculated at each iteration. The iteration process continues until reaching the new converged state where the residual displacement $\{\Delta \mathbf{U}_{fR}\}_i^j$ reduces to a specified tolerance. Upon convergence of the global equilibrium iteration, the sensitivity of the load factor and nodal displacements with respect to model parameters can be computed, as described in the following section.

3.3 Top-Level Response Sensitivity Equations

To formulate the equations of response sensitivity at the structural level, the equilibrium equations (Eq. (3.1)) are differentiated with respect to the parameter h

$$[\mathbf{K}_T]_i^j \frac{\partial \{\mathbf{U}_f\}_i^j}{\partial h} = \frac{\partial \{\mathbf{P}_f\}_i^j}{\partial h} - \left. \frac{\partial \{\mathbf{P}_r\}_i^j}{\partial h} \right|_{\mathbf{U}_f} \tag{3.17}$$

The vector $\partial \{\mathbf{P}_r\}_i^j / \partial h \big|_{\mathbf{U}_f}$ represents the derivative of the resisting force vector evaluated with fixed displacements, and it is assembled from element contributions by standard finite element procedures [72]. Physically, this vector represents the

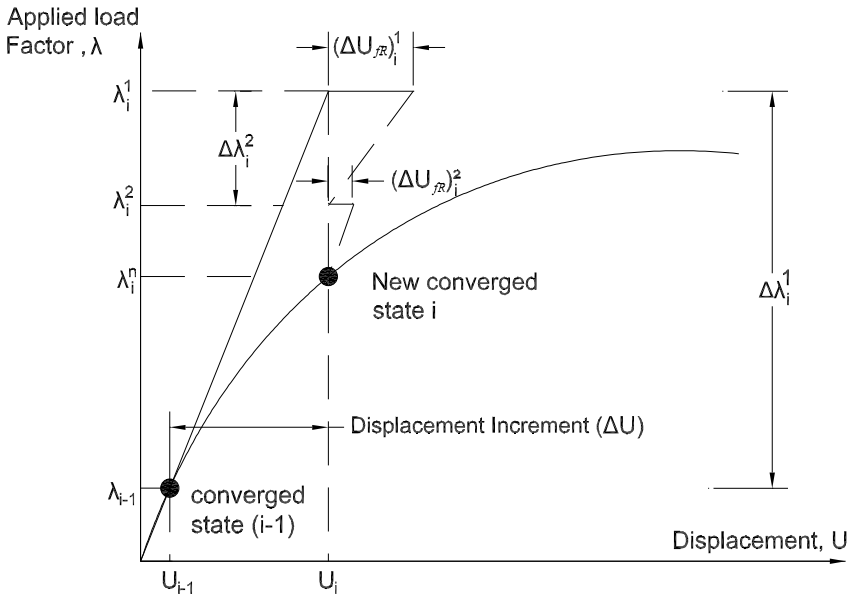

Figure 3.1: Displacement control method for single degree of freedom system.

forces that must be applied to the structure to keep the nodal displacements fixed due to changes in the parameter h. The vector $\partial\{\mathbf{P}_f\}_i^j/\partial h$ represents the derivative of the external forces (Eq. (3.2)) with respect to the parameter h.

$$\frac{\partial\{\mathbf{P}_f\}_i^j}{\partial h} = \frac{\partial\lambda_i^j}{\partial h}\{\mathbf{P}_{ref}\} + \lambda_i^j\frac{\partial\{\mathbf{P}_{ref}\}}{\partial h} \tag{3.18}$$

Combining Eq. (3.18) with Eq. (3.17) gives the following expression for the nodal displacement sensitivity

$$[\mathbf{K}_T]_i^j\frac{\partial\{\mathbf{U}_f\}_i^j}{\partial h} = \frac{\partial\lambda_i^j}{\partial h}\{\mathbf{P}_{ref}\} + \lambda_i^j\frac{\partial\{\mathbf{P}_{ref}\}}{\partial h} - \left.\frac{\partial\{\mathbf{P}_r\}_i^j}{\partial h}\right|_{\mathbf{U}_f} \tag{3.19}$$

where $\partial\{\mathbf{P}_{ref}\}/\partial h$ is the derivative of the reference load pattern with respect to h. After convergence of the top-level equilibrium iteration, this equation can be solved for each parameter in the structural model after assembling the right-hand side sensitivity vector. While the conditional derivative of the resisting forces is assembled from element contributions using standard finite element techniques, the sensitivity of the load factor, $\partial\lambda_i^j/\partial h$, must be determined during equilibrium iteration within the time step, as shown in the following section.

3.4 Sensitivity Analysis of Displacement Control Method

Direct differentiation of the governing incremental-iterative equations [13] must be carried out in order to find the sensitivity of the load factor, $\partial\lambda_i^j/\partial h$, in Eq. (3.19). Similar to the displacement-controlled response, the sensitivity separates the first iteration in a time step from the subsequent iterations.

To make the proposed derivations applicable to all element types and all system of equations, the tangent stiffness is considered constant ($\partial[\mathbf{K}_T]_i^j/\partial h = \mathbf{0}$). Due to this assumption, the derivative of the load factor will be handled via the derivative of the residual displacement vector ($\partial\{\Delta\mathbf{U}_{fR}\}_i^j/\partial h$) in subsequent iterations. An example to verify the redundancy of the derivative of the tangent stiffness is provided in the appendix.

3.4.1 First Iteration

The sensitivity of the tangent displacements, $\mathbf{U}_{fT}$, with respect to a parameter, h, at the first iteration is found using a differential form of Eq. (3.3)

$$\frac{\partial\{\mathbf{U}_{fT}\}_i^1}{\partial h} = \left([\mathbf{K}_T]_i^0\right)^{-1} \frac{\partial\{\mathbf{P}_{ref}\}}{\partial h} \tag{3.20}$$

With the sensitivity of the tangent displacement vector, the sensitivity of the initial load increment factor, $\partial\Delta\lambda_i^1/\partial h$, can be calculated by differentiating Eq. (3.4) with respect to h

$$\frac{\partial\Delta\lambda_i^1}{\partial h} = -\frac{\Delta U_c \left(\{\mathbf{g}\}^T \frac{\partial\{\mathbf{U}_{fT}\}_i^1}{\partial h}\right)}{\left(\{\mathbf{g}\}^T\{\mathbf{U}_{fT}\}_i^1\right)^2} \tag{3.21}$$

where it is noted that the analyst-specified displacement increment, ΔU_c, is constant and does not depend on any parameter. The sensitivity of the load factor is then updated with the sensitivity of the load factor increment

$$\frac{\partial\lambda_i^1}{\partial h} = \frac{\partial\lambda_{i-1}}{\partial h} + \frac{\partial\Delta\lambda_i^1}{\partial h} \tag{3.22}$$

Computations for the sensitivity of the load factor with respect to h at subsequent iterations are shown next.

3.4.2 Subsequent Iterations

The sensitivity of the tangent displacements computed at subsequent iterations can be obtained from a differential form of Eq. (3.14)

$$\frac{\partial\{\mathbf{U}_{fT}\}_i^j}{\partial h} = \left([\mathbf{K}_T]_i^{j-1}\right)^{-1} \frac{\partial\{\mathbf{P}_{ref}\}}{\partial h} \tag{3.23}$$

Recognizing that the residual force vector, $\{\mathbf{R}_f\}_i^{j-1}$, goes to zero as the equilibrium iteration converges, the derivative of the residual displacements with respect to h is obtained using a differential form of Eq. (3.13)

$$\frac{\partial\{\Delta\mathbf{U}_{fR}\}_i^j}{\partial h} = \left([\mathbf{K}_T]_i^{j-1}\right)^{-1} \frac{\partial\{\mathbf{R}_f\}_i^{j-1}}{\partial h} \tag{3.24}$$

The sensitivity of the residual forces on the right-hand side of Eq. (3.24) is evaluated by differentiating Eq. (3.11) with respect to parameter h

$$\frac{\partial\{\mathbf{R}_f\}_i^{j-1}}{\partial h} = \frac{\partial\lambda_i^{j-1}}{\partial h}\{\mathbf{P}_{ref}\} + \lambda_i^{j-1}\frac{\partial\{\mathbf{P}_{ref}\}}{\partial h} - \left.\frac{\partial\{\mathbf{P}_r\}_i^{j-1}}{\partial h}\right|_{\mathbf{U}_f} \tag{3.25}$$

where the first two terms on the right-hand side of Eq. (3.25) are obtained from the differentiation of the external forces in Eq. (3.2). The last term on the right-hand side of Eq. (3.25) is the conditional derivative of the resisting force vector.

Then, the sensitivity of the incremental load factor can be evaluated by differ-

entiating Eq. (3.15) with respect to h

$$\frac{\partial \Delta\lambda_i^j}{\partial h} = \frac{\left(\{\mathbf{g}\}^T\{\mathbf{U}_{fT}\}_i^j\right)\left(-\{\mathbf{g}\}^T\frac{\partial\{\Delta\mathbf{U}_{fR}\}_i^j}{\partial h}\right) + \left(\{\mathbf{g}\}^T\{\Delta\mathbf{U}_{fR}\}_i^j\right)\left(\{\mathbf{g}\}^T\frac{\partial\{\mathbf{U}_{fT}\}_i^j}{\partial h}\right)}{\left(\{\mathbf{g}\}^T\{\mathbf{U}_{fT}\}_i^j\right)^2} \tag{3.26}$$

where the vector $\mathbf{g}$ selects derivatives from the tangent displacement vector $\partial\{\mathbf{U}_{fT}\}_i^j/\partial h$ and the residual displacement vector $\partial\{\Delta\mathbf{U}_{fR}\}_i^j/\partial h$, defined in Eqs. (3.23) and (3.24)and, respectively. The sensitivity of the total load factor is then updated according to the derivative of Eq. (3.9)

$$\frac{\partial \lambda_i^j}{\partial h} = \frac{\partial \lambda_i^{j-1}}{\partial h} + \frac{\partial \Delta\lambda_i^j}{\partial h} \tag{3.27}$$

After equilibrium is achieved at the end of the time step, the sensitivity of the load factor can be used to determine the applied load sensitivity, $\partial\mathbf{P}_f/\partial h$, and the nodal response sensitivity, $\partial\mathbf{U}_f/\partial h$, according to Eqs. (3.18) and (3.19), respectively. After all sensitivity calculations for the current time step are complete, uncertainties can be quantified and gradient-based computations can be made, then the simulation advances to the next time step, according to the process depicted in Fig. 3.2.

3.5 Numerical Examples

The foregoing response sensitivity equations for the displacement control method have been implemented in the OpenSees finite element software framework [43, 61]. To verify the equations and their implementation, standalone sensitivity analyses

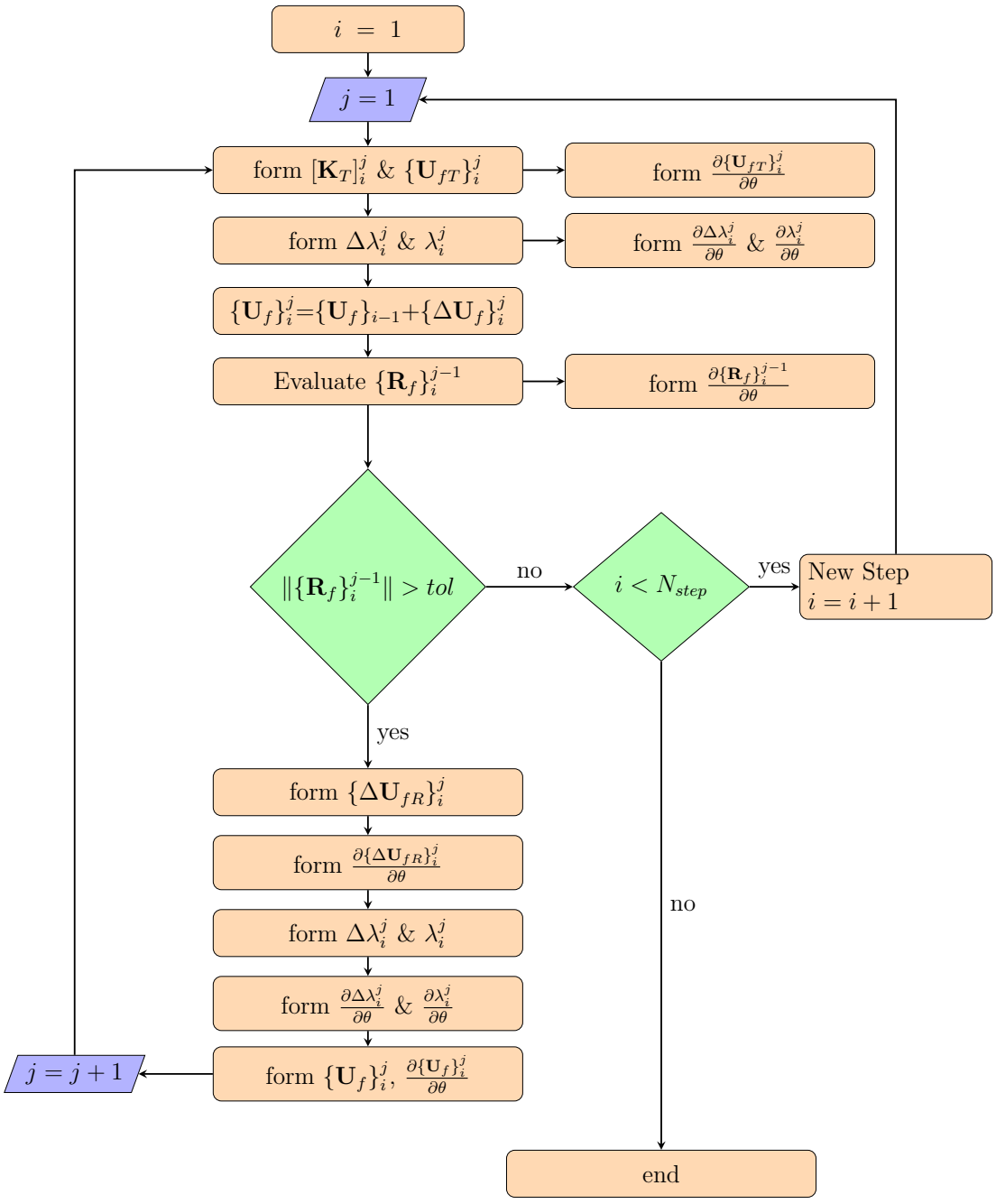

Figure 3.2: Computations for load factor and its sensitivity in the displacement control method.

are performed in the first two examples, one with geometric and one with material nonlinearity. The last example shows the reliability analysis of a multistory steel frame where the performance function is defined in terms of the frame's lateral load resistance.

3.5.1 Shallow Truss

An analysis is performed for the shallow truss shown in Fig. 3.3, which is a common benchmark example for geometric nonlinearity. Four elastic beam-column elements in a corotational mesh [18] are used for each member. Each element has elastic modulus E=200,000 MPa, cross-section area A=0.1 m^2, and second moment of cross-section area, I=0.002 m^4.

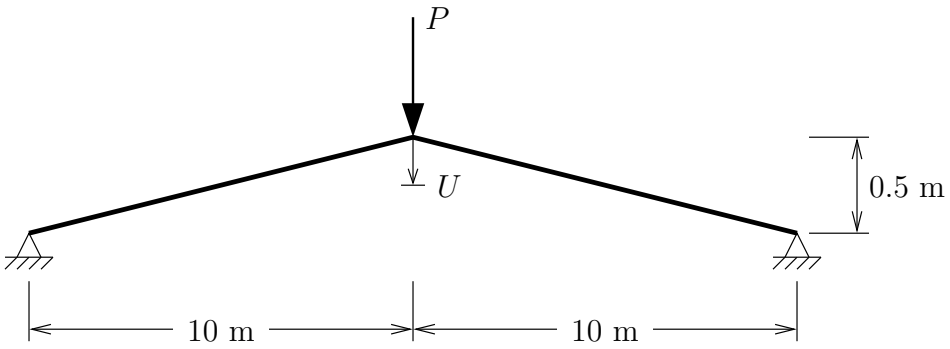

Figure 3.3: Shallow truss subjected to midspan load.

The midspan load-displacement response is shown in Fig. 3.4 using both the load and displacement control methods. As expected, the load controlled solution is not able to capture the snap through behavior, but is able to capture the tension stiffening response that ensues. On the other hand, the displacement controlled

solution (using ΔU_c=0.01 m for the midspan vertical displacement) is able to capture the entire range of snap through and tension stiffening response.

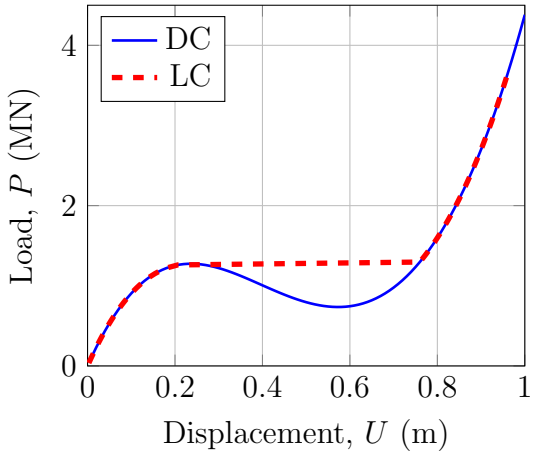

Figure 3.4: Load-displacement relationship using displacement and load control methods.

To verify the DDM equations and implementation for the displacement control method, the sensitivity is computed at each time step and compared with FDM computations. According to the finite difference approximation, the FDM results should converge to the DDM for decreasing parameter perturbations, i.e.,

$$\lim_{\Delta\theta\to 0} \frac{\lambda(\theta+\Delta\theta)-\lambda(\theta)}{\Delta\theta} = \frac{\partial\lambda}{\partial h} \tag{3.28}$$

where a forward finite difference is used. For small finite difference perturbations, similarity of FDM and DDM results implies that the DDM computations are correct.

A comparison of DDM and FDM load factor sensitivity with respect to the section area, A, and second moment of area, I, of the shallows truss is shown in

Fig. 3.5. The DDM results are compared to a finite difference perturbation of 0.001 times the nominal parameter values, which is sufficiently small to satisfy Eq. (3.28). In each plot, the sensitivities are scaled by the nominal parameter value so that they have the same units as the response. As shown in Fig. 3.5 (a), the section area initially acts as a resistance variable ($\partial\lambda/\partial h > 0$), where increasing this parameter will lead to an increase in the load required to reach the same displacement. The section area then acts as a load variable ($\partial\lambda/\partial h < 0$) as the truss snaps through to a stable equilibrium solution. As the truss response continues to stiffen in tension, the section area returns to its role as a resistance variable. The second moment of section area, I, acts as a resistance variable throughout the entire load path, as shown in Fig. 3.5 (b).

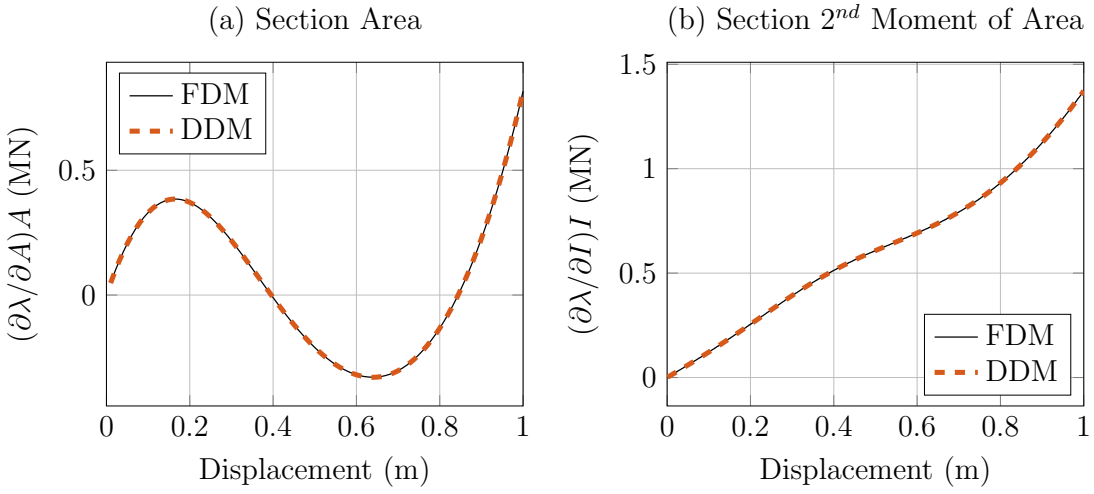

Figure 3.5: Response sensitivity of load factor with respect to shallow truss cross-section properties: (a) section area, A; (b) second moment of section area, I.

The sensitivity of the applied load with respect to X and Y coordinates of the midspan node is shown in Fig. 3.6. The X coordinate is a load variable where

increasing the horizontal coordinate of the midspan node (making the truss more shallow) leads to a reduction in the load required to follow the load-displacement path. In contrast, increases in the Y coordinate of the midspan node (making the truss more steep) make this parameter a resistance variable where the load required to follow the snap through path must increase. However, as the truss enters tension stiffening response, the Y coordinate switches to a load variable.

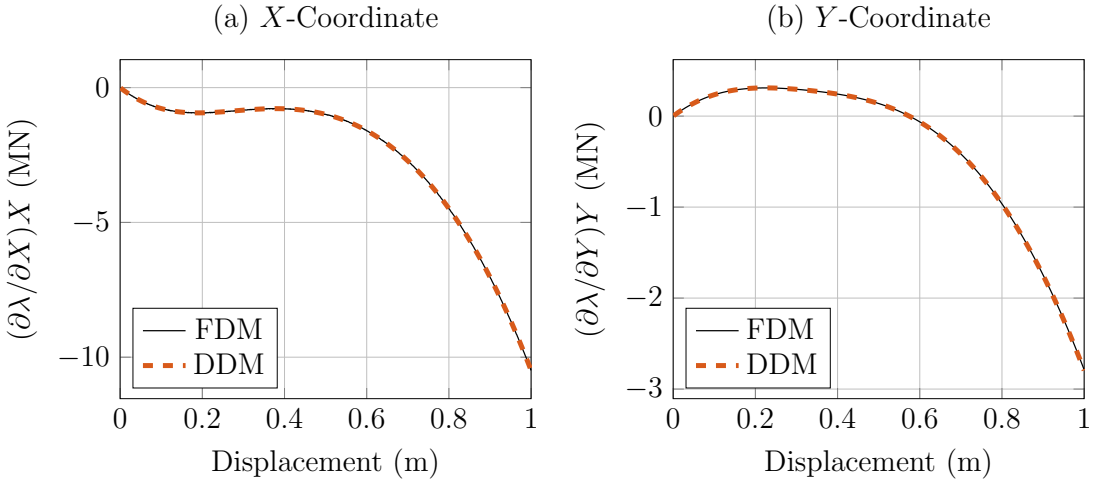

Figure 3.6: Response sensitivity of load factor with respect to nodal coordinates at apex of shallow truss: (a) horizontal X-coordinate; (b) vertical Y-coordinate.

3.5.2 Reinforced Concrete Bridge Pier

A reinforced concrete bridge pier, specimen 7 in the tests of [67] is used in this example. The geometry and reinforcement details of the bridge pier are shown in Fig. 3.7. Due to confinement, the concrete compressive strength is f'_c=39 MPa, and the peak compressive strain is ε_c=0.0052. In addition, the residual concrete

compressive strength is f_{cu}=11.7 MPa, and the corresponding strain ε_u=0.0248. A bilinear stress-strain relationship is assumed for the steel reinforcement with yield stress, f_y= 510 MPa, elastic modulus, E=200,000 MPa, and 1% strain hardening ratio.

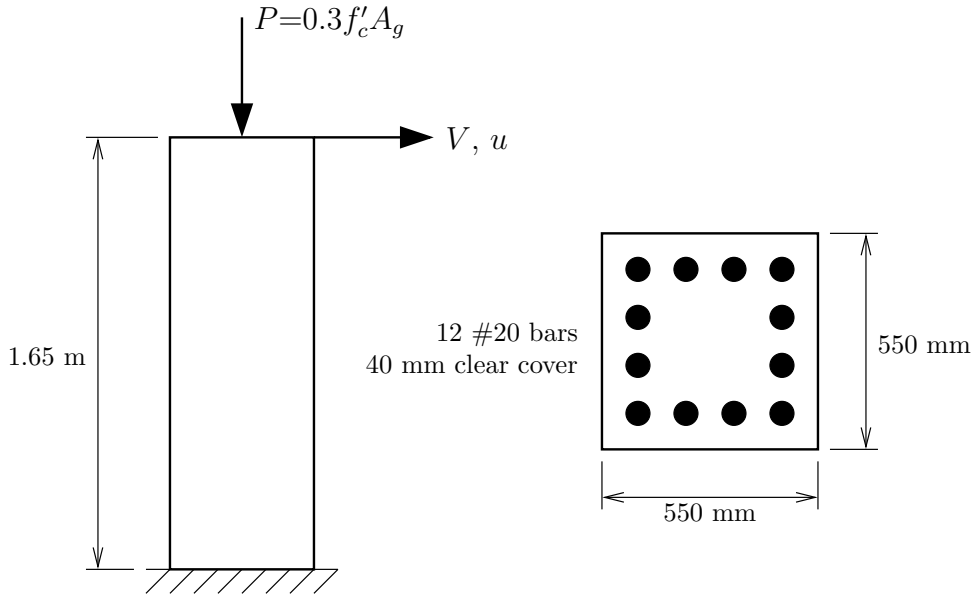

Figure 3.7: Reinforced concrete bridge pier configuration, reinforcement details, and material properties.

One force-based beam column element [47] with four Gauss-Lobatto integration points is used to simulate the bridge pier response. A fiber discretization of the cross section accounts for the effect of axial-moment interaction based on the prescribed stress-strain relationships for the concrete and reinforcing steel. A constant gravity load equal to 30% of the gross section capacity is applied to the bridge pier. The base shear-lateral displacement response computed using the displacement control method is shown in Fig. 3.8 where the pier reaches its peak lateral

load resistance at a displacement of approximately 1.3 cm. After this displacement, the pier forms a plastic hinge and loses load carrying capacity.

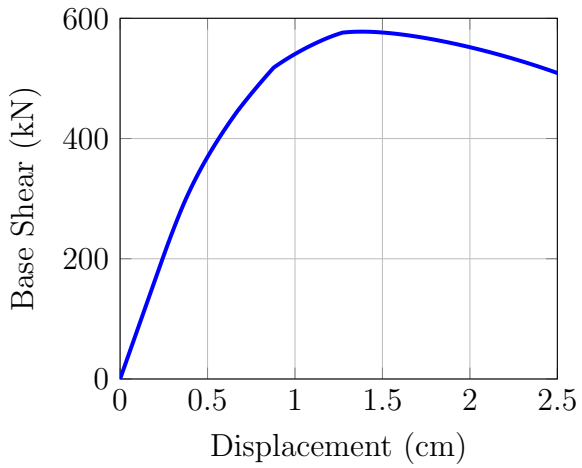

Figure 3.8: Base shear-lateral displacement relationship for reinforced concrete bridge pier.

The sensitivity of the base shear computed with respect to the section strength parameters of concrete, f'_c, and reinforcing steel, f_y, is shown in Fig. 3.9. As in the first example, the sensitivities are multiplied by the nominal parameter value in order to achieve consistent units. In addition to verifying that the DDM implementation is correct by comparisons with finite difference computations using $\Delta\theta = 0.001$ times the nominal parameter value, Fig. 3.9 shows that both f'_c and f_y are resistance variables where increasing their values leads to an increase in the load required to reach the same lateral displacement. The discrete jumps observed in Fig. 3.9 (b) occur when the steel reinforcing bars yield, i.e., the parameter f_y becomes active in the DDM computations. The final jump occurs when the plastic hinge forms at 1.3 cm lateral displacement, where the response sensitivity

is roughly equal with respect to both the concrete and steel strength. However, at the final lateral displacement of 2.5 cm, the sensitivity with respect to f_c' is higher than that for f_y. These results confirm engineering judgment that both the concrete and steel strength affect the peak load capacity of the pier while the concrete strength plays a more important role on the residual capacity.

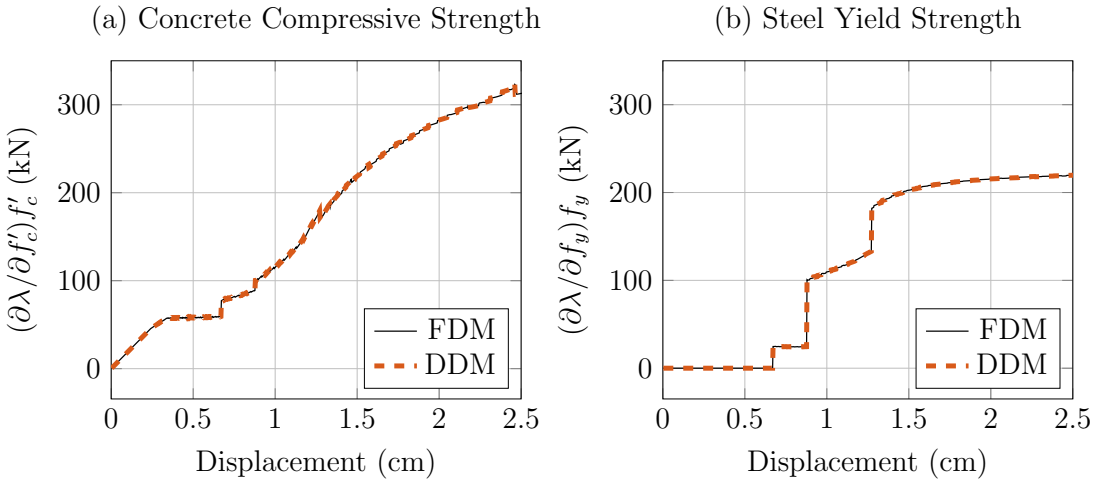

Figure 3.9: Response sensitivity of load factor with respect to section strength parameters: (a) concrete compressive strength, f_c'; (b) steel yield strength, f_y.

The base shear sensitivity for two post-yield constitutive properties: the concrete residual strength, f_{cu}, and the steel hardening modulus, H_{kin}, is shown in Fig. 3.10. The displacements at which the response sensitivities become non-zero indicate where these parameters become active, with the steel yielding prior to the concrete core reaching its peak compressive strength. Compared to the section strength parameters in Fig. 3.9, neither of the post-yield parameters has a significant influence on the load resistance of the bridge pier.

The response sensitivity of the base shear with respect to geometric parameters

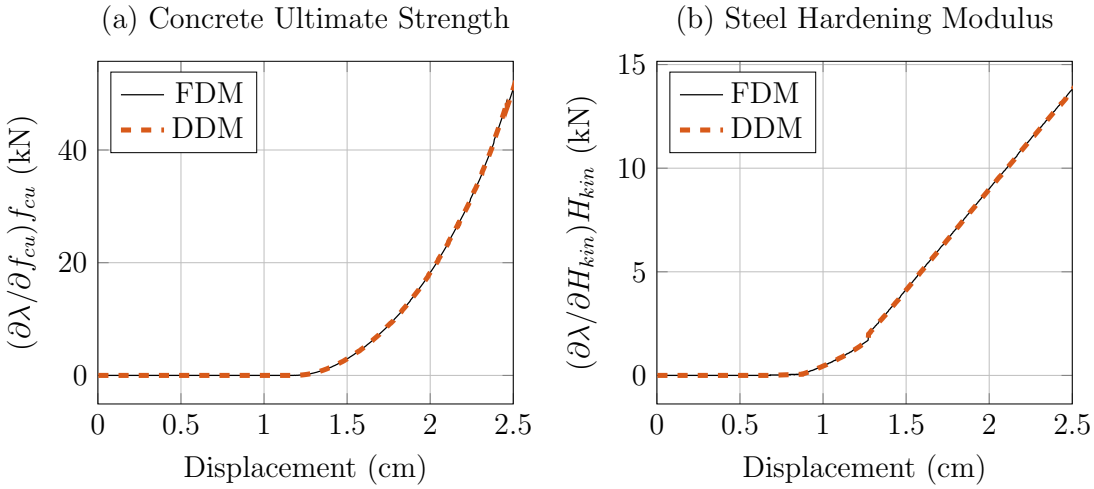

Figure 3.10: Response sensitivity of load factor with respect to section post-yield constitutive parameters: (a) concrete ultimate strength, f_{cu}; (b) steel hardening modulus.

of bridge pier length, L, and cross-section depth, d, is shown in Fig. 3.11. The results shown in Fig. 3.11 (a) indicate an increase in the bridge pier length will result in a reduction of the lateral load carrying capacity, i.e., the pier length is a load variable. Conversely, Fig. 3.11 (b) shows that the section depth, d, is a resistance variable. Both the length and the section depth have a large influence on the lateral load carrying capacity of the bridge pier. As the pier reaches its peak load capacity at 1.3 cm displacement and forms a plastic hinge, the response sensitivity with respect to length reduces. On the other hand, the sensitivity with respect to the section depth remains approximately unchanged in its contribution to the post-peak residual capacity of the bridge pier after the plastic hinge forms.

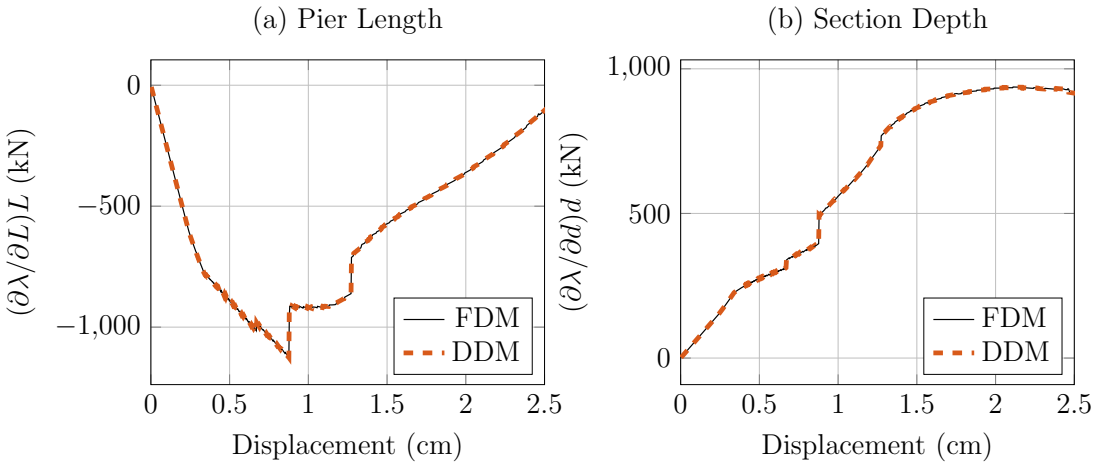

Figure 3.11: Response sensitivity of load factor with respect to geometric properties of the bridge pier: (a) pier length, L; (b) cross-section depth, d.

3.5.3 Reliability Analysis of Steel Frame

In addition to computing the sensitivity of load resistance to uncertain modeling parameters, this example shows how computations of load factor sensitivity can be used for reliability analyses of structural systems whose performance is defined by load capacity. The model shown in Fig. 3.12 is based on the exterior moment resisting frame of a "Pre-Northridge" Los Angeles SAC steel building [24]. All members are wide flange sections with the shapes indicated in the figure for the floor girders (A36 steel) and the interior and exterior columns (A572 Gr. 50 steel). The floor dead load is 4.6 kPa while the (reduced) live load is 0.96 kPa. The tributary width for the floor loads is 4.6 m.

A single force-based beam-column element [47] simulates the response of each member. Four Gauss-Lobatto integration points are used in each element where

a fiber model represents the section force-deformation relationship. A uniaxial, bilinear constitutive relationship is assumed for each steel fiber with E=200,000 MPa and strain-hardening ratio 0.02. There are five fibers in each flange and 25 fibers in the web at each element integration point. The vertical distribution of lateral loads shown in Fig. 3.12 is based on the first mode effective earthquake forces.

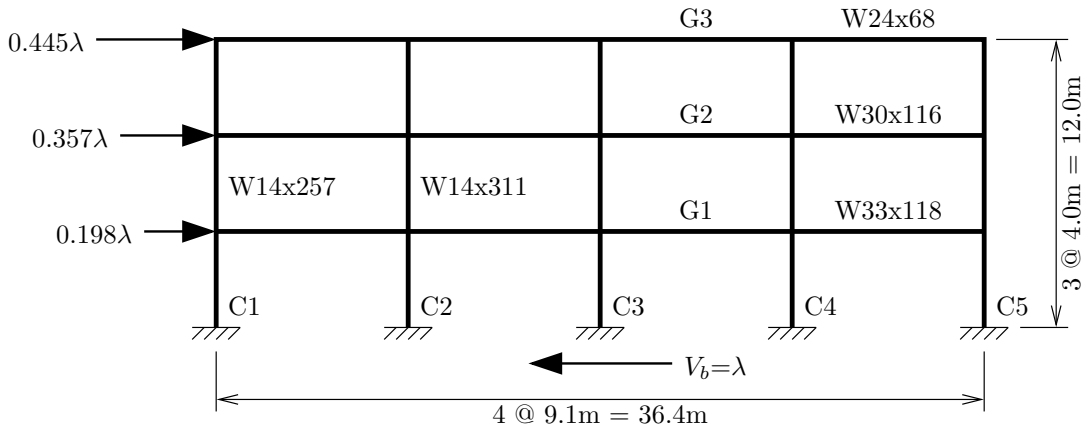

Figure 3.12: Steel moment frame for reliability example.

All material and geometric parameters are considered uncertain. The elastic modulus E of each member is a lognormal random variable with mean value 200,000 MPa, coefficient of variation (cov) 5%, and correlation coefficient 0.6 with the elastic modulus of the other members. The yield strength f_y of each member is a lognormal random variable with mean value 300 MPa, 10% cov, and correlation coefficient 0.6 with f_y of the other members. The strain hardening ratio α of each member is a lognormal random variable with mean 0.02, 10% cov, and correlation coefficient 0.6 with α of the other members. The cross-section dimensions of each

member are modeled as uncorrelated normal random variables with mean values based on the nominal wide-flange dimensions and 2% cov. The gravity and lateral loads are considered deterministic.

A nonlinear static pushover analysis is performed on the frame with the mean realization of all random variables. The lateral response of the frame shown in Fig. 3.13 reaches a base shear of 6000 kN at a lateral roof displacement of 0.49 m. Two first order reliability method (FORM) analyses are carried out based on this ultimate mean response. The first performance function seeks the probability that the lateral roof displacement exceeds 0.7 m when the peak load level is reached

$$g_1 = 0.7 - U_{roof} \text{ (m)} \tag{3.29}$$

where U_{roof} is the horizontal displacement of the roof. This performance function requires a load-controlled pushover analysis and FORM analysis reveals a reliability index of β=1.53, which corresponds to an 6.3% probability of the roof exceeding the prescribed displacement. The load-displacement response at the design point is shown in Fig. 3.13 and the ranking of the 20 most important random variables is shown in Table 3.1 (a) using the measures proposed by [30].

The second performance function seeks the probability that the frame's load carrying capacity is less than 5500 kN when the peak lateral displacement is reached

$$g_2 = V_b - 5500 \text{ (kN)} \tag{3.30}$$

where V_b is the base shear. A displacement-controlled analysis is required in order

to evaluate this performance function. Based on FORM analysis, the reliability index for this performance function is β=3.32, indicating a 0.044% probability that the lateral load resistance of the frame will be less than 5500 kN at the peak roof displacement. The load-displacement response corresponding to the realization of the random variables at the design point is shown in Fig. 3.13. The 20 most important random variables are shown in Table 3.1 (b). Similar to the first performance function, the yield strength and depth of the girders have the largest influence on failure of the frame for this limit state. Although the two performance functions were not defined to give similar levels of safety, the importance rankings resulting from the respective FORM analyses are virtually the same. The first performance function leads to a higher probability of failure (lower reliability index) because, compared to reducing the base shear, it is relatively easy to increase the roof displacement after the frame has yielded and the member stiffnesses have reduced.

3.6 Conclusion

Response sensitivity equations were derived for the displacement control method by applying the direct differentiation method (DDM) to the incremental-iterative equations developed by [13]. The derived equations were implemented in the finite element software framework OpenSees, and the equations were verified by comparing the DDM equations with the finite difference computations through stand-alone sensitivity analysis of structural models with geometric and material

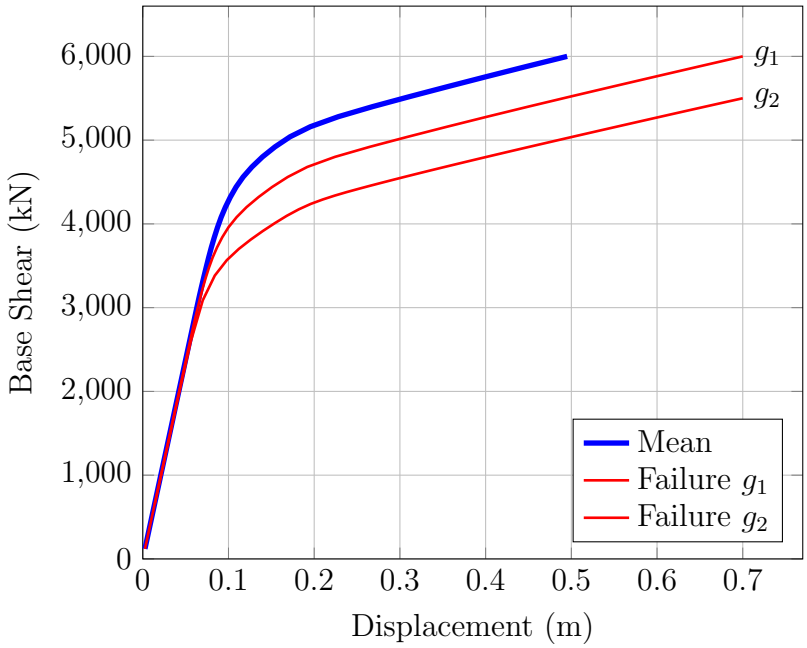

Figure 3.13: Load-displacement response at the mean and failure realizations of the random variables for the steel moment-resisting frame.

nonlinearity. Probabilistic analyses of a multistory steel frame using the first order reliability method give the reliability index, probability of failure, and importance measures for displacement-controlled analyses. Future work will extend DDM sensitivity analysis to other continuation methods such as the arc-length and minimum unbalanced displacement norm approaches [13].

Acknowledgments

This research was made possible through the support of the Higher Committee for Education Development (HCED) in Iraq. Any opinions, findings, and conclusions

Table 3.1: Ranking of the 20 most important parameters in the steel frame example using performance functions based on load and displacement control methods.

(a) Load Control, g_1

Member	**Property**	**Importance**
G2	f_y	-0.5449
G1	f_y	-0.5345
G3	f_y	-0.4145
G1	d	-0.2612
G2	d	-0.25
C2	f_y	-0.1395
C3	f_y	-0.139
C4	f_y	-0.1374
G3	d	-0.1155
C1	f_y	-0.1127
C5	f_y	-0.1115
C2	d	-0.06377
C3	d	-0.06274
C4	d	-0.0616
C1	d	-0.05177
C5	d	-0.0459
G2	E	-0.02502
G1	E	-0.02373
G3	E	-0.01365
C2	E	-0.01227

(b) Displacement Control, g_2

Member	**Property**	**Importance**
G2	f_y	-0.5405
G1	f_y	-0.5149
G3	f_y	-0.4249
G1	d	-0.2675
G2	d	-0.2571
C2	f_y	-0.1456
C3	f_y	-0.1451
C4	f_y	-0.1435
G3	d	-0.1187
C1	f_y	-0.1179
C5	f_y	-0.1167
C2	d	-0.06768
C3	d	-0.06634
C4	d	-0.06507
C1	d	-0.05608
C5	d	-0.04891
G2	E	-0.01964
G1	E	-0.01783
C1	E	-0.01253
C2	E	-0.01177

or recommendations expressed in this material are those of the authors and do not necessarily reflect the views of the HCED.

4 Corotational Post-Buckling Sensitivity Analysis of Space Frame Structures

Accurate and efficient response sensitivity computations for nonlinear geometry are required in structural reliability, optimization, and system identification. The response sensitivity equations using direct differentiation method (DDM) have been formulated for material nonlinear analysis. For geometric nonlinear analysis, the DDM has been developed only for two dimensional simulations. The proposed research develops DDM sensitivity for the corotational formulation of space frame elements. The main problem in the corotational formulation of space frame elements is that the finite rotations are not true vector quantities and the structural response depends on the order in which rotations are applied and hence complex algorithm, presented by Crisfield [19], is used to create a local system that is invariant with respect to the definition of the local axes . The response sensitivity equations are obtained for corotational formulation of space frame elements and implemented in OpenSees software framework. To verify the accuracy of the derived sensitivity equations, standalone sensitivity analysis is used by comparing the proposed DDM with finite difference method (FDM) for simple and complex structures. Future applications that require the present formulation are: structural reliability and optimization of three dimensional structures undergoing large displacements.

4.1 Introduction

Response sensitivity analysis measures the change in structural response due to changes in system properties [35]. Sensitivity analysis helps to identify the most important parameters that affect structural response for different limit states. The most common applications that require sensitivity gradients, which are the results of the sensitivity analysis, are optimization, system identification, and reliability analysis. For instance, sensitivity analysis can be used to minimize the structural cost, and it also helps to minimize the difference between the measured and numerical response for system identification purposes [3].

Different methods are available to perform sensitivity analysis such as the finite difference method (FDM), the complex perturbation method (CPM), the adjoint system method (ASM), and the direct differentiation method (DDM). The FDM requires rerunning the structural analysis with perturbed parameter values to estimate the response sensitivity. As a result, it is computationally intensive. Furthermore, the accuracy of the FDM depends on the perturbation value. For instance, too small perturbation value leads to round-off errors, while too large perturbation value leads to inaccurate response sensitivity results. The ASM, which is based on Lagrangian multipliers, is more accurate than FDM especially for linear analysis. However, ASM is not recommended for path dependent problems [35]. In the CPM, all sensitivity parameters and response quantities in a finite element analysis are represented using complex numbers and all finite element computations are carried out using complex algebra. By performing structural analysis using CPM,

the real component of the complex response represents the structural response and the imaginary component of the complex response represents the response sensitivity. In spite of giving very accurate response sensitivity results, CPM requires full re-analysis for each parameter in the finite element model and hence it is computationally intensive. The DDM is an attractive alternative to FDM. In the DDM, the analytical response sensitivity equations are derived and implemented within the finite element response algorithm. The DDM computes sensitivity gradients using the same solver as the ordinary response while the simulation proceeds rather than by complete re-analysis for each parameter. Many researchers have contributed to the development of sensitivity analysis such as [53, 31, 57, 53, 36, 5, 27, 62, 34].

Geometric nonlinear behavior can be captured using either a total Lagrangian, an updated Lagrangian or a corotational formulations. The difference between the aforementioned formulations is in the reference configuration system that describes the motion of the body. For instance, in the total Lagrangian formulation, the structural deformations are calculated based on the undeformed element configuration. In the updated Lagrangian formulation, The structural deformations are calculated based on the last deformed element configuration. The corotational formulation removes the rigid-body mode which allows to separate material nonlinearity due to large deformation inside the basic system from geometric nonlinearity due to large displacement outside the basic system. Many studies have shown the advantage of using the corotational formulation over the Lagrangian formulations such as [68] and [71].

For two and three dimensional linear transformations, the implementation of

response gradients is straightforward. Under the rigid body mode assumption, the local-global coordinate transformation is linear and the local-basic coordinate transformation is based on the undeformed configuration. In the 2D corotational system, an exact transformation of displacements and forces can be obtained in two steps (basic to local and local to global). However, the transformation for 3D frame elements is more complex than that for 2D elements. This is because finite rotations in three dimensional space elements do not comply with the rules of vector operations, non-vectorial nature, and the results depend on the order in which the rotations are applied. To overcome the problem of violating vector properties, Crisfield algorithm [19] is used to obtain the triads of the deformed configuration of the space frame element.

The objective of this paper is to derive the response sensitivity equations for 3D space frame element using DDM. The derivation requires following Crisfield algorithm [19] to obtain the element triads and their sensitivities in the deformed configuration. The derived equations are implemented in the OpenSees finite element framework software and verified through a set of standalone sensitivity analyses for simple and complex structures.

4.2 Global and Basic Coordinate Systems

For three-dimensional frame elements, there are 12 nodal degrees of freedom (six DOFs at each connected node, I and J) as shown in Fig. 4.1. For notational

convenience, the global DOFs are grouped as

$$\mathbf{u}^T = \begin{bmatrix} \mathbf{u}_I^T & \boldsymbol{\gamma}_I^T & \mathbf{u}_J^T & \boldsymbol{\gamma}_J^T \end{bmatrix} \tag{4.1}$$

where $\mathbf{u}_I$ and $\mathbf{u}_J$ are the global translational displacement components while $\boldsymbol{\gamma}_I$ and $\boldsymbol{\gamma}_J$ represent the global rotations at each end of the element.

$$\mathbf{u}_I = \begin{bmatrix} u_1 \\ u_2 \\ u_3 \end{bmatrix} \qquad \boldsymbol{\gamma}_I = \begin{bmatrix} u_4 \\ u_5 \\ u_6 \end{bmatrix} \tag{4.2}$$

$$\mathbf{u}_J = \begin{bmatrix} u_7 \\ u_8 \\ u_9 \end{bmatrix} \qquad \boldsymbol{\gamma}_J = \begin{bmatrix} u_{10} \\ u_{11} \\ u_{12} \end{bmatrix} \tag{4.3}$$

With the corotational formulation, it is necessary to remove the rigid body displacement modes from the element displacement field. For frame elements in three dimensions, there are six rigid body displacement modes and six deformation modes. This leads to the six basic DOFs shown in Fig. 4.1 that describe the deformation of the element

$$\mathbf{u}_b = \begin{bmatrix} u_{b1} \\ u_{b2} \\ u_{b3} \\ u_{b4} \\ u_{b5} \\ u_{b6} \end{bmatrix} = \begin{bmatrix} L_d - L \\ \theta_{I3} \\ \theta_{J3} \\ -\theta_{I2} \\ -\theta_{J2} \\ \theta_{J1} - \theta_{I1} \end{bmatrix} \tag{4.4}$$

where u_{b1} is the change in length of the element (the difference between the deformed length, L_d, and the original length, L) and u_{b6} is the torsional deformation. Basic DOFs u_{b2} through u_{b5} represent the flexural deformations of the element. The nodal rotations, θ_{I1} through θ_{J3}, are measured about the local element axes. The non-vectorial nature of these rotations in three dimensions makes the transformation of displacements and forces between the global and basic systems complicated. As a result, an approximate algorithm is required to describe the rotation of a space frame element in the deformed configuration.

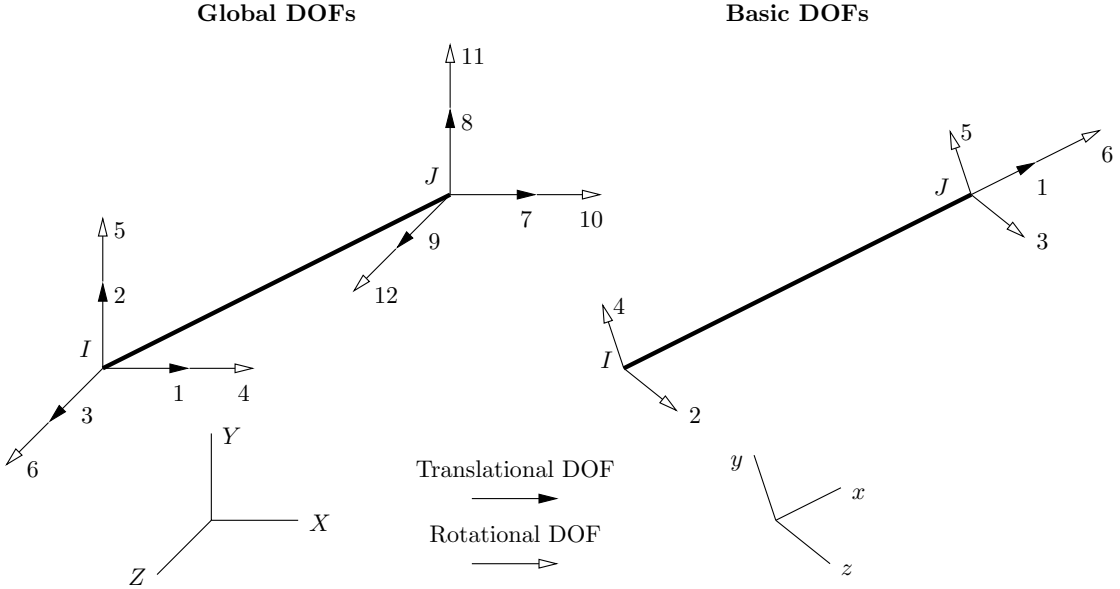

Figure 4.1: Force and displacement degrees of freedom of global and basic coordinate systems of space frame (3D) element.

4.3 Rotation Matrix for Large Rotations-Rodrigues Formula

The vector $\mathbf{V}_0$ shown in Fig. 4.2 describes the position of a point P_0 with respect to a fixed reference system (X, Y, Z). To describe the transition of point P_0 to a new position Q, the vector $\mathbf{V}_0$ has to be rotated to describe the new position. To do so, Rodrigues formula, which describes the rotation of a vector in space, can be used. The derivation of Rodrigues rotation formula was presented by many researchers such as [4], [18], [20], and [23]. The formula describes rotation of a vector $\mathbf{V}_0$ about a unit vector $\mathbf{t}$ by an angle θ to a new vector $\mathbf{V}_1$ as shown in Fig. 4.2

$$\mathbf{V}_1 = \mathbf{R}(\boldsymbol{\theta}_1)\mathbf{V}_0 \tag{4.5}$$

where $\boldsymbol{\theta}_1$ is the pseudo rotation vector with magnitude equal to the rotation angle θ about an axis of rotation described by the unit vector $\mathbf{t}$.

$$\boldsymbol{\theta} = \begin{bmatrix} \theta_1 & \theta_2 & \theta_3 \end{bmatrix}^T = \theta\mathbf{t} \tag{4.6}$$

where the rotation angle θ is

$$\theta = \|\boldsymbol{\theta}\| = \sqrt{\theta_1^2 + \theta_2^2 + \theta_3^2} \tag{4.7}$$

The vector $\boldsymbol{\theta}$ that describes the angle of rotation is called the "pseudo rotation vector" because it violates the properties of vector addition (non-vectorial nature).

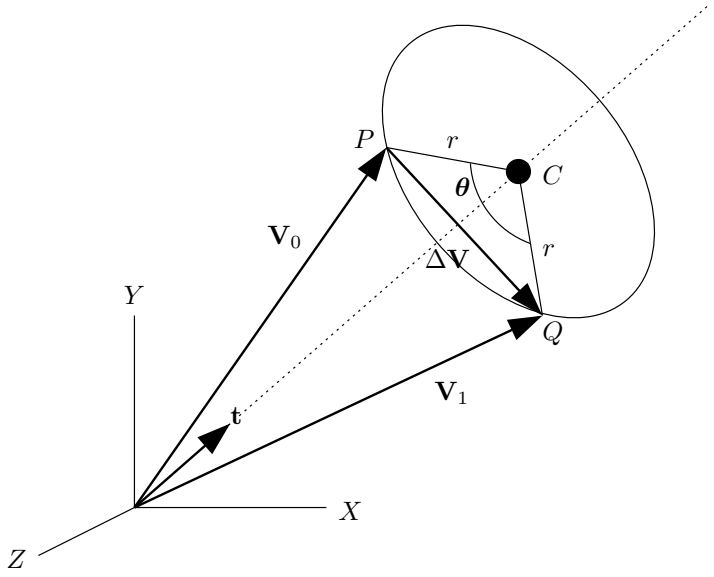

Figure 4.2: Rotation of a vector in space.

The rotation matrix $\mathbf{R}(\boldsymbol{\theta})$ can be obtained using Rodrigues formula [19]

$$\mathbf{R}(\boldsymbol{\theta}) = \mathbf{I} + \frac{\sin(\theta)}{\theta}\mathbf{S}(\boldsymbol{\theta}) + \frac{(1-\cos(\theta))}{\theta^2}\mathbf{S}(\boldsymbol{\theta}) \tag{4.8}$$

An alternative expression for the rotation matrix $\mathbf{R}(\boldsymbol{\theta})$ can be obtained using the tangent scaled pseudo vector $\boldsymbol{\omega}$ instead of $\boldsymbol{\theta}$, where $\boldsymbol{\omega}$ is defined in terms of $\boldsymbol{\theta}$, about the same unit vector $\mathbf{t}$, as

$$\boldsymbol{\omega} = w\mathbf{t} = 2\tan(\theta/2)\mathbf{t} = 2\frac{\tan(\theta/2)}{\theta}\boldsymbol{\theta} \tag{4.9}$$

Substituting Eq. (4.9) in to Eq. (4.8) gives the rotation matrix $\mathbf{R}(\boldsymbol{\omega})$

$$\mathbf{R}(\boldsymbol{\omega}) = \mathbf{I} + \frac{1}{1+\frac{1}{4}\boldsymbol{\omega}^T\boldsymbol{\omega}}\left[\mathbf{S}(\boldsymbol{\omega}) + \frac{1}{2}\mathbf{S}(\boldsymbol{\omega})\mathbf{S}(\boldsymbol{\omega})\right] \tag{4.10}$$

where the spin tensor $\mathbf{S}(\boldsymbol{\omega})$ can be represented as a skew symmetric matrix that contains infinitesimal rotations about the orthogonal local axes

$$\mathbf{S}(\boldsymbol{\omega}) = \begin{bmatrix} 0 & -\omega_3 & \omega_2 \\ \omega_3 & 0 & -\omega_1 \\ -\omega_2 & \omega_1 & 0 \end{bmatrix} \tag{4.11}$$

It is noted that Eq. (4.10) is not applicable when θ equals 180^o and odd multiples thereof, in which case the tangent scaled pseudo vector, $\boldsymbol{\omega}$, becomes infinite and the rotation matrix $\mathbf{R}$ becomes singular. One approach to overcome this obstacle is to use the normalized unit quaternion [70, 65] instead of the pseudo rotation vector $\boldsymbol{\theta}$. The normalized quaternion vector consists of the quaternion scalar element, q_0, and a vector of three components. The vector components are represented by a sine-scaled pseudo vector in the same direction as the unit vector $\mathbf{t}$. The scalar component q_0 is represented by a cosine of pseudo rotation and is used to extract the pseudo rotation vector $\boldsymbol{\theta}$ out of the rotation matrix $\mathbf{R}(\boldsymbol{\omega})$. Note that the length of the quaternion vector is one, i.e., $\mathbf{q}^T\mathbf{q} = 1$.

$$\mathbf{q} = \begin{bmatrix} q_0 \\ q_1 \\ q_2 \\ q_3 \end{bmatrix} = \begin{bmatrix} \cos(\theta/2) \\ \sin(\theta/2)\mathbf{t} \end{bmatrix} \tag{4.12}$$

Using the half angle formulas for cosine and sine of the angle of rotation, θ.

$$\cos\theta = \cos^2\left(\frac{\theta}{2}\right) - \sin^2\left(\frac{\theta}{2}\right) = 1 - 2\sin^2\left(\frac{\theta}{2}\right) \tag{4.13}$$

$$\sin\theta = 2\cos\left(\frac{\theta}{2}\right)\sin\left(\frac{\theta}{2}\right) \tag{4.14}$$

substitution of Eq. (4.13) and Eq. (4.14) into Eq. (4.8) gives

$$\mathbf{R}(\boldsymbol{\theta}) = \mathbf{I} + 2\cos\left(\frac{\theta}{2}\right)\sin\left(\frac{\theta}{2}\right)\mathbf{S}(\mathbf{t}) + \left[1 - \cos^2\left(\frac{\theta}{2}\right) + \sin^2\left(\frac{\theta}{2}\right)\right]\mathbf{S}\left(\mathbf{t}\right)^2 \tag{4.15}$$

where $\mathbf{S}(\mathbf{t})^2$ is the square of the skew symmetric matrix which can be expressed as

$$\mathbf{S}(\mathbf{t})^2 = \mathbf{t}\mathbf{t}^T - \mathbf{I} \tag{4.16}$$

By substituting Eq. (4.16) in Eq. (4.15), the equation of the rotation matrix becomes

$$\mathbf{R}(\boldsymbol{\theta}) = \left[\cos^2\left(\frac{\theta}{2}\right) - \sin^2\left(\frac{\theta}{2}\right)\right]\mathbf{I} + 2\cos\left(\frac{\theta}{2}\right)\sin\left(\frac{\theta}{2}\right)\mathbf{S}(\mathbf{t}) + \left[2\sin^2\left(\frac{\theta}{2}\right)\right]\mathbf{t}\mathbf{t}^T \tag{4.17}$$

The final form of the rotation matrix $\mathbf{R}$ in terms of the normalized quaternion can be obtained by substituting Eq. (4.12) in to Eq. (4.17).

$$\mathbf{R}(\mathbf{q}) = 2\begin{bmatrix} q_0^2 + q_1^2 - \frac{1}{2} & q_1q_2 - q_0q_3 & q_1q_3 + q_0q_2 \\ q_2q_1 + q_0q_3 & q_0^2 + q_2^2 - \frac{1}{2} & q_2q_3 - q_1q_0 \\ q_3q_1 - q_0q_2 & q_3q_2 + q_0q_1 & q_0^2 + q_3^2 - \frac{1}{2} \end{bmatrix} \tag{4.18}$$

To extract the tangent-scaled pseudo vector $\boldsymbol{\omega}$ from the rotation matrix, the quaternion vector has to be extracted first. To this end, the Spurrier algorithm, which was introduced first by [37] and improved later by [66], is the most efficient al-

gorithm for extracting the normalized quaternion from the rotation matrix. Many researchers have shown the robustness of the Spurrier algorithm[49, 64, 17, 1, 20], which is based on using the square root operation to compute only the largest of the trace of $\mathbf{R}$ and the diagonal elements of $\mathbf{R}$. Then, only this largest component is used as a divisor in computing the other components of the quaternion as shown in Fig. 4.3 where i, j, k is the cyclic permutation of 1,2,3. After obtaining the normalized quaternion via the Spurrier algorithm, the tangent scaled pseudo vector, $\boldsymbol{\omega}$, can be obtained by combining Eq. (4.9) and Eq. (4.12)

$$\boldsymbol{\omega} = 2 \tan\left(\frac{\theta}{2}\right) \mathbf{t} = \frac{2}{q_0}\mathbf{q} \tag{4.19}$$

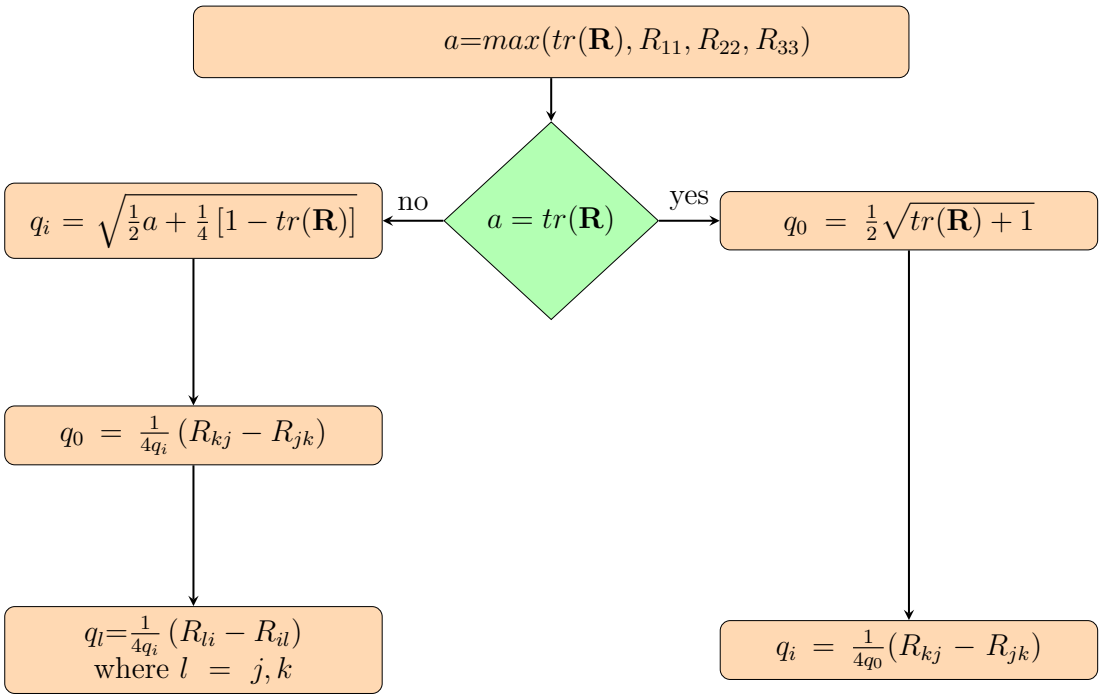

Figure 4.3: Extraction of the unit quaternion from the rotation matrix using Spurrier algorithm.

4.3.1 Compound Rotations

The result of successive large rotations depends on the order in which they are applied. For example, consider a vector $\mathbf{v_0}$ that is rotated to a vector $\mathbf{v}_1$ using pseudo angle $\boldsymbol{\theta}_1$ and then rotated to another vector $\mathbf{v}_2$ using pseudo angle $\boldsymbol{\theta}_2$ via the following operations

$$\begin{aligned} \mathbf{v}_1 &= \mathbf{R}(\boldsymbol{\theta}_1)\mathbf{v}_0 \\ \mathbf{v}_2 &= \mathbf{R}(\boldsymbol{\theta}_2)\mathbf{v}_1 \end{aligned} \tag{4.20}$$

The new vector $\mathbf{v}_2$ can then be expressed in terms of $\mathbf{v}_0$

$$\mathbf{v}_2 = \mathbf{R}(\boldsymbol{\theta}_2)\mathbf{R}(\boldsymbol{\theta}_1)\mathbf{v}_0 \tag{4.21}$$

Alternatively, the new vector $\mathbf{v}_2$ can be obtained using the quaternion product operation [65]

$$\begin{aligned} \mathbf{v}_2 &= \mathbf{R}(\mathbf{q}_2)\mathbf{R}(\mathbf{q}_1)\mathbf{v}_0 \\ \mathbf{v}_2 &= \mathbf{R}(\mathbf{q}_{12})\mathbf{v}_0 \end{aligned} \tag{4.22}$$

where $\mathbf{R}(\mathbf{q}_{12})$ can be calculated using Eq. (4.18) and $\mathbf{q}_{12}$ represents the quaternion product

$$\mathbf{q}_{12} = \mathbf{q}_2\mathbf{q}_1 = \begin{bmatrix} q_{10}q_{20} - \mathbf{q}_1^T\mathbf{q}_2 \\ q_{10}\mathbf{q}_2 + q_{20}\mathbf{q}_1 - \mathbf{q}_1 \times \mathbf{q}_2 \end{bmatrix} \tag{4.23}$$

Note that the first row is the scalar component and the second row is the vector component. Furthermore, the quaternion product is not a commutative operation due to the presence of the vector cross-product ($\mathbf{q}_1 \times \mathbf{q}_2 = -\mathbf{q}_2 \times \mathbf{q}_1$).

4.4 Displaced Local Frame

Three node triads are defined for the deformed element: two nodal triads, $\mathbf{N}_I$ and $\mathbf{N}_J$, are defined at the element ends along with one local element base triad $\hat{\mathbf{E}}$, as shown in Fig. 4.4. The triads $\mathbf{N}_I$ and $\mathbf{N}_J$ represent the nodal rotations at the

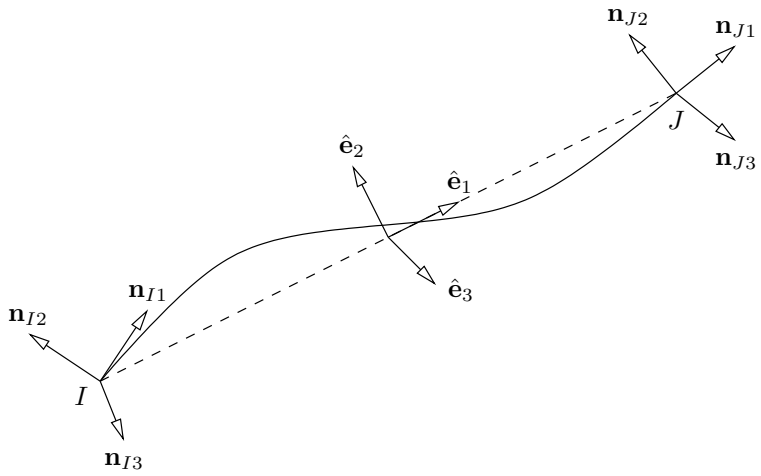

Figure 4.4: Three nodal triads of the deformed element.

element ends, each in terms of three base vectors

$$\mathbf{N}_I = \begin{bmatrix} \mathbf{n}_{I1} & \mathbf{n}_{I2} & \mathbf{n}_{I3} \end{bmatrix} \qquad \mathbf{N}_J = \begin{bmatrix} \mathbf{n}_{J1} & \mathbf{n}_{J2} & \mathbf{n}_{J3} \end{bmatrix} \tag{4.24}$$

The local element base triad $\hat{\mathbf{E}}$, which corresponds to a rotation matrix that transforms vectors from global to local coordinate system, consists of three unit base vectors

$$\hat{\mathbf{E}} = \begin{bmatrix} \hat{\mathbf{e}}_1 & \hat{\mathbf{e}}_2 & \hat{\mathbf{e}}_3 \end{bmatrix} \tag{4.25}$$

The unit base vector $\hat{\mathbf{e}}_1$ lies along the element between nodes I and J. In the deformed configuration, $\hat{\mathbf{e}}_1$ can be computed by considering the end displacements of the element.

$$\hat{\mathbf{e}}_1 = \frac{\mathbf{X}_{IJ} + \mathbf{u}_{IJ}}{L_d} \tag{4.26}$$

where $\mathbf{X}_{IJ}$ and $\mathbf{u}_{IJ}$ are the difference between global coordinates and displacements of nodes I and J, respectively, as shown in Fig. 4.5.

$$\mathbf{X}_{IJ} = \mathbf{X}_J - \mathbf{X}_I \tag{4.27}$$

$$\mathbf{u}_{IJ} = \mathbf{u}_J - \mathbf{u}_I \tag{4.28}$$

The deformed length of the element, L_d, is

$$L_d = \|\mathbf{X}_{IJ} + \mathbf{u}_{IJ}\| = \left[(\mathbf{X}_{IJ} + \mathbf{u}_{IJ})^T(\mathbf{X}_{IJ} + \mathbf{u}_{IJ})\right]^{\frac{1}{2}} \tag{4.29}$$

which is easily computed from the original nodal coordinates and the translational nodal displacements.

Note that the geometric linear transformation that is performed in the undeformed configuration can be retrieved by setting $\mathbf{u}_{IJ}$ to zero. For linear transformation, the unit base vectors $\hat{\mathbf{e}}_2$ and $\hat{\mathbf{e}}_3$ that give the orientation of the element cross-section after deformation can be computed using a vector, $\mathbf{v}$, lying on the x-z plane that can be specified as a user input data such that

$$\hat{\mathbf{e}}_2 = \frac{\mathbf{v} \times \hat{\mathbf{e}}_1}{\|\mathbf{v} \times \hat{\mathbf{e}}_1\|} \tag{4.30}$$

$$\hat{\mathbf{e}}_3 = \hat{\mathbf{e}}_1 \times \hat{\mathbf{e}}_2 \tag{4.31}$$

where $\times$ denotes the vector cross-product operation.

On the other hand, for the corotational transformation, the vectors $\hat{\mathbf{e}}_2$ and $\hat{\mathbf{e}}_3$

cannot be computed directly because their formulations depend on the rotations of nodal triads in the deformed configuration. The most common approach to obtain $\hat{\mathbf{e}}_2$ and $\hat{\mathbf{e}}_3$ independently from the orientation of the local axes (x, y, z) is the Crisfield algorithm [19], which will be discussed next.

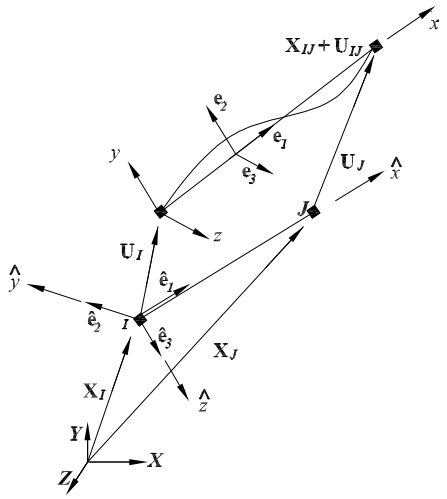

Figure 4.5: Deformed configuration of frame in space.

4.4.1 Crisfield Algorithm

The pseudo rotation increment vector of node I and J can be described as

$$\Delta\boldsymbol{\theta}_I = \{\boldsymbol{\theta}_I\}_i^j - \{\boldsymbol{\theta}_I\}_i^{j-1} \tag{4.32}$$

$$\Delta\boldsymbol{\theta}_J = \{\boldsymbol{\theta}_J\}_i^j - \{\boldsymbol{\theta}_J\}_i^{j-1} \tag{4.33}$$

where the subscript i refers to the time step and the superscript j refers to the iteration number within the time step. The increment of the pseudo rotation vectors is used to compute the quaternion vector $\mathbf{q}(\Delta\boldsymbol{\theta})$ by applying Eq. (4.12). The orientation of the deformed sections located at the ends of the element is represented by the nodal triads ($\mathbf{N}_I$ and $\mathbf{N}_J$) and can be obtained by applying Eq. (4.18).

To combine the triads $\mathbf{N}_I$ and $\mathbf{N}_J$, Crisfield used the compound rotation formula

$$\mathbf{N}_J = \mathbf{R}(\boldsymbol{\zeta})\mathbf{N}_I \tag{4.34}$$

where $\boldsymbol{\zeta}$ is the tangent-scaled pseudo rotation vector that connects the nodal rotations $\mathbf{N}_I$ and $\mathbf{N}_J$. The matrix $\mathbf{R}(\boldsymbol{\zeta})$ is the rotation matrix that corresponds to the rotation from triad $\mathbf{N}_I$ to triad $\mathbf{N}_J$. By multiplying both sides of Eq. (4.34) by $\mathbf{N}_I^T$ and considering that $\mathbf{N}_I$ is an orthogonal matrix gives

$$\mathbf{R}(\boldsymbol{\zeta}) = \mathbf{N}_J\mathbf{N}_I^T \tag{4.35}$$

To get the $\boldsymbol{\zeta}$ vector out of the rotation matrix $\mathbf{R}(\boldsymbol{\zeta})$, the quaternion vector has to be extracted first by using Spurrier algorithm [66] and then using Eq. (4.19) to get $\boldsymbol{\zeta}$ out of the quaternion vector. The average rotation matrix can be calculated now in terms of the pseudo rotation vector, $\boldsymbol{\zeta}$, using Eq. (4.10).

$$\bar{\mathbf{R}} = \mathbf{R}\left(\frac{\boldsymbol{\zeta}}{2}\right)\mathbf{N}_I \tag{4.36}$$

The mean triad ($\bar{\mathbf{R}}$) is a 3×3 matrix and each column in this matrix corresponds to the local axes orientation in the deformed configuration

$$\bar{\mathbf{R}} = \left[\begin{array}{ccc} \bar{\mathbf{r}}_1 & \bar{\mathbf{r}}_2 & \bar{\mathbf{r}}_3 \end{array} \right] \tag{4.37}$$

To find the triad $\hat{\mathbf{E}}$, Crisfield made an assumption that $\bar{\mathbf{r}}_1$ coincides with $\hat{\mathbf{e}}_1$ via small possible rotations while $\hat{\mathbf{e}}_2$ and $\hat{\mathbf{e}}_3$ are

$$\hat{\mathbf{e}}_2 = \bar{\mathbf{r}}_2 - \frac{\bar{\mathbf{r}}_2^T \hat{\mathbf{e}}_1}{2}(\bar{\mathbf{r}}_1 + \hat{\mathbf{e}}_1) \tag{4.38}$$

$$\hat{\mathbf{e}}_3 = \bar{\mathbf{r}}_3 - \frac{\bar{\mathbf{r}}_3^T \hat{\mathbf{e}}_1}{2}(\bar{\mathbf{r}}_1 + \hat{\mathbf{e}}_1) \tag{4.39}$$

After defining the unit base vectors ($\hat{\mathbf{e}}_1$, $\hat{\mathbf{e}}_2$, $\hat{\mathbf{e}}_3$) and the nodal rotations ($\mathbf{N}_I$ and $\mathbf{N}_J$) in the deformed configuration, the displacements in the local and basic systems are defined next.

4.5 Transformation From Local to Basic Coordinates

As in the planar case, the axial deformation (u_{l1}) produces extension which is the difference between the deformed and the initial length (L_n)

$$u_{l1} = L_d - L_n = \frac{1}{L_d + L_n} \left(2\mathbf{X}_{IJ} + \mathbf{u}_{IJ}\right)^T \mathbf{u}_{IJ} \tag{4.40}$$

Once the three triads ($\mathbf{N}_I$, $\mathbf{N}_J$, and $\hat{\mathbf{E}}$) are determined, the local rotations at the ends of the element (node I and J) can be obtained using the Crisfield algo-

rithm [19]. The local displacement vector $\mathbf{u}_l$ can be represented by

$$\mathbf{u}_l = \begin{bmatrix} u_{l1} \\ u_{l2} \\ u_{l3} \\ u_{l4} \\ u_{l5} \\ u_{l6} \\ u_{l7} \end{bmatrix} = \begin{bmatrix} \theta_{I_1} \\ \theta_{I_3} \\ \theta_{I_2} \\ \theta_{J_1} \\ \theta_{J_3} \\ \theta_{J_2} \\ u_{l1} \end{bmatrix} \tag{4.41}$$

where

$$\theta_{I_1} = \arcsin\left[\frac{1}{2}\left(\hat{\mathbf{e}}_3^T\mathbf{n}_{I_2} - \hat{\mathbf{e}}_2^T\mathbf{n}_{I_3}\right)\right] \tag{4.42}$$

$$\theta_{I_2} = \arcsin\left[\frac{1}{2}\left(\hat{\mathbf{e}}_1^T\mathbf{n}_{I_3} - \hat{\mathbf{e}}_3^T\mathbf{n}_{I_1}\right)\right] \tag{4.43}$$

$$\theta_{I_3} = \arcsin\left[\frac{1}{2}\left(\hat{\mathbf{e}}_2^T\mathbf{n}_{I_1} - \hat{\mathbf{e}}_1^T\mathbf{n}_{I_2}\right)\right] \tag{4.44}$$

$$\theta_{J_1} = \arcsin\left[\frac{1}{2}\left(\hat{\mathbf{e}}_3^T\mathbf{n}_{J_2} - \hat{\mathbf{e}}_2^T\mathbf{n}_{J_3}\right)\right] \tag{4.45}$$

$$\theta_{J_2} = \arcsin\left[\frac{1}{2}\left(\hat{\mathbf{e}}_1^T\mathbf{n}_{J_3} - \hat{\mathbf{e}}_3^T\mathbf{n}_{J_1}\right)\right] \tag{4.46}$$

$$\theta_{J_3} = \arcsin\left[\frac{1}{2}\left(\hat{\mathbf{e}}_2^T\mathbf{n}_{J_1} - \hat{\mathbf{e}}_1^T\mathbf{n}_{J_2}\right)\right] \tag{4.47}$$

The element deformations vector $\mathbf{v}$ within the corotational basic system can be obtained by

$$\mathbf{v} = \mathbf{T}_{bl}\mathbf{u}_l \tag{4.48}$$

and the equilibrium between the basic forces, $\mathbf{p}_b$, and forces in the local coordinate system, $\mathbf{p}_l$, is described by

$$\mathbf{p}_l = \mathbf{T}_{bl}^T\mathbf{p}_b \tag{4.49}$$

where $\mathbf{T}_{bl}$ is a 6x7 local-basic transformation matrix

$$\mathbf{T}_{bl} = \begin{bmatrix} 0 & 0 & 0 & 0 & 0 & 0 & 1 \\ 0 & 1 & 0 & 0 & 0 & 0 & 0 \\ 0 & 0 & 0 & 0 & 1 & 0 & 0 \\ 0 & 0 & -1 & 0 & 0 & 0 & 0 \\ 0 & 0 & 0 & 0 & 0 & -1 & 0 \\ -1 & 0 & 0 & 1 & 0 & 0 & 0 \end{bmatrix} \tag{4.50}$$

4.6 Transformation From Global to Local Coordinates

The first components in the corotational theory is the transformation of element displacements from global coordinate system to local coordinate system which can be described by the matrix-vector product

$$\mathbf{u}_l = \mathbf{T}\mathbf{u} \tag{4.51}$$

where $\mathbf{u}$ is the dispacement vector in the global coordinate system. The size of the local and global displacement vectors are 7 and 12, respectively. Therefore, the

size of the local-global transformation matrix $\mathbf{T}$ is 7×12.

The vector of the local element forces, $\mathbf{p}_l$, transforms to the vector of the global forces, $\mathbf{p}$, by the contragradient relationship

$$\mathbf{p} = \mathbf{T}^T \mathbf{p}_l \tag{4.52}$$

Unlike the 2D corotational formulation, in which the local-global transformation matrix $\mathbf{T}$ is a linear function, the transformation matrix $\mathbf{T}$ of the 3D corotational formulation is a function of displacements in the deformed configuration ($\mathbf{T}(\mathbf{u}(h))$. More information about the derivation of the transformation matrix $\mathbf{T}$ can be found in [19] and [20], and is omitted here for brevity. The first component in the transformation matrix is $\mathbf{t}_1$ that corresponds to global-local transformation of axial deformations and forces. The global-local transformation components $\mathbf{t}_2, \mathbf{t}_3, \mathbf{t}_4$, and $\mathbf{t}_5$ correspond to the transformation of element end rotations. The last tow components $\mathbf{t}_{6I}$ and $\mathbf{t}_{6J}$ correspond to the transformation of torsional rotations at element ends, node I and node J. The final form of the the end of the element.

$$\mathbf{T}^T = \begin{bmatrix} \mathbf{t}_1^T & \mathbf{t}_2^T & \mathbf{t}_3^T & \mathbf{t}_4^T & \mathbf{t}_5^T & \mathbf{t}_{6I}^T & \mathbf{t}_{6J}^T \end{bmatrix} \tag{4.53}$$

where

$$\mathbf{t}_1 = \begin{bmatrix} -\hat{\mathbf{e}}_1^T & \mathbf{0}^T & \hat{\mathbf{e}}_1^T & \mathbf{0}^T \end{bmatrix} \tag{4.54}$$

$$\mathbf{t}_2 = \frac{1}{2\cos(\theta_{I_3})} \left[\mathbf{L}(\bar{\mathbf{r}}_2)\mathbf{n}_{I_1} + \mathbf{h}_{I_3}\right]^T \tag{4.55}$$

$$\mathbf{t}_3 = \frac{1}{2\cos(\theta_{J_3})}\left[\mathbf{L}(\bar{\mathbf{r}}_2)\mathbf{n}_{J_1} + \mathbf{h}_{J_3}\right]^T \tag{4.56}$$

$$\mathbf{t}_4 = \frac{1}{2\cos(\theta_{I_2})}\left[-\mathbf{L}(\bar{\mathbf{r}}_3)\mathbf{n}_{I_1} - \mathbf{h}_{I_2}\right]^T \tag{4.57}$$

$$\mathbf{t}_5 = \frac{1}{2\cos(\theta_{J_2})}\left[-\mathbf{L}(\bar{\mathbf{r}}_3)\mathbf{n}_{J_1} - \mathbf{h}_{J_2}\right]^T \tag{4.58}$$

$$\mathbf{t}_{6J} = \frac{1}{2\cos(\theta_{J_1})}\left[\mathbf{L}(\bar{\mathbf{r}}_3)\mathbf{n}_{J_2} - \mathbf{L}(\bar{\mathbf{r}}_2)\mathbf{n}_{J_3} + \mathbf{h}_{J_1}\right] \tag{4.59}$$

$$\mathbf{t}_{6I} = \frac{1}{2\cos(\theta_{I_1})}\left[\mathbf{L}(\bar{\mathbf{r}}_3)\mathbf{n}_{I_2} - \mathbf{L}(\bar{\mathbf{r}}_2)\mathbf{n}_{I_3} + \mathbf{h}_{I_1}\right]^T \tag{4.60}$$

The matrix $\mathbf{L}$ is produced as a result of taking the variation of the base vectors $\hat{\mathbf{e}}_2$ and $\hat{\mathbf{e}}_3$, respectively.

$$\delta\hat{\mathbf{e}}_k = \mathbf{L}(\bar{\mathbf{r}}_k)^T\delta\mathbf{u} \tag{4.61}$$

for $k = 1, 2$ and the matrix $\mathbf{L}$ is

$$\mathbf{L}(\bar{\mathbf{r}}_k)^T = \begin{bmatrix} \mathbf{L}_1(\bar{\mathbf{r}}_k)^T & \mathbf{L}_2(\bar{\mathbf{r}}_k)^T & -\mathbf{L}_1(\bar{\mathbf{r}}_k)^T & \mathbf{L}_2(\bar{\mathbf{r}}_k)^T \end{bmatrix} \tag{4.62}$$

with

$$\mathbf{L}_1(\bar{\mathbf{r}}_k) = \frac{1}{2}(\bar{\mathbf{r}}_k^T\hat{\mathbf{e}}_1\mathbf{A} + \mathbf{A}\bar{\mathbf{r}}_k(\hat{\mathbf{e}}_1 + \bar{\mathbf{r}}_1)^T) \tag{4.63}$$

and

$$\mathbf{L}_2(\bar{\mathbf{r}}_k) = \frac{1}{2}\mathbf{S}(\bar{\mathbf{r}}_k) - \frac{1}{4}\bar{\mathbf{r}}_k^T\hat{\mathbf{e}}_1\mathbf{S}(\bar{\mathbf{r}}_1) - \frac{1}{4}\mathbf{S}(\bar{\mathbf{r}}_k)\hat{\mathbf{e}}_1(\hat{\mathbf{e}}_1 + \bar{\mathbf{r}}_1)^T \tag{4.64}$$

The matrix $\mathbf{A}$ is obtained by taking the variation of the base vector $\hat{\mathbf{e}}_1$

$$\delta\hat{\mathbf{e}}_1 = \mathbf{A}\delta\mathbf{u}_{IJ} \tag{4.65}$$

$$\mathbf{A} = \frac{1}{L_d}(\mathbf{I} - \hat{\mathbf{e}}_1\hat{\mathbf{e}}_1^T) \tag{4.66}$$

Finally the vector $\mathbf{h}$ is obtained as a result of taking the variation of the rotation vectors Eq. (4.42) through Eq. (4.47)

$$\mathbf{h}_{I_1}^T = \begin{bmatrix} \mathbf{0}^T & (\mathbf{S}(\mathbf{n}_{I_2})\hat{\mathbf{e}}_3 - \mathbf{S}(\mathbf{n}_{I_3})\hat{\mathbf{e}}_2)^T & \mathbf{0}^T & \mathbf{0}^T \end{bmatrix} \tag{4.67}$$

$$\mathbf{h}_{I_2}^T = \begin{bmatrix} (\mathbf{A}\mathbf{n}_{I_3})^T & (\mathbf{S}(\mathbf{n}_{I_1})\hat{\mathbf{e}}_3 - \mathbf{S}(\mathbf{n}_{I_3})\hat{\mathbf{e}}_1)^T & -(\mathbf{A}\mathbf{n}_{I_3})^T & \mathbf{0}^T \end{bmatrix} \tag{4.68}$$

$$\mathbf{h}_{I_3}^T = \begin{bmatrix} (\mathbf{A}\mathbf{n}_{I_2})^T & (\mathbf{S}(\mathbf{n}_{I_1})\hat{\mathbf{e}}_2 - \mathbf{S}(\mathbf{n}_{I_2})\hat{\mathbf{e}}_1)^T & -(\mathbf{A}\mathbf{n}_{I_2})^T & \mathbf{0}^T \end{bmatrix} \tag{4.69}$$

$$\mathbf{h}_{J_1}^T = \begin{bmatrix} \mathbf{0}^T & \mathbf{0}^T & \mathbf{0}^T(\mathbf{S}(\mathbf{n}_{J_2})\hat{\mathbf{e}}_3 - \mathbf{S}(\mathbf{n}_{J_3})\hat{\mathbf{e}}_2)^T \end{bmatrix} \tag{4.70}$$

$$\mathbf{h}_{J_2}^T = \begin{bmatrix} (\mathbf{A}\mathbf{n}_{J_3})^T & \mathbf{0}^T & (-\mathbf{A}\mathbf{n}_{J_3})^T(\mathbf{S}(\mathbf{n}_{J_1})\hat{\mathbf{e}}_3 - \mathbf{S}(\mathbf{n}_{J_3})\hat{\mathbf{e}}_1)^T \end{bmatrix} \tag{4.71}$$

$$\mathbf{h}_{J_3}^T = \begin{bmatrix} (\mathbf{A}\mathbf{n}_{J_2})^T & \mathbf{0}^T & (-\mathbf{A}\mathbf{n}_{J_2})^T(\mathbf{S}(\mathbf{n}_{J_1})\hat{\mathbf{e}}_2 - \mathbf{S}(\mathbf{n}_{J_2})\hat{\mathbf{e}}_1)^T \end{bmatrix} \tag{4.72}$$

Up to here, the finite element corotational formulation of space frame elements

is completed and the DDM response sensitivity equations are defined next.

4.7 Sensitivity of The Unit Base Vectors

Derivation of sensitivity begins with the displaced local frame, which is defines by element triads and unit base vectors. The sensitivity derivations of the element triad $\hat{\mathbf{E}}$ in the deformed configuration start by differentiating the unit base vector $\hat{\mathbf{e}}_1$ in Eq. (4.26) with respect to parameter h

$$\frac{d\hat{\mathbf{e}}_1}{dh} = \frac{L_d(\frac{d\mathbf{X}_{IJ}}{dh} + \frac{d\mathbf{u}_{IJ}}{dh}) - (\mathbf{X}_{IJ} + \mathbf{u}_{IJ})\frac{dL_d}{dh}}{L_d^2} \tag{4.73}$$

where the sensitivity of the deformed length can be obtained by differentiating Eq. (4.29) with respect to parameter h

$$\frac{dL_d}{dh} = \frac{(\mathbf{X}_{IJ} + \mathbf{u}_{IJ})^T(\frac{\partial\mathbf{X}_{IJ}}{\partial h} + \frac{\partial\mathbf{u}_{IJ}}{\partial h})}{L_d} \tag{4.74}$$

where $\frac{\partial\mathbf{u}_{IJ}}{\partial h}$ is the sensitivity of the nodal displacement. The sensitivity of the nodal coordinates $d\mathbf{X}_{IJ}/dh$ is nonzero only when the parameter h corresponds to a nodal coordinate at the element ends.

The derivatives of the other unit base vectors $\hat{\mathbf{e}}_2$ and $\hat{\mathbf{e}}_3$ are more complex and require following the Crisfield algorithm which starts by taking the derivative of the pseudo rotation increment defined in Eq. (4.32) and Eq. (4.33)

$$\frac{d\Delta\boldsymbol{\theta}_I}{dh} = \frac{d\{\boldsymbol{\theta}_I\}_i^j}{dh} - \frac{d\{\boldsymbol{\theta}_I\}_i^{j-1}}{dh} \tag{4.75}$$

$$\frac{d\Delta\boldsymbol{\theta}_J}{dh} = \frac{d\{\boldsymbol{\theta}_J\}_i^j}{dh} - \frac{d\{\boldsymbol{\theta}_J\}_i^{j-1}}{dh} \tag{4.76}$$

The next step of the derivation is to differentiate the unit quaternion vector defined in Eq. (4.12), with respect to the parameter h

$$\frac{d\mathbf{q}}{dh} = \begin{bmatrix} \frac{dq_0}{dh} \\ \frac{dq_1}{dh} \\ \frac{dq_2}{dh} \\ \frac{dq_3}{dh} \end{bmatrix} = \begin{bmatrix} -\frac{1}{2}\sin(\theta/2)\frac{d\theta}{dh} \\ \frac{\sin(\theta/2)}{\theta}\frac{d\boldsymbol{\theta}}{dh} + \frac{(\frac{\theta}{2}\frac{d\theta}{dh}\cos(\theta/2) - \frac{d\theta}{dh}\sin(\theta/2))}{\theta^2}\boldsymbol{\theta} \end{bmatrix} \tag{4.77}$$

where the sensitivity of the magnitude of the pseudo rotation, θ, can be obtained by differentiating Eq. (4.7) with respect to parameter h

$$\frac{d\theta}{dh} = \frac{\theta_1\frac{d\theta_1}{dh} + \theta_2\frac{d\theta_2}{dh} + \theta_3\frac{d\theta_3}{dh}}{\theta} \tag{4.78}$$

The sensitivity of the updated rotations requires the derivative of the quaternion product, which can be obtained by differentiating Eq. (4.23) with respect to parameter h

$$\frac{\mathbf{q}_{12}}{dh} = \begin{bmatrix} q_{10}\frac{dq_{20}}{dh} + \frac{dq_{10}}{dh}\mathbf{q}_{20} - (\mathbf{q}_1^T\frac{d\mathbf{q}_2}{dh} + \frac{d\mathbf{q}_1^T}{dh}\mathbf{q}_2) \\ q_{10}\frac{d\mathbf{q}_2}{dh} + \frac{dq_{10}}{dh}\mathbf{q}_2 + q_{20}\frac{d\mathbf{q}_1}{dh} + \frac{dq_{20}}{dh}\mathbf{q}_1 - \frac{d(\mathbf{q}_1\times\mathbf{q}_2)}{dh} \end{bmatrix} \tag{4.79}$$

The sensitivities of the rotation triads $\mathbf{N}_I$ and $\mathbf{N}_J$ are ready to be evaluated by differentiating Eq. (4.18) with respect to parameter h. For instance, to get $d\mathbf{N}_I/dh$, it is necessary to apply the quaternion vector and its derivative corresponding to node I

$$\frac{d\mathbf{R}}{dh} = \begin{bmatrix} 2q_0\frac{dq_0}{dh} + 2q_1\frac{dq_1}{dh} & q_1\frac{dq_2}{dh} + \frac{dq_1}{dh}q_2 - (q_0\frac{dq_3}{dh} + \frac{dq_0}{dh}q_3) & q_1\frac{dq_3}{dh} + \frac{dq_1}{dh}q_3 + q_0\frac{dq_2}{dh} + \frac{dq_0}{dh}q_2 \\ q_2\frac{dq_1}{dh} + \frac{dq_2}{dh}q_1 + q_0\frac{dq_3}{dh} + \frac{dq_0}{dh}q_3 & 2q_0\frac{dq_0}{dh} + 2q_2\frac{dq_2}{dh} & q_2\frac{dq_3}{dh} + \frac{dq_2}{dh}q_3 - q_1\frac{dq_0}{dh} - \frac{dq_1}{dh}q_0 \\ q_3\frac{dq_1}{dh} + \frac{dq_3}{dh}q_1 - q_0\frac{dq_2}{h} - \frac{dq_0}{dh}q_2 & q_3\frac{dq_2}{dh} + \frac{dq_3}{dh}q_2 + q_0\frac{dq_1}{dh} + \frac{dq_0}{dh}q_1 & 2q_0\frac{dq_0}{dh} + 2q_3\frac{dq_3}{dh} \end{bmatrix} \tag{4.80}$$

The sensitivity of the rotation triad from node I to node J can be evaluated now by differentiation Eq. (4.35)

$$\frac{d\mathbf{R}(\boldsymbol{\zeta})}{dh} = \mathbf{N}_J\frac{d\mathbf{N}_I^T}{dh} + \frac{d\mathbf{N}_J}{dh}\mathbf{N}_I^T \tag{4.81}$$

To obtain the sensitivity of the average tangent scaled pseudo vector, $\boldsymbol{\zeta}$, the sensitivity derivation has to be extended to include the Spurrier algorithm as shown in Fig. 4.6.

After obtaining the sensitivity of the unit quaternion vector, the sensitivity of the tangent scaled pseudo vector can be computed by differentiating Eq. (4.19) with respect to the parameter h

$$\frac{d\boldsymbol{\zeta}}{dh} = \frac{2\left(q_0\frac{d\mathbf{q}}{dh} - \frac{dq_0}{dh}\mathbf{q}\right)}{q_0^2} \tag{4.82}$$

The sensitivity of the mean rotation triad is ready to be evaluated now by differentiating Eq. (4.36) with respect to h.

$$\frac{d\bar{\mathbf{R}}}{dh} = \mathbf{R}(\frac{\boldsymbol{\zeta}}{2})\frac{\partial\mathbf{N}_I}{\partial h} + \frac{\partial\mathbf{R}(\frac{\boldsymbol{\zeta}}{2})}{\partial h}\mathbf{N}_I \tag{4.83}$$

The sensitivity of the rotation Matrix $\mathbf{R}(\boldsymbol{\zeta}/2)$ can be obtained by differentiat-

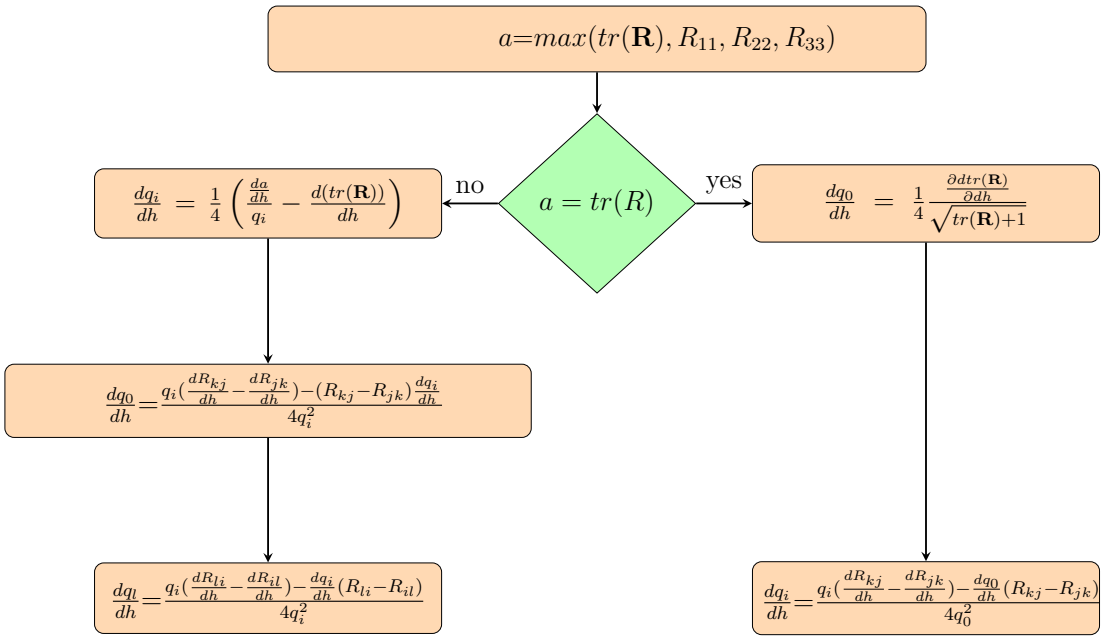

Figure 4.6: Extraction the sensitivity of the unit quaternion from the rotation matrix using Spurrier's algorithm.

ing Eq. (4.10) with respect to parameter h where the tangent scaled vector $\boldsymbol{\omega}$ is evaluated at $\boldsymbol{\zeta}/2$.

$$\frac{\partial \mathbf{R}(\boldsymbol{\omega})}{\partial h} = \frac{1}{1+\frac{1}{4}\boldsymbol{\omega}^T\boldsymbol{\omega}}\left[\frac{\partial \mathbf{S}(\boldsymbol{\omega})}{\partial h} + \frac{1}{2}\frac{\partial(\mathbf{S}(\boldsymbol{\omega})\mathbf{S}(\boldsymbol{\omega}))}{\partial h}\right] - \frac{\frac{1}{2}\boldsymbol{\omega}^T\frac{\partial \boldsymbol{\omega}}{\partial h}}{\left(1+\frac{1}{4}\boldsymbol{\omega}^T\boldsymbol{\omega}\right)^2}\left[\mathbf{S}(\boldsymbol{\omega}) + \frac{1}{2}\mathbf{S}(\boldsymbol{\omega})\mathbf{S}(\boldsymbol{\omega})\right] \tag{4.84}$$

where the derivative of the spin tensor $\frac{\partial \mathbf{S}}{\partial h}$ and its square $\frac{\partial(\mathbf{S}(\boldsymbol{\omega})\mathbf{S}(\boldsymbol{\omega}))}{\partial h}$ are

$$\frac{\partial \mathbf{S}(\boldsymbol{\omega})}{\partial h} = \begin{bmatrix} 0 & -\frac{\partial \omega_3}{\partial h} & \frac{\partial \omega_2}{\partial h} \\ \frac{\partial \omega_3}{\partial h} & 0 & -\frac{\partial \omega_1}{\partial h} \\ -\frac{\partial \omega_2}{\partial h} & \frac{\partial \omega_1}{\partial h} & 0 \end{bmatrix} \tag{4.85}$$

$$\frac{\partial(\mathbf{S}(\boldsymbol{\omega})\mathbf{S}(\boldsymbol{\omega}))}{\partial h} = \begin{bmatrix} -2\omega_3\frac{\partial\omega_3}{\partial h} - 2\omega_2\frac{\partial\omega_2}{\partial h} & \omega_1\frac{\partial\omega_2}{\partial h} + \frac{\partial\omega_1}{\partial h}\omega_2 & \omega_3\frac{\partial\omega_1}{\partial h} + \omega_1\frac{\partial\omega_3}{\partial h} \\ \omega_1\frac{\partial\omega_2}{\partial h} + \omega_2\frac{\partial\omega_1}{\partial h} & -2\omega_3\frac{\partial\omega_3}{\partial h} - 2\omega_1\frac{\partial\omega_1}{\partial h} & \omega_3\frac{\partial\omega_2}{\partial h} + \omega_2\frac{\partial\omega_3}{\partial h} \\ \omega_3\frac{\partial\omega_1}{\partial h} + \frac{\partial\omega_3}{\partial h}\omega_1 & \omega_3\frac{\partial\omega_2}{\partial h} + \omega_2\frac{\partial\omega_3}{\partial h} & -2\omega_2\frac{\partial\omega_2}{\partial h} - 2\omega_1\frac{\partial\omega_1}{\partial h} \end{bmatrix} \tag{4.86}$$

The derivative of the tangent scaled pseudo vector $\frac{\partial\boldsymbol{\omega}}{\partial h}$ where $\boldsymbol{\omega}$ is evaluated at $\boldsymbol{\zeta}/2$ are calculated by Eq. (4.82).

Note that the components of $d\hat{\mathbf{R}}/dh$ are

$$\frac{d\bar{\mathbf{R}}}{dh} = \begin{bmatrix} \frac{d\bar{\mathbf{r}}_1}{dh} & \frac{d\bar{\mathbf{r}}_2}{dh} & \frac{d\bar{\mathbf{r}}_3}{dh} \end{bmatrix} \tag{4.87}$$

The sensitivity of the unit base vectors $\hat{\mathbf{e}}_2$ and $\hat{\mathbf{e}}_3$ can be computed now based on the derivatives of $d\bar{\mathbf{r}}_2/dh$ and $d\bar{\mathbf{r}}_3/dh$, respectively.

$$\frac{d\hat{\mathbf{e}}_2}{dh} = \frac{d\bar{\mathbf{r}}_2}{dh} - \frac{1}{2}\left[\frac{d\bar{\mathbf{r}}_2^T}{dh}\hat{\mathbf{e}}_1 + \bar{\mathbf{r}}_2^T\frac{d\hat{\mathbf{e}}_1}{dh}(\bar{\mathbf{r}}_1 + \hat{\mathbf{e}}_1) + \bar{\mathbf{r}}_2^T\hat{\mathbf{e}}_1\left(\frac{d\bar{\mathbf{r}}_1}{dh} + \frac{d\hat{\mathbf{e}}_1}{dh}\right)\right] \tag{4.88}$$

$$\frac{d\hat{\mathbf{e}}_3}{dh} = \frac{d\bar{\mathbf{r}}_3}{dh} - \frac{1}{2}\left[\frac{d\bar{\mathbf{r}}_3^T}{dh}\hat{\mathbf{e}}_1 + \bar{\mathbf{r}}_3^T\frac{d\hat{\mathbf{e}}_1}{dh}(\bar{\mathbf{r}}_1 + \hat{\mathbf{e}}_1) + \bar{\mathbf{r}}_3^T\hat{\mathbf{e}}_1\left(\frac{d\bar{\mathbf{r}}_1}{dh} + \frac{d\hat{\mathbf{e}}_1}{dh}\right)\right] \tag{4.89}$$

4.8 Sensitivity Derivations in The Element Level

The sensitivity of the global-local transformation starts by differentiating Eq. (4.52) with respect to parameter h

$$\frac{\partial \mathbf{p}}{\partial h} = \mathbf{T}^T \frac{\partial \mathbf{p}_l}{\partial h} + \frac{\partial \mathbf{T}^T}{\partial h} \mathbf{p}_l \tag{4.90}$$

where $\partial \mathbf{p}/\partial h$ and $\partial \mathbf{p}_l/\partial h$ represent the sensitivity of the element forces in the global and local coordinate systems, respectively. The sensitivity of the global-local transformation matrix is presented by $\partial \mathbf{T}^T/\partial h$. By applying the chain rule in the differentiation of $\mathbf{p}(\mathbf{u}, h)$ and $\mathbf{p}_l(\mathbf{u}_l, h)$ with respect to parameter h, Eq. (4.90) expands to

$$\mathbf{K}_g \frac{\partial \mathbf{u}}{\partial h} + \left.\frac{\partial \mathbf{p}}{\partial h}\right|_{\mathbf{u}} = \mathbf{T}^T \left(\mathbf{K} \frac{\partial \mathbf{u}_l}{\partial h} + \left.\frac{\partial \mathbf{p}_l}{\partial h}\right|_{\mathbf{u}_l} \right) + \frac{\partial \mathbf{T}^T}{\partial h} \mathbf{p}_l \tag{4.91}$$

where $\mathbf{K}_g$ and $\mathbf{K}$ are global and local stiffness matrices. The conditional derivative of the external force vector is $\partial \mathbf{p}/\partial h|_{\mathbf{u}}$. The derivatives $\partial \mathbf{u}/\partial h$ and $\partial \mathbf{u}_l/\partial h$ represent the nodal displacement sensitivities in the global and local coordinate systems, respectively.

It is necessary to obtain the relationship between the derivative of the global displacements $\mathbf{u}$ and the local displacements $\mathbf{u}_l$ by

$$\frac{\partial \mathbf{u}_l}{\partial h} = \mathbf{T} \frac{\partial \mathbf{u}}{\partial h} + \frac{\partial \mathbf{T}}{\partial h} \mathbf{u} \tag{4.92}$$

Then, Eq. (4.106) and Eq. (4.91) are combined to give the following expression

$$\mathbf{K}_g \frac{\partial \mathbf{u}}{\partial h} + \left.\frac{\partial \mathbf{p}}{\partial h}\right|_{\mathbf{u}} = \mathbf{T}^T \left(\mathbf{K}\mathbf{T}\frac{\partial \mathbf{u}}{\partial h} + \mathbf{K}\frac{\partial \mathbf{T}}{\partial h}\mathbf{u} + \left.\frac{\partial \mathbf{p}_l}{\partial h}\right|_{\mathbf{u}_l} \right) + \frac{\partial \mathbf{T}}{\partial h}\mathbf{p}_l \tag{4.93}$$

Note that the relationship between the global and local stiffness matrices is

$$\mathbf{K}_g = \mathbf{T}^T \mathbf{K} \mathbf{T} \tag{4.94}$$

By applying Eq. (4.94) in Eq. (4.93), the first terms in the left and right-hand sides of Eq. (4.93) are equal and hence they cancel out. As a result, Eq. (4.93) gives the following expression for the conditional derivative of the element forces

$$\left.\frac{\partial \mathbf{p}}{\partial h}\right|_{\mathbf{u}} = \mathbf{T}^T \left(\mathbf{K}\frac{\partial \mathbf{T}}{\partial h}\mathbf{u} + \mathbf{T}^T \left.\frac{\partial \mathbf{p}_l}{\partial h}\right|_{\mathbf{u}_l} \right) + \frac{\partial \mathbf{T}}{\partial h}\mathbf{p}_l \tag{4.95}$$

4.8.1 Sensitivity of The Local-Basic Transformation

To determine the conditional derivative of the element forces, $\partial \mathbf{p}_l / \partial h|_{\mathbf{u}_l}$ in Eq. (4.95), Eq. (4.49) has to be differentiated by a procedure identical to that which led to Eq. (4.93)

$$\mathbf{K}\frac{\partial \mathbf{u}_l}{\partial h} + \left.\frac{\partial \mathbf{p}_l}{\partial h}\right|_{\mathbf{u}_l} = \mathbf{T}_{bl}^T \left(\mathbf{k}_b \frac{\partial \mathbf{v}}{\partial h} + \left.\frac{\partial \mathbf{p}_b}{\partial h}\right|_{\mathbf{v}} \right) + \frac{\partial \mathbf{T}_{bl}^T}{\partial h}\mathbf{p}_b \tag{4.96}$$

Note that the local-basic transformation matrix is constant and accordingly its derivative $\partial \mathbf{T}_{bl}^T / \partial h$ is equal to zero. The derivative of the element deformations in the basic system is $\partial \mathbf{v} / \partial h$ and the conditional derivative of the basic forces is

$\partial \mathbf{q}/\partial h|_{\mathbf{v}}$. The derivative of the element deformations $\partial \mathbf{v}/\partial h$ is obtained by the chain rule of differentiation

$$\frac{\partial \mathbf{v}}{\partial h} = \mathbf{T}_{bl}\frac{\partial \mathbf{u}_l}{\partial h} + \left.\frac{\partial \mathbf{v}}{\partial h}\right|_{\mathbf{u}_l} \tag{4.97}$$

Note that the conditional derivative of the basic displacements, $\frac{\partial \mathbf{v}}{\partial h}\big|_{\mathbf{u}_l}$, is zero because of the constant local-basic transformation matrix ,$\mathbf{T}_{bl}$. Following the same derivation procedure as that employed for the gradient of the transformation from global to local coordinates, inserting Eq. (4.97) into Eq. (4.96) gives

$$\mathbf{K}\frac{\partial \mathbf{u}_l}{\partial h} + \left.\frac{\partial \mathbf{p}_l}{\partial h}\right|_{\mathbf{u}_l} = \mathbf{T}_{bl}^T\left(\mathbf{k}_b\mathbf{T}_{bl}\frac{\partial \mathbf{u}_l}{\partial h} + \left.\frac{\partial \mathbf{p}_b}{\partial h}\right|_{\mathbf{v}}\right) + \frac{\partial \mathbf{T}_{bl}^T}{\partial h}\mathbf{p}_b \tag{4.98}$$

After simplification, the final form of the conditional derivative of the element forces is

$$\left.\frac{\partial \mathbf{p}_l}{\partial h}\right|_{\mathbf{u}_l} = \mathbf{T}_{bl}^T\left.\frac{\partial \mathbf{p}_b}{\partial h}\right|_{\mathbf{v}} \tag{4.99}$$

The formulation of the conditional derivatives, $\partial \mathbf{p}_b/\partial h|_{\mathbf{v}}$ in the basic system depends on the type of element formulation used in the structural analysis. More information about $\partial \mathbf{p}_b/\partial h|_{\mathbf{v}}$ can be found in [59], [31], and [57]. The derivative of the local displacements, $\partial \mathbf{u}_l/\partial h$, and the global-local transformation matrix, $\partial \mathbf{T}/\partial h$, are defined next.

4.9 Sensitivity of The Local and Basic Displacements

The sensitivity of the local rotation can be obtained directly by differentiating Eq. (4.42) through Eq. (4.47) with respect to parameter h

$$\frac{d\theta_{I_1}}{dh} = \frac{\frac{1}{2}\left(\hat{\mathbf{e}}_3^T \frac{d\mathbf{n}_{I2}}{dh} + \frac{d\hat{\mathbf{e}}_3^T}{dh}\mathbf{n}_{I2} - \hat{\mathbf{e}}_2^T \frac{d\mathbf{n}_{I3}}{dh} - \frac{d\hat{\mathbf{e}}_2^T}{dh}\mathbf{n}_{I3}\right)}{1 - \frac{1}{4}\left(\hat{\mathbf{e}}_3^T \mathbf{n}_{I2} - \hat{\mathbf{e}}_2^T \mathbf{n}_{I3}\right)^{1/2}} \tag{4.100}$$

$$\frac{d\theta_{I_2}}{dh} = \frac{\frac{1}{2}\left(\hat{\mathbf{e}}_1^T \frac{d\mathbf{n}_{I_3}}{dh} + \frac{d\hat{\mathbf{e}}_1^T}{dh}\mathbf{n}_{I_3} - \hat{\mathbf{e}}_3^T \frac{d\mathbf{n}_{I_1}}{dh} - \frac{d\hat{\mathbf{e}}_3^T}{dh}\mathbf{n}_{I_1}\right)}{1 - \frac{1}{4}\left(\hat{\mathbf{e}}_1^T \mathbf{n}_{I_3} - \hat{\mathbf{e}}_3^T \mathbf{n}_{I_1}\right)^{1/2}} \tag{4.101}$$

$$\frac{d\theta_{I_3}}{dh} = \frac{\frac{1}{2}\left(\hat{\mathbf{e}}_2^T \frac{d\mathbf{n}_{I_1}}{dh} + \frac{d\hat{\mathbf{e}}_2^T}{dh}\mathbf{n}_{I_1} - \hat{\mathbf{e}}_1^T \frac{d\mathbf{n}_{I_2}}{dh} - \frac{d\hat{\mathbf{e}}_1^T}{dh}\mathbf{n}_{I_2}\right)}{1 - \frac{1}{4}\left(\hat{\mathbf{e}}_2^T \mathbf{n}_{I_1} - \hat{\mathbf{e}}_1^T \mathbf{n}_{I_2}\right)^{1/2}} \tag{4.102}$$

$$\frac{d\theta_{J_1}}{dh} = \frac{\frac{1}{2}\left(\hat{\mathbf{e}}_3^T \frac{d\mathbf{n}_{J2}}{dh} + \frac{d\hat{\mathbf{e}}_3^T}{dh}\mathbf{n}_{J_2} - \hat{\mathbf{e}}_2^T \frac{d\mathbf{n}_{J_3}}{dh} - \frac{d\hat{\mathbf{e}}_2^T}{dh}\mathbf{n}_{J_3}\right)}{1 - \frac{1}{4}\left(\hat{\mathbf{e}}_3^T \mathbf{n}_{J_2} - \hat{\mathbf{e}}_2^T \mathbf{n}_{J_3}\right)^{1/2}} \tag{4.103}$$

$$\frac{d\theta_{J_2}}{dh} = \frac{\frac{1}{2}\left(\hat{\mathbf{e}}_1^T \frac{d\mathbf{n}_{J_3}}{dh} + \frac{d\hat{\mathbf{e}}_1^T}{dh}\mathbf{n}_{J_3} - \hat{\mathbf{e}}_3^T \frac{d\mathbf{n}_{J_1}}{dh} - \frac{d\hat{\mathbf{e}}_3^T}{dh}\mathbf{n}_{J_1}\right)}{1 - \frac{1}{4}\left(\hat{\mathbf{e}}_1^T \mathbf{n}_{J_3} - \hat{\mathbf{e}}_3^T \mathbf{n}_{J_1}\right)^{1/2}} \tag{4.104}$$

$$\frac{d\theta_{J_3}}{dh} = \frac{\frac{1}{2}\left(\hat{\mathbf{e}}_2^T \frac{d\mathbf{n}_{J_1}}{dh} + \frac{d\hat{\mathbf{e}}_2^T}{dh}\mathbf{n}_{J_1} - \hat{\mathbf{e}}_1^T \frac{d\mathbf{n}_{J_2}}{dh} - \frac{d\hat{\mathbf{e}}_1^T}{dh}\mathbf{n}_{J_2}\right)}{1 - \frac{1}{4}\left(\hat{\mathbf{e}}_2^T \mathbf{n}_{J_1} - \hat{\mathbf{e}}_1^T \mathbf{n}_{J_2}\right)^{1/2}} \tag{4.105}$$

The sensitivity of the axial displacement (with reference to the basic system) can be obtained by taking the derivative of Eq. (4.40) with respect to parameter h.

$$\frac{du_1}{dh} = \frac{1}{L_d + L}\left[(2\mathbf{X}_{IJ} + \mathbf{u}_{IJ})^T \frac{d\mathbf{u}_{IJ}}{dh} + (2\frac{d\mathbf{X}_{IJ}}{dh} + \frac{d\mathbf{u}_{IJ}}{dh})^T \mathbf{u}_{IJ}\right] - \frac{\frac{dL_d}{dh} + \frac{dL_n}{dh}}{(L_d + L_n)^2}(2\mathbf{X}_{IJ} + \mathbf{u}_{IJ})^T \mathbf{u}_{IJ} \tag{4.106}$$

4.10 Sensitivity of The Global-Local Transformation Matrix

The sensitivity of the global-local transformation matrix can be obtained by differentiating Eq. (4.54) though Eq. (4.60) with respect to parameter h. The sensitivities of the auxiliary matrices, $\mathbf{A}$, $\mathbf{L}$, and $\mathbf{h}$, are omitted here for brevity and provided in appendix B.

$$\frac{d\mathbf{t}_1}{dh} = \begin{bmatrix} -\frac{d\hat{\mathbf{e}}_1^T}{dh} & \mathbf{0}^T & \frac{d\hat{\mathbf{e}}_1^T}{dh} & \mathbf{0}^T \end{bmatrix} \tag{4.107}$$

$$\frac{d\mathbf{t}_2}{dh} = \frac{1}{2\cos(\theta_{I_3})}\left[\mathbf{L}(\bar{\mathbf{r}}_2)\frac{d\mathbf{n}_{I_1}}{dh} + \frac{d\mathbf{L}(\bar{\mathbf{r}}_2)}{dh}\mathbf{n}_{I_1} + \frac{d\mathbf{h}_{I_3}}{dh}\right]^T + \frac{\sin(\theta_{I_3})}{2\cos^2(\theta_{I_3})}\frac{d\theta_{I_3}}{dh}\left[\mathbf{L}(\bar{\mathbf{r}}_2)\mathbf{n}_{I_1} + \mathbf{h}_{I_3}\right]^T \tag{4.108}$$

where $\mathbf{n}_{I_1}$ is finite component of $\mathbf{N}_I$, similar for others.

$$\frac{d\mathbf{t}_3}{dh} = \frac{1}{2\cos(\theta_{J_3})}\left[\mathbf{L}(\bar{\mathbf{r}}_2)\frac{d\mathbf{n}_{J_1}}{dh} + \frac{d\mathbf{L}(\bar{\mathbf{r}}_2)}{dh}\mathbf{n}_{J_1} + \frac{d\mathbf{h}_{J_3}}{dh}\right]^T + \frac{\sin(\theta_{J_3})}{2\cos^2(\theta_{J_3})}\frac{d\theta_{J_3}}{dh}\left[\mathbf{L}(\bar{\mathbf{r}}_2)\mathbf{n}_{J_1} + \mathbf{h}_{J_3}\right]^T \tag{4.109}$$

$$\frac{d\mathbf{t}_4}{dh} = \frac{1}{2\cos(\theta_{I_2})}\left[-\mathbf{L}(\bar{\mathbf{r}}_3)\frac{d\mathbf{n}_{I_1}}{dh} - \frac{d\mathbf{L}(\bar{\mathbf{r}}_3)}{dh}\mathbf{n}_{I_1} - \frac{d\mathbf{h}_{I_2}}{dh}\right]^T + \frac{\sin(\theta_{I_2})}{2\cos^2(\theta_{I_2})}\frac{d\theta_{I_2}}{dh}\left[-\mathbf{L}(\bar{\mathbf{r}}_3)\mathbf{n}_{I_1} - \mathbf{h}_{I_2}\right]^T \tag{4.110}$$

$$\frac{d\mathbf{t}_5}{dh} = \frac{1}{2\cos(\theta_{J_2})}\left[-\mathbf{L}(\bar{\mathbf{r}}_3)\frac{d\mathbf{n}_{J_1}}{dh} - \frac{d\mathbf{L}(\bar{\mathbf{r}}_3)}{dh}\mathbf{n}_{J_1} - \frac{d\mathbf{h}_{J_2}}{dh}\right]^T + \frac{\sin(\theta_{J_2})}{2\cos^2(\theta_{J_2})}\frac{d\theta_{J_2}}{dh}\left[-\mathbf{L}(\bar{\mathbf{r}}_3)\mathbf{n}_{J_1} - \mathbf{h}_{J_2}\right]^T \tag{4.111}$$

$$\frac{d\mathbf{t}_{6J}}{dh} = \frac{1}{2\cos(\theta_{J_1})}\left[\mathbf{L}(\bar{\mathbf{r}}_3)\frac{d\mathbf{n}_{J_2}}{dh} + \frac{d\mathbf{L}(\bar{\mathbf{r}}_3)}{dh}\mathbf{n}_{J_2} - \mathbf{L}(\bar{\mathbf{r}}_2)\frac{d\mathbf{n}_{J_3}}{dh} - \frac{d\mathbf{L}(\bar{\mathbf{r}}_2)}{dh}\mathbf{n}_{J_3} + \frac{d\mathbf{h}_{J_1}}{dh}\right]^T + \frac{\sin(\theta_{J_1})}{2\cos(\theta_{J_1})}\frac{d\theta_{J_1}}{dh}\left[\mathbf{L}(\bar{\mathbf{r}}_3)\mathbf{n}_{J_2} - \mathbf{L}(\bar{\mathbf{r}}_2)\mathbf{n}_{J_3} + \mathbf{h}_{J_1}\right]^T \tag{4.112}$$

$$\frac{d\mathbf{t}_{6_I}}{dh} = \frac{1}{2\cos(\theta_{I_1})}\left[\mathbf{L}(\bar{\mathbf{r}}_3)\frac{d\mathbf{n}_{I_2}}{dh} + \frac{d\mathbf{L}(\bar{\mathbf{r}}_3)}{dh}\mathbf{n}_{I_2} - \mathbf{L}(\bar{\mathbf{r}}_2)\frac{\mathbf{n}_{I_3}}{dh} - \frac{d\mathbf{L}(\bar{\mathbf{r}}_2)}{dh}\mathbf{n}_{I_3} + \frac{d\mathbf{h}_{I_1}}{dh}\right]^T + \frac{\sin(\theta_{I_1})}{2\cos(\theta_{I_1})}\frac{d\theta_{I_1}}{dh}\left[\mathbf{L}(\bar{\mathbf{r}}_3)\mathbf{n}_{I_2} - \mathbf{L}(\bar{\mathbf{r}}_2)\mathbf{n}_{I_3} + \mathbf{h}_{I_1}\right]^T \tag{4.113}$$

4.11 Numerical Examples

The derived DDM sensitivity formulation for corotational space frame elements have been implemented in OpenSees and verified through standalone sensitivity analyses for a cantilever beam and multistory steel frame structure.

4.11.1 Cantilever Example

The cantilever shown in Fig. 4.7 is a commonly used verification example for geometrically nonlinear frame element formulations [38, 51]. A bilinear stress-strain relationship is assumed with yield stress, f_y= 30.0 ksi, elastic modulus, E=30,000 ksi, kinematic hardening, H_{kin}=3000.0 ksi, and Poisson's ratio, ν=0.3. The length, L, is 5 in and the section is rectangular with dimensions 0.1 in by 0.5 in. Geometric nonlinear analysis is performed using one force based beam-column element with four Gauss-Lobatto integration points. The section is discretized into 30 by 30 fibers. Previous work with this example included shear deformation at the section and material level; however, these effects are neglected here as the focus is on DDM sensitivity of the corotational formulation, which is independent of the material formulation. A vertical displacement is applied at the free end and the structural analysis is performed using displacement control solution method. The shear force-displacement relationship is recorded as shown in Fig. 4.8.

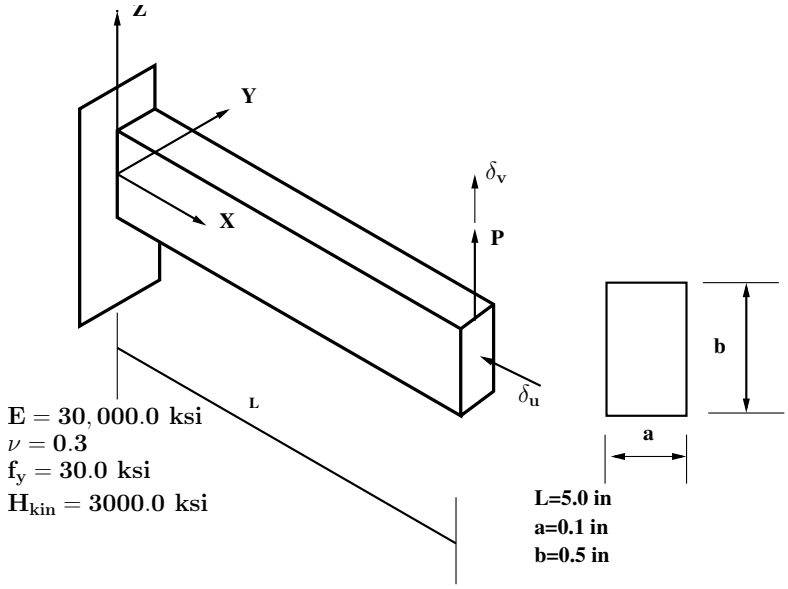

Figure 4.7: Cantilever beam subjected to shear force at the free end.

Standalone sensitivity analyses of the load factor and the free end rotation are performed with respect to the modulus of elasticity E, yield strength, f_y, and the kinematic hardening, H_{Kin}. The perturbed value used with FDM is 0.0001 times the value of the uncertain parameter. Compatible results are obtained for both DDM and FDM as shown in Fig. 4.9, Fig. 4.10, and Fig. 4.11.

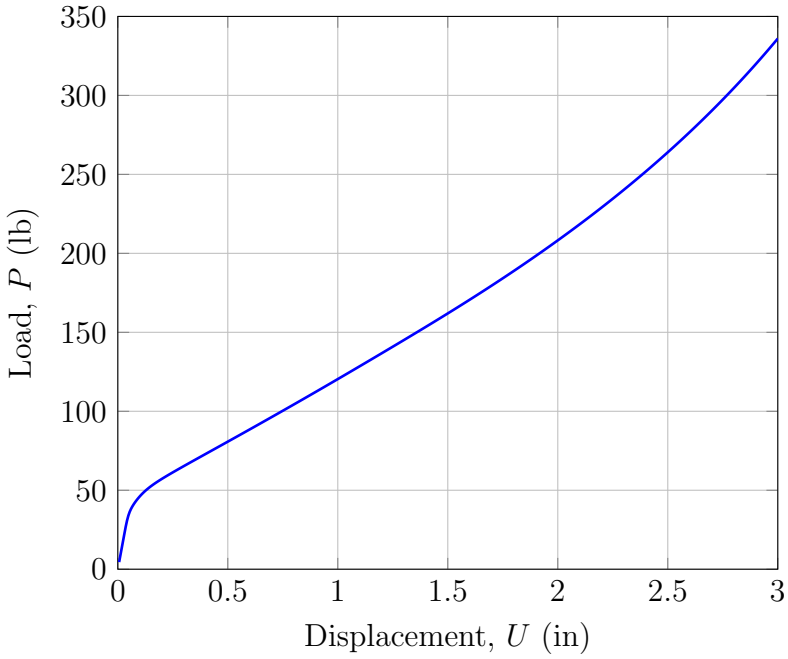

Figure 4.8: Load-displacement relationship at the free end of the Cantilever beam.

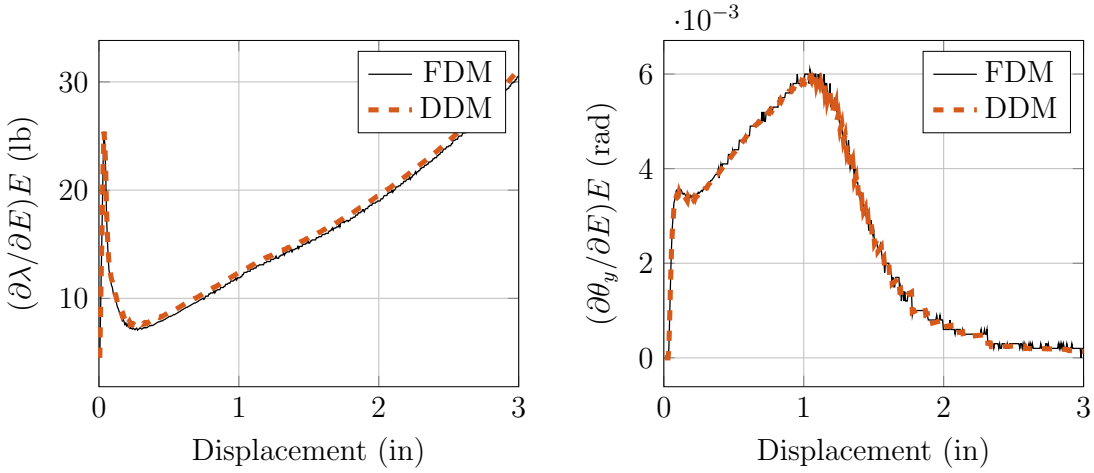

Figure 4.9: Response sensitivity of load factor and free end rotation with respect to the modulus of elasticity, E.

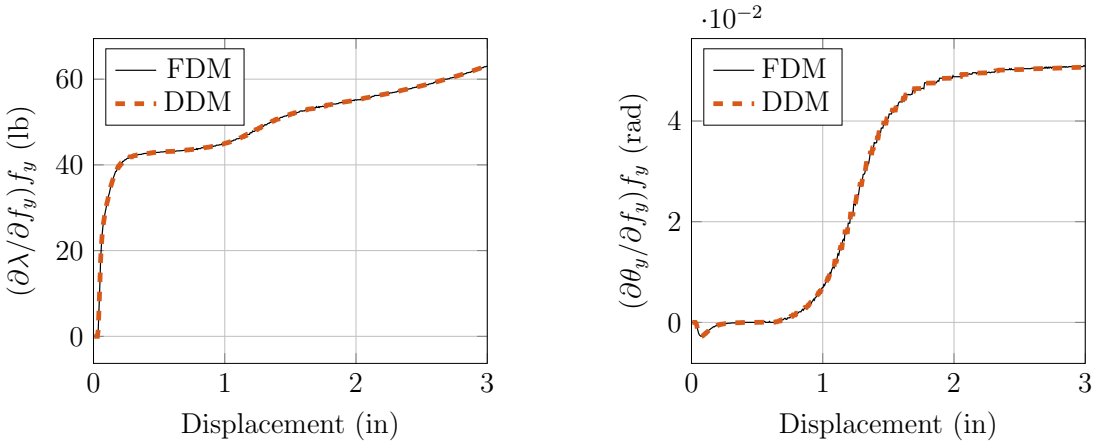

Figure 4.10: Response sensitivity of load factor and free end rotation with respect to the yield strength, f_y.

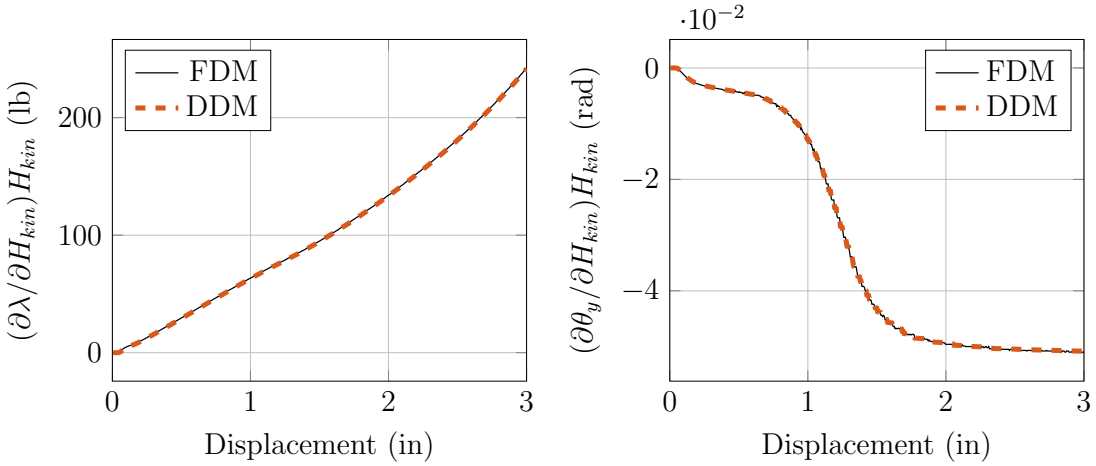

Figure 4.11: Response sensitivity of load factor and free end rotation with respect to the kinematic strain hardening, H_{kin}.

4.11.2 Two-Story Three-Dimensional Frame

A three-dimensional frame, which was analyzed by many researchers such as [4], [1], and [20], is used in this example. Elastic perfectly plastic material is used with elastic modulus, E=19613 MPa, yield strength, f_y=98 MPa, and Poisson's ratio ν=0.17. Beam and column sections are rectangular with dimensions shown in Fig. 4.12.

The section is discretized into 30 by 30. Geometric nonlinear analysis is performed using one force beam-column element per member with five Lobatto integration points. The analysis is performed by controlling the horizontal roof displacement, and the lateral load-displacement relationship is recorded as shown in Fig. 4.13

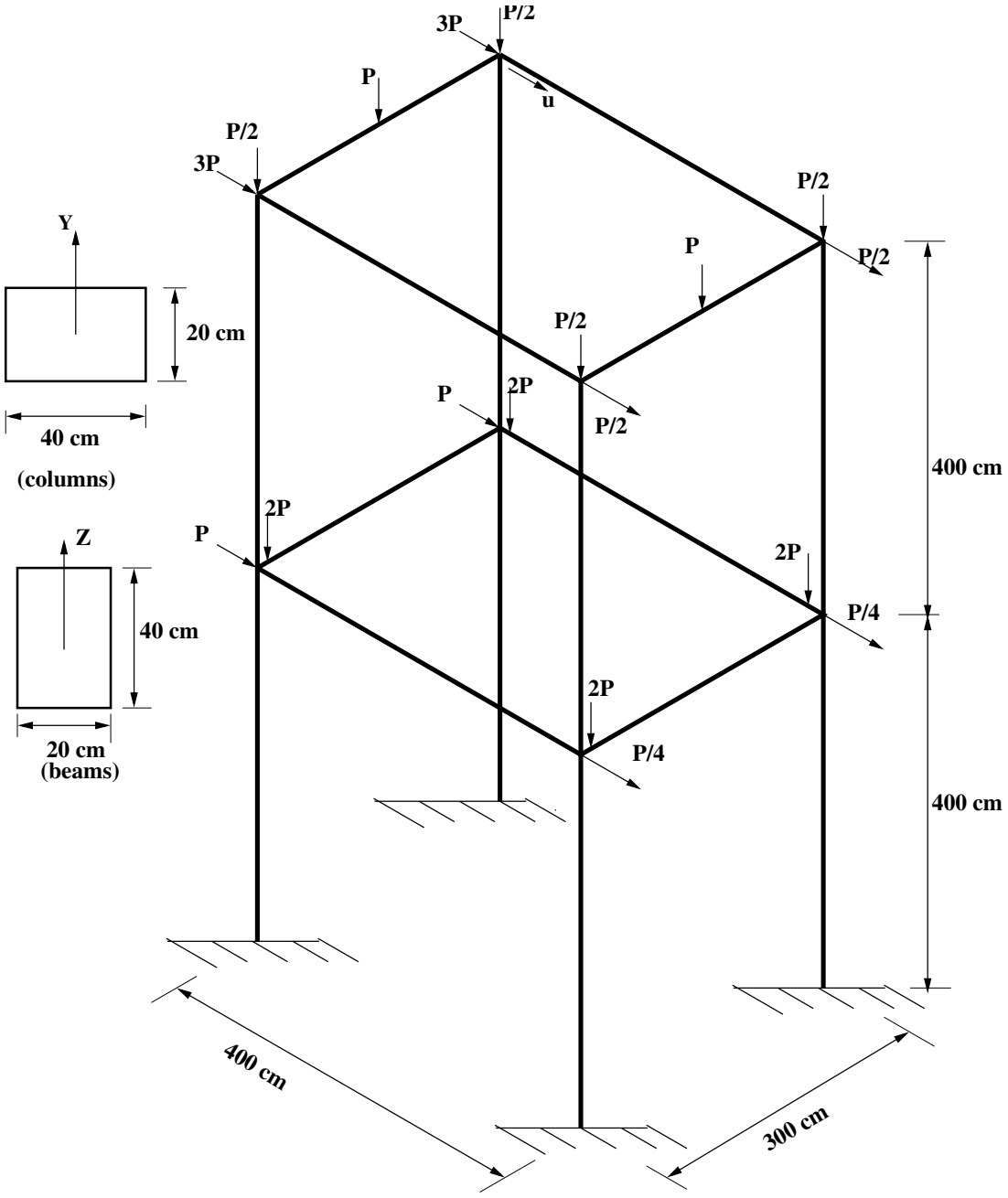

Figure 4.12: Two-story frame.

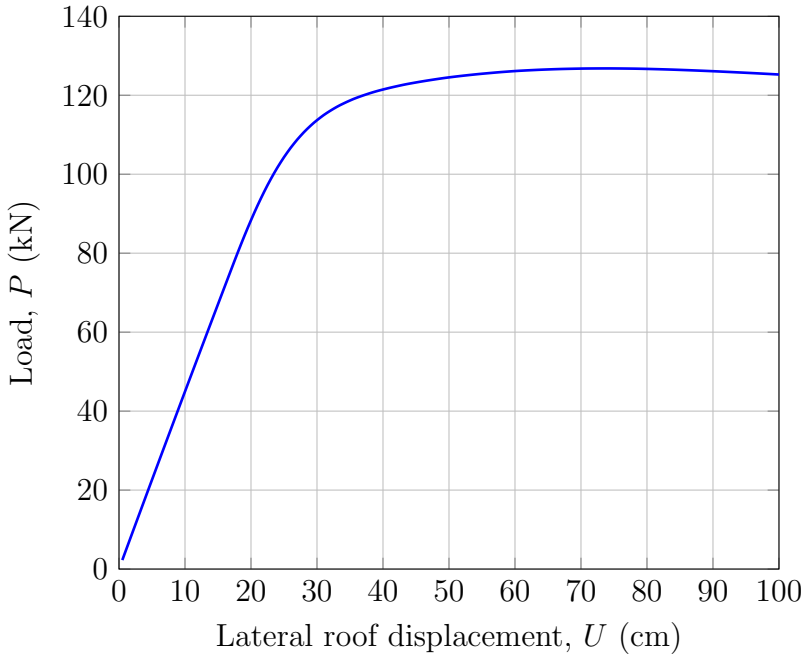

Figure 4.13: Load-displacement relationship for two-story frame.

Standalone sensitivity analyses of the load factor and the horizontal roof displacement are performed with respect to the modulus of elasticity, E and yield strength, f_y. The perturbed value used with FDM is 0.0001 times the value of the uncertain parameter. Compatible results are obtained for both DDM and FDM, as shown in Fig. 4.14 and Fig. 4.15. Note that the effect of f_y parameter starts at displacement of 18.5 cm. The discrete jumps observed in Fig. 4.15 and Fig. 4.14 occur when the steel section yields at lateral roof displacement of 34 cm.

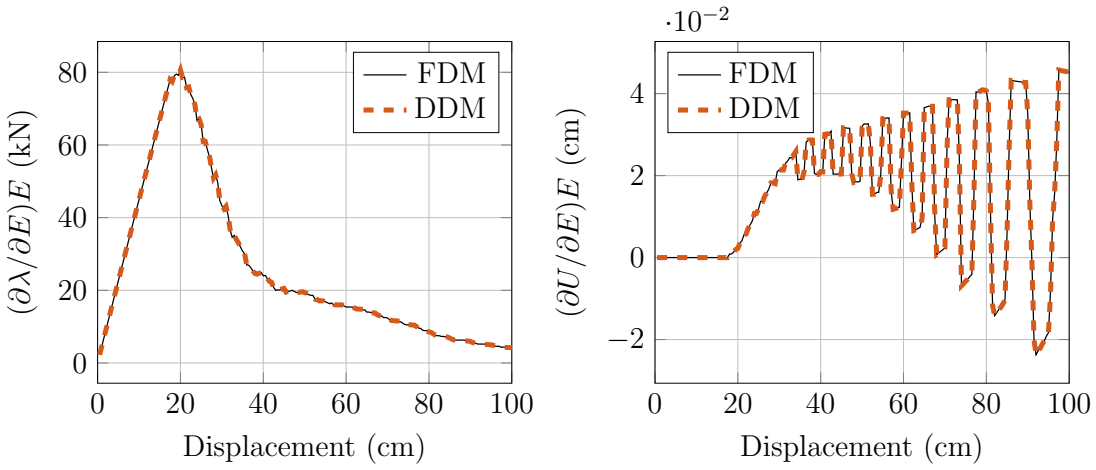

Figure 4.14: Response sensitivity of load factor and lateral roof displacement with respect to the modulus of elasticity, E.

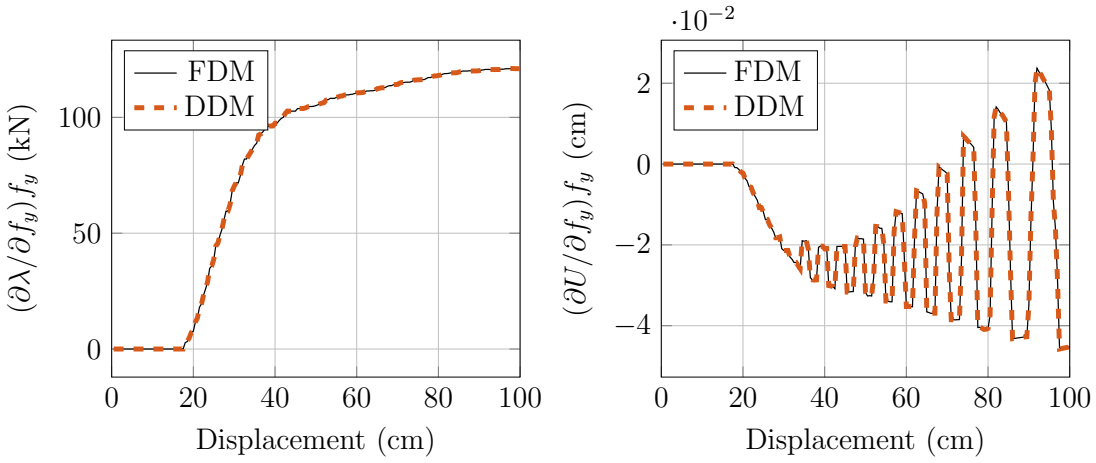

Figure 4.15: Response sensitivity of load factor and lateral roof displacement with respect to the yield strength, f_y.

4.12 Conclusion

Response sensitivity equations using direct differentiation method (DDM) are obtained for corotational space frame finite elements. In order to overcome the problem of violating vector properties, Crisfield algorithm [19] is used to obtain the triads of the deformed configuration. The derived equations are implemented in OpenSees software and verified with finite difference method (FDM) through a set of standalone sensitivity analyses for simple and complex structures. The response sensitivity results obtained by DDM are compatible with those obtained by FDM. By including sensitivity equations in the implementation of 3D corotational space frame elements, the DDM response sensitivity can be used in simulating material and geometric nonlinear formulations of frame finite elements in three dimensional simulations, giving researchers a powerful tool for gradient-based applications that can help prevent man-made and natural hazards from becoming disasters through robust reliability-based design optimization.

Acknowledgments

This research was made possible through the support of the Higher Committee for Education Development (HCED) in Iraq. Any opinions, findings, and conclusions or recommendations expressed in this material are those of the authors and do not necessarily reflect the views of the HCED.

5 Conclusion

The response sensitivity equations of geometric nonlinear finite element formulations including geometric-nonlinear displacement-based frame finite elements, displacement control solution method, and the three dimensional space frame element have been obtained. Direct differentiation method (DDM) is used to derive the response sensitivity equations for the aforementioned formulations where the sensitivity equations are derived within the finite element algorithm. The derived equations are implemented in OpenSees software framework. Standalone sensitivity analyses are used to verify the accuracy of the derived equations by comparing the response sensitivity results obtained by DDM with those obtained by finite difference method (FDM).

Analytical response sensitivity of geometrically nonlinear displacement-based frame finite elements is developed for uncertain material, cross-section dimension, nodal coordinate, and load parameters. The derivation is based on moderate rotations within the element basic system which leads to additional terms in the conditional derivative of basic forces. Examples of standalone sensitivity analysis verify the DDM implementation for the geometrically nonlinear formulation. Finite element reliability analysis of a steel frame shows that a lower reliability index is obtained compared to the standard geometrically linear formulation; however, the importance measures differ only slightly with axial loads having higher

importance with the geometrically nonlinear formulation. These results indicate that modeling decisions are important for estimating the probability of failure, but not necessarily the importance ranking when comparing geometrically linear and nonlinear displacement-based formulations.

Furthermore, displacement control solution method is extended by including the response sensitivity equations using the direct differentiation method (DDM). The DDM sensitivity derivations are applied to the incremental-iterative equations developed by [13]. The derived equations are implemented in the finite element software framework OpenSees, and the equations are verified by comparing the DDM equations with the finite difference computations through stand-alone sensitivity analysis of structural models with geometric and material nonlinearity. Probabilistic analyses of a multistory steel frame using the first order reliability method give the reliability index, probability of failure, and importance measures for displacement-controlled analyses. Future work will extend DDM sensitivity analysis to other continuation methods such as the arc-length and minimum unbalanced displacement norm approaches [13].

For 3D space frame element. response sensitivity equations using direct differentiation method (DDM) are obtained. In order to overcome the problem of violating vector properties, Crisfield algorithm [19] is used to obtain the triads of the deformed configuration in the formulation of large displacement of space frame. The derived equations are implemented OpenSees software and verified with finite difference method (FDM) through a set of standalone sensitivity analyses for simple and complex structures. The response sensitivity results obtained by DDM are

compatible with those obtained by FDM. By including sensitivity equations in the implementation of 3D corotational space frame element, the DDM response sensitivity can be used in simulating material and geometric nonlinear formulations of frame finite elements in three dimensional simulations, giving researchers a powerful tool for gradient-based applications that can help prevent man-made and natural hazards from becoming disasters through robust reliability-based design optimization.

Bibliography

[1] Reza Abbasnia and Aslam Kassimali. Large deformation elastic-plastic analysis of space frames. *Journal of Constructional Steel Research*, 35(3):275 – 290, 1995.

[2] Md.Iftekharul Alam and Dookie Kim. Effect of constitutive material models on seismic response of two-story reinforced concrete frame. *International Journal of Concrete Structures and Materials*, 6(2):101–110, 2012.

[3] Kevin R. Collins Anderizej S. Nowak. *Reliability of structures*. Taylor and Francis Group, 2nd edition, 2012.

[4] John Argyris. An excursion into large rotations. *Computer Methods in Applied Mechanics and Engineering*, 32(1):85 – 155, 1982.

[5] M. Barbato and J. P. Conte. Finite element response sensitivity analysis: A comparison between force-based and displacement-based frame element models. *Computer Methods in Applied Mechanics and Engineering*, 194:1479–1512, 2005.

[6] M. Barbato and J. P. Conte. Finite element structural response sensitivity and reliability analyses using smooth versus non-smooth material constitutive models. *International Journal of Reliability and Safety*, 1(1/2):3–39, 2006.

[7] M. Barbato, A. Zona, and J. P. Conte. Finite element response sensitivity analysis using three-field mixed formulation: general theory and application to frame structures. *International Journal for Numerical Methods in Engineering*, 69(1):114–161, 2007.

[8] Jean-Louis Batoz and Gouri Dhatt. Incremental displacement algorithms for nonlinear problems. *International Journal for Numerical Methods in Engineering*, 14(8):1262–1267, 1979.

[9] A. Bebamzadeh and T. Haukaas. Second-order sensitivities of inelastic finite-element response by direct differentiation. *Journal of Engineering Mechanics*, 134(10):867–880, 2008.

[10] A. Bebamzadeh, T. Haukaas, R. Vaziri, A. Poursartip, and G. Fernlund. Application of response sensitivity in composite processing. *Journal of Composite Materials*, 44(15):1821–1840, 2010.

[11] W. Chen and S. Chan. Second-order inelastic analysis of steel frames using element with midspan and end springs. *Journal of Structural Engineering*, 121(3):530–541, 1995.

[12] Kyung K Choi and Nam-Ho Kim. *Structural sensitivity analysis and optimization 1: linear systems*. Springer Science & Business Media, 2006.

[13] M. J. Clarke and G. J. Hancock. A study of incremental-iterative strategies for non-linear analyses. *International Journal for Numerical Methods in Engineering*, 29:1365–1391, 1990.

[14] J. P. Conte, M. Barbato, and E. Spacone. Finite element response sensitivity analysis using force-based frame models. *International Journal of Numerical Methods in Engineering*, 59(13):1781–1820, 2004.

[15] R. D. Cook, D. S. Malkus, M. E. Plesha, and R. J. Witt. *Concepts and Applications of Finite Element Analysis*. John Wiley & Sons, 4th edition, 2002.

[16] M. A. Crisfield. A fast incremental/iterative solution procedure that handles snap-through. *Computers & Structures*, 13(13):55 –62, 1981.

[17] M. A. Crisfield. A consistent co-rotational formulation for non-linear, three dimensional beam elements. *Computer Methods in Applied Mechanics and Engineering*, 81:131–150, 1990.

[18] M. A. Crisfield. *Non-linear Finite Element Analysis of Solids and Structures*, volume 1. John Wiley & Sons, 1991.

[19] M. A. Crisfield. *Non-linear Finite Element Analysis of Solids and Structures*, volume 2. John Wiley & Sons, 1997.

[20] R. M. De Souza. *Force-Based Finite Element for Large Displacement Inelastic Analsysis of Frames*. PhD thesis, University of California, Berkeley, CA, 2000.

[21] M. H. El-Zanaty and D. W. Murray. Nonlinear finite element analysis of steel frames. *Journal of Structural Engineering*, pages 353–369, 1983.

[22] M. Fafard and B. Massicotte. Geometrical interpretation of the arc-length method. *Computers & Structures*, 46(4):603 – 615, 1993.

[23] C. A. Felippa and B. Haugen. A unified formulation of small-strain corotational finite elements: I. Theory. *Computer Methods in Applied Mechanics and Engineering*, 194(21-24):2285–2335, 2005.

[24] FEMA. State of the art report on systems performance of steel moment frames subject to earthquake ground shaking. Technical Report FEMA-355C, Federal Emergency Management Association, 2000.

[25] Y. T. Feng, D. Peri, and D. R.J. Owen. A new criterion for determination of initial loading parameter in arc-length methods. *Computers & Structures*, 58(3):479–485, 1996.

[26] P. Franchin. Reliability of uncertain inelastic structures under earthquake excitation. *Journal of Engineering Mechanics*, 130(2):180–191, 2004.

[27] Yanglin Gong, Lei Xu, and Don E. Grierson. Sensitivity analysis of steel moment frames accounting for geometric and material nonlinearity. *Computers and Structures*, 84(7):462–475, 2006.

[28] Q. Gu, M. Barbato, and J. P. Conte. Handling of constraints in finite-element response sensitivity analysis. *Journal of Engineering Mechanics*, 135(12):1427–1438, 2009.

[29] Q. Guo and A. Jeffers. Direct differentiation method for response sensitivity analysis of structures in fire. *Engineering Structures*, 10.1016/j.engstruct.2014.06.025, 2014.

[30] T. Haukaas and A. Der Kiureghian. Parameter sensitivity and importance measures in nonlinear finite element reliability analysis. *Journal of Engineering Mechanics*, 131(10):1013–1026, 2005.

[31] Terje Haukaas and Michael H. Scott. Shape sensitivities in the reliability analysis of nonlinear frame structures. *Computers & Structures*, 84(15-16):964 – 977, 2006.

[32] K.D. Hjelmstad. *Fundamentals of Structural Mechanics*. Springer US, 2010.

[33] D. C. Kent and R. Park. Flexural members with confined concrete. *Journal of the Structural Division, ASCE*, 97(7):1969–1990, 1971.

[34] Ravi Kiran, Lei Li, and Kapil Khandelwal. Complex perturbation method for sensitivity analysis of nonlinear trusses. *Journal of Structural Engineering*, 0(0):04016154, 2016.

[35] M. Kleiber, H. Antunez, T. D. Hien, and P. Kowalczyk. *Parameter Sensitivity in Nonlinear Mechanics*. John Wiley & Sons, 1997.

[36] M. Kleiber and T. D. Hien. Parameter sensitivity of inelastic buckling and post-buckling response. *Computer Methods in Applied Mechanics and Engineering*, 145(3-4):239–262, 1997.

[37] A. R. Klumpp. Singularity-free extraction of a quaternion from a direction-cosine matrix. *Journal of Spacecraft and Rockets*, 13(12):754–755, 1976.

[38] K. Kondoh and S. N. Atluri. Large-deformation, elasto-plastic analysis of frames under nonconservative loading, using explicitly derived tangent stiffnesses based on assumed stresses. *Computational Mechanics*, 2(1):1–25, 1987.

[39] C.-L. Lee and F. C. Filippou. Frame elements with mixed formulation for singular section response. *International Journal for Numerical Methods in Engineering*, 78(11):1320–1344, 2009.

[40] H. O. Madsen, S. Krenk, and N. C. Lind. *Methods of Structural Safety*. Dover, 2006.

[41] J. B. Mander, M. J. N. Priestley, and R. Park. Theoretical stress-strain model for confined concrete. *Journal of Structural Engineering*, 114(8):1804–1826, August 1988.

[42] I. M. May, J. H. Naji, and T. H. Ganaba. Displacement control for the non-linear analysis of reinforced concrete structures. *Engineering Computations*, 5:266–273, 1988.

[43] F. McKenna, M. H. Scott, and G. L. Fenves. Nonlinear finite-element analysis software architecture using object composition. *Journal of Computing in Civil Engineering*, 24(1):95–107, 2010.

[44] J.L. Meek and Hoon Swee Tan. Geometrically nonlinear analysis of space frames by an incremental iterative technique. *Computer Methods in Applied Mechanics and Engineering*, 47(3):261 – 282, 1984.

[45] Robert E. Melchers. *Structural Reliability Analysis and Prediction, 2nd Edition.* Wiley., 1999.

[46] B. A Memon and X. Z. Su. Arc-length for nonlinear finite element analysis. *J Zhejiang Univ Sci*, 5:618–628., 2004.

[47] A. Neuenhofer and F. C. Filippou. Evaluation of nonlinear frame finite-element models. *Journal of Structural Engineering*, 123(7):958–966, July 1997.

[48] A. Neuenhofer and F. C. Filippou. Geometrically nonlinear flexibility-based frame finite element. *Journal of Structural Engineering*, 124(6):704–711, June 1998.

[49] B. Nour-Omid and C.C. Rankin. Finite rotation analysis and consistent linearization using projectors. *Computer Methods in Applied Mechanics and Engineering*, 93(3):353 – 384, 1991.

[50] A.S. Nowak and K.R. Collins. *Reliability of Structures, Second Edition.* Taylor & Francis, 2012.

[51] M. S. Park and B. C. Lee. Geometrically non-linear and elastoplastic three-dimensional shear flexible beam element of Von-Mises-type hardening material. *International Journal for Numerical Methods in Engineering*, 39:383–408, 1996.

[52] Graham Powell and Jeffrey Simons. Improved iteration strategy for nonlinear structures. *International Journal for Numerical Methods in Engineering*, 17(10):1455–1467, 1981.

[53] M. H. Scott. Evaluation of force-based frame element response sensitivity formulations. *Journal of Structural Engineering*, 138(1):72–80, January 2012.

[54] M. H. Scott. Response sensitivity of geometrically nonlinear force-based frame elements. *Journal of Structural Engineering*, 139(11):1963–1972, 2013.

[55] M. H. Scott. Response sensitivity of geometrically nonlinear force-based frame elements. *Journal of Structural Engineering*, 139(11):1963–1972, November 2013.

[56] M. H. Scott and F. C. Filippou. Exact response gradients for large displacement nonlinear beam-column elements. *Journal of Structural Engineering*, 133(2):155–165, February 2007.

[57] M. H. Scott and F. C. Filippou. Response gradients for nonlinear beam-column elements under large displacements. *Journal of Structural Engineering*, 133(2):155–165, 2007.

[58] M. H. Scott, P. Franchin, G. L. Fenves, and F. C. Filippou. Response sensitivity for nonlinear beam-column elements. *Journal of Structural Engineering*, 130(9):1281–1288, September 2004.

[59] M. H. Scott, P. Franchin, G. L. Fenves, and F. C. Filippou. Response sensitivity for nonlinear beam-column elements. *Journal of Structural Engineering*, 130(9):1281–1288, September 2004.

[60] M. H. Scott and O. M. Hamutçuoğlu. Analytical sensitivity of interpolatory quadrature in force-based frame elements. *Communications in Numerical Methods in Engineering*, 26(12):1586–1595, 2010.

[61] M. H. Scott and T. Haukaas. Software framework for parameter updating and finite-element response sensitivity analysis. *Journal of Computing in Civil Engineering*, 22(5):281–291, 2008.

[62] O Sergeyev and Z Mroz. Sensitivity analysis and optimal design of 3d frame structures for stress and frequency constraints. *Computers & Structures*, 75(2):167–185, 2000.

[63] M. S. A. Siddiquee, T. Tanaka, and F. Tatsuoka. Tracing the equilibrium path by dynamic relaxation in materially nonlinear problems. *International Journal for Numerical and Analytical Methods in Geomechanics*, 19(11):749–767, 1995.

[64] J.C. Simo and L. Vu-Quoc. A three-dimensional finite-strain rod model. part ii: Computational aspects. *Computer Methods in Applied Mechanics and Engineering*, 58(1):79 – 116, 1986.

[65] Kerry W. Spring. Euler parameters and the use of quaternion algebra in the manipulation of finite rotations: A review. *Mechanism and Machine Theory*, 21(5):365 – 373, 1986.

[66] R. A Spurrier. Comment on singularity-free extraction of a quaternion from a direction-cosine matrix. *Journal of Spacecraft and Rocket*, 15(4):255 – 256, 1978.

[67] H. Tanaka and R. Park. Effect of lateral confining reinforcement on the ductile behaviour of reinforced concrete columns. Technical Report 90-2, Dept. of Civil Engineering, University of Canterbury, U.K., 1990.

[68] Lip H. Teh and Murray J. Clarke. Co-rotational and lagrangian formulations for elastic three-dimensional beam finite elements. *Journal of Constructional Steel Research*, 48(23):123 – 144, 1998.

[69] J. J. Tsay and J. S. Arora. Nonlinear structural design sensitivity analysis for path dependent problems. Part I: General theory. *Computer Methods in Applied Mechanics and Engineering*, 81:183–208, 1990.

[70] Roger A. Wehage. *Quaternions and Euler Parameters — A Brief Exposition*, pages 147–180. Springer Berlin Heidelberg, Berlin, Heidelberg, 1984.

[71] Xi Zhang, KJR Rasmussen, and H Zhang. Formulation and implementation of threedimensional doubly symmetric beam-column analyses with warping effect in opensees. Technical report, Research Report R917, 2011.

[72] Y. Zhang and A. Der Kiureghian. Dynamic response sensitivity of inelastic structures. *Computer Methods in Applied Mechanics and Engineering*, 108:23–36, 1993.

[73] H. Zheng, D. F. Liu, C. F. Lee, and L. G. Tham. Displacement-controlled method and its applications to material non-linearity. *International Journal for Numerical and Analytical Methods in Geomechanics*, 29(3):209–226, 2005.

[74] Minjie Zhu and Michael H. Scott. Direct differentiation of the particle finite-element method for fluid-structure interaction. *Journal of Structural Engineering*, 142(3):04015159, 2016.

APPENDIX

A Spring Example

A.1 Spring Example

The goal of the following example is to illustrate the redundancy of the derivative of the structural tangent stiffness on the proposed sensitivity equations of displacement control solution method. A simple spring system is presented in this example. The system has two unconstrained displacements with three spring elements as shown in Fig. A.1. The basic force-deformation relationship is presented by Eq.(A.1), Fig. A.2, and Fig. A.3.

$$P_b\left(U_b\right) = P_{bo}\left(\left(3\frac{U_b}{U_{bo}}\right) - \left(\frac{U_b}{U_{bo}}\right)^3\right) \tag{A.1}$$

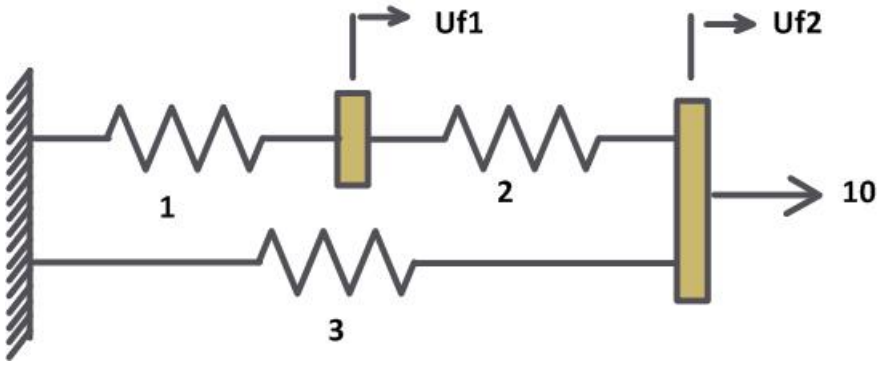

Figure A.1: Two-DOF spring example

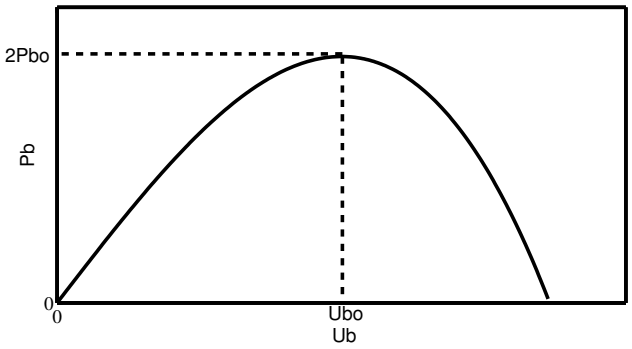

Figure A.2: Force-deformation values of each spring element

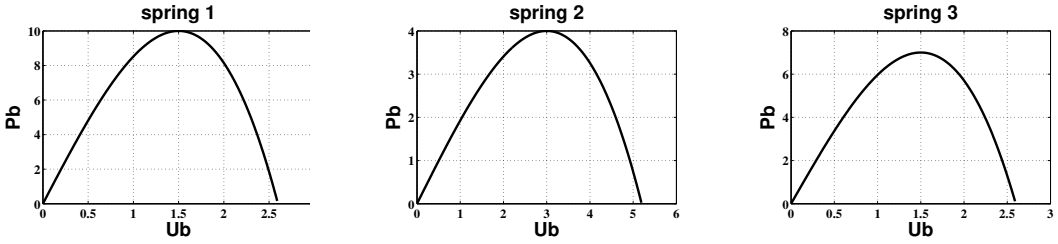

Figure A.3: Force-deformation values of each spring element

The values of U_{bo} and P_{bo} are shown in table A.1.

Table A.1: Force-deformation values of each spring element

Springnumber	P_{bo}	U_{bo}
1	5	1.5
2	2	3
3	3.5	1.5

The sensitivity of the load factor to the peak response force at the spring element one is plotted using both DDM and FDM methods as shown in Fig. A.4. One step of analysis is performed twice. The first analysis considers $\partial[\mathbf{K}_T]_i^j/\partial h = 0$ while the second analysis considers $\partial[\mathbf{K}_T]_i^j/\partial h \neq 0$ and the sensitivity of the load factor to the maximum load (Pb_{01}) of spring 1 is recorded .

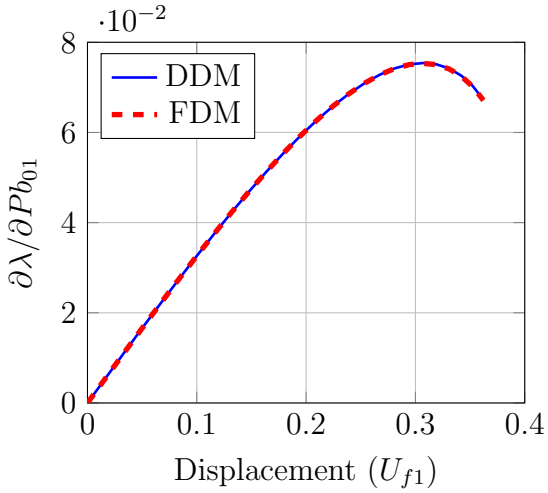

Figure A.4: Sensitivity of the load factor to the peak response force of spring element one

A.1.1 Case 1: $\partial[\mathbf{K}_T]_i^j/\partial h = 0$

For this example, the sensitivity of the tangent displacement vector is zero, where no solution for the sensitivity of the load factor can be attained in the first iteration. The solution is achieved after three iterations.

A.1.2 The First Iterative Cycle, j=1

The tangent stiffness matrix of all iterations can be obtained via the matrix-triple product.

$[\mathbf{K}_T]_i^j = \mathbf{A}_f^T[\mathbf{K}_b]_i^j\mathbf{A}_f$

where $\mathbf{A}_f$ is the compatibility matrix.

$[\mathbf{K}_T]_1^1 = \begin{bmatrix} 11.9977 & -1.9977 \\ -1.9977 & 8.9666 \end{bmatrix}$

The reference load vector is defined as

$\{\mathbf{P}_{ref}\} = \{0, 1\}^T$

The tangent displacement vector and its derivative can be obtained by applying Eq. (3.3) and Eq. (3.20), respectively.

$\{\mathbf{U}_{ft}\}_1^1 = \{0.0193, 0.1158\}^T$

$\frac{\partial\{\mathbf{U}_{ft}\}_1^1}{\partial P b_{01}} = \{0, 0\}^T$ Because of the zero sensitivity of the tangent displacement, the sensitivity of the load factor is zero at this iteration.

$\frac{\partial \lambda_1^1}{\partial P b_{01}} = 0$

The residual force vector and its derivative can be evaluated by applying Eq. (3.11) and Eq. (3.25), respectively.

$\{\mathbf{R}_f\}_1^1 = \{0.1999, -0.0354\}^T$

$\frac{\partial\{\mathbf{R}_f\}_1^1}{\partial P_{b0}} = \{0, 0\}^T$

More iterations are required to minimize the residual force vector to a specified tolerance (10^-6).

A.1.3 The Subsequent Iterative Cycles, $j > 1$

By following the aforementioned steps for the subsequent iterations, the residual displacement vector and its derivative can be calculated based on the residual force vector of the previous iteration as illustrated in Eqs. (3.13) and (3.24), respectively.

$\{\Delta\mathbf{U}_R\}_1^2 = \{0.01662, -0.00025\}^T$

$\frac{\partial\{\Delta\mathbf{U}_R\}_1^2}{\partial Pb_{01}} = \{0,0\}^T$

The sensitivity of the load factor can be evaluated based on the derivatives of the tangent and the residual displacements using Eq. (3.27)

$\frac{\partial\lambda_1^2}{\partial Pb_{01}} = 0$

An additional iteration is required to converge the results which leads to the exact solution for the sensitivity of the load factor ($\frac{\partial\lambda_1^3}{\partial Pb_{01}}$).

$\{\mathbf{R}_f\}_1^2 = \{0.1027 * 10^{-5}, 0.5827 * 10^{-5}\}^T$

$\frac{\partial\{\mathbf{R}_f\}_1^2}{\partial Pb_{01}} = \{-0.033325, 0\}^T$

$\frac{\partial\{\Delta\mathbf{U}_R\}_1^3}{\partial Pb_{01}} = \{-0.00288, -0.00064\}^T$

$\frac{\partial\lambda_1^3}{\partial Pb_{01}} = 0.00555$

A.1.4 Case 2: $\partial[\mathbf{K}_T]_i^j/\partial h \neq 0$

In this case the sensitivity of the tangent displacement can be obtained by

$$[\mathbf{K}_T]_i^j \frac{\partial\{\mathbf{U}_{fT}\}_i^j}{\partial h} = \frac{\partial\{\mathbf{P}_{ref}\}}{\partial h} - \frac{\partial[\mathbf{K}_T]_i^j}{\partial h}\{\mathbf{U}_{fT}\}_i^j \tag{A.2}$$

where the derivative of the stiffness matrix ($\partial[\mathbf{K}_T]_i^j/\partial h$) is based on the sensitivity of the basic stiffness matrix as shown in Eq. (A.3). Note that the sensitivity of the compatibility matrix is zero because of not considering the geometric parameters in the analysis.

$$\frac{\partial[\mathbf{K}_T]_i^j}{\partial P_{01}} = \mathbf{A}_f^T \frac{\partial[\mathbf{K}_b]_i^j}{\partial P_{01}} \mathbf{A}_f \tag{A.3}$$

A.1.5 The First Iterative Cycle, j=1

Same as before, the stiffness matrix is

$$[\mathbf{K}_T]_1^1 = \begin{bmatrix} 11.9977 & -1.9977 \\ -1.9977 & 8.9666 \end{bmatrix}$$

The derivative of the stiffness matrix can be obtained by applying Eq. (A.3)

$$\frac{\partial[\mathbf{K}_T]_1^1}{\partial Pb_{01}} = \begin{bmatrix} 2 & 0 \\ 0 & 0 \end{bmatrix}$$

The reference force and the tangent displacement vectors are repeated for clarity.

$\{\mathbf{P}_{ref}\}= \{0, 1\}^T$

$\{\mathbf{U}_{ft}\}_1^1 = \{0.0193, 0.1158\}^T$

The sensitivity of the tangent displacement vector can be obtained by applying Eq. (A.2) $\frac{\partial\{\mathbf{U}_{ft}\}_1^1}{\partial Pb_{01}}$=$\{-0.0033387, -0.0007438\}^T$ Most of the solution for the sensitivity of the load factor is captured at the end of this iterative cycle ($j = 1$)

$\frac{\partial\lambda_1^1}{\partial P_{b0}} = 0.005545$

As expected, one iteration is not enough to satisfy the equilibrium condition that is represented by minimizing the residual force vector to a specified tolerance (10^{-6})

$\{\mathbf{R}_f\}_1^1 = \{0.1999, -0.0354\}^T$

Because of the nonzero derivative value of the load factor and according to Eq. (3.25), the derivative of the residual force vector is not zero. $\frac{\partial\{\mathbf{R}_f\}_1^1}{\partial P_{b0}} = \{0, 0.005545\}^T$

As in case 1, more iterations are required to satisfy the tolerance condition.

A.1.6 The Subsequent Iterative Cycles, $j > 1$

As in subsequent iterations of case 1, the residual displacement and its derivative vectors are obtained by applying Eqs. (3.13) and (3.24), respectively.

$\{\Delta \mathbf{U}_R\}_1^2 = \{0.01662, -0.00025\}^T$

$\frac{\partial \{\Delta \mathbf{U}_R\}_1^2}{\partial P b_{01}} = \{-0.00277, 0.000001158\}^T$

The sensitivity of the load factor can be updated by applying Eq. (3.27)

$\frac{\partial \lambda_1^2}{\partial P b_{01}} = 0.00555$

The residual force vector and its derivative are updated for the next iteration.

$\{\mathbf{R}_f\}_1^2 = \{0.1027 * 10^{-5}, 0.5827 * 10^{-5}\}^T$

$\frac{\partial \{\mathbf{R}_f\}_1^2}{\partial P_{b0}} = \{-0.0333, 0.00555\}^T$

The residual displacement vector and its derivative are updated using the residual force vector of previous iteration.

$\{\mathbf{U}_R\}_1^3 = \{0.20134 * 10^-6, 0.6947 * 10^-6\}^T$

$\frac{\partial \{\Delta \mathbf{U}_R\}_1^3}{\partial P b_{01}} = \{-0.0028, -2.2948 * 10^-7\}^T$

The sensitivity of the load factor is attained after three iterations.

$\frac{\partial \lambda_1^3}{\partial P b_{01}} = 0.00555$

B Sensitivity of **A**, **L**, and **h** Matrices With Respect to Parameter h

The derivative of the **A** matrix can be obtained by deriving Eq. (4.66) with respect to parameter h

$$\frac{d\mathbf{A}}{dh} = \frac{-L_d(\frac{d\hat{\mathbf{e}}_1\hat{\mathbf{e}}_1^T)}{dh} - (\mathbf{I} - \hat{\mathbf{e}}_1\hat{\mathbf{e}}_1^T)\frac{dL_d}{dh}}{L_d^2} \tag{B.1}$$

where dL_d/dh is the derivative of the deformed length which is defined in Eq. (4.74). The derivative of the $\hat{\mathbf{e}}_1\hat{\mathbf{e}}_1^T$ is

$$\frac{d\hat{\mathbf{e}}_1\hat{\mathbf{e}}_1^T}{dh} = \hat{\mathbf{e}}_1\frac{d\hat{\mathbf{e}}_1}{dh}^T + \frac{d\hat{\mathbf{e}}_1}{dh}\hat{\mathbf{e}}_1^T \tag{B.2}$$

The derivative of the **L** matrix is

$$\frac{d\mathbf{L}(\bar{\mathbf{r}}_k)^T}{dh} = \begin{bmatrix} \frac{d\mathbf{L}_1(\bar{\mathbf{r}}_k)^T}{dh} & \frac{d\mathbf{L}_2(\bar{\mathbf{r}}_k)^T}{dh} & \frac{d-\mathbf{L}_1(\bar{\mathbf{r}}_k)^T}{dh} & \frac{d\mathbf{L}_2(\bar{\mathbf{r}}_k)^T}{dh} \end{bmatrix} \tag{B.3}$$

where $\frac{d\mathbf{L}_1(\bar{\mathbf{r}}_k)^T}{dh}$ can be obtained by taking the derivative of Eq. (4.63) with respect to parameter h.

$$\frac{d\mathbf{L}_1(\bar{\mathbf{r}}_k)}{dh} = \frac{1}{2}\left[(\bar{\mathbf{r}}_k^T\hat{\mathbf{e}}_1)\frac{d\mathbf{A}}{dh} + \frac{d(\bar{\mathbf{r}}_k^T\hat{\mathbf{e}}_1)}{dh}\mathbf{A} + \mathbf{A}\frac{d(\bar{\mathbf{r}}_k(\hat{\mathbf{e}}_1 + \bar{\mathbf{r}}_1))}{dh} + \frac{d\mathbf{A}}{dh}\bar{\mathbf{r}}_k(\hat{\mathbf{e}}_1 + \bar{\mathbf{r}}_1)^T\right] \tag{B.4}$$

where the derivative of $\bar{\mathbf{r}}_k^T\hat{\mathbf{e}}1$ can be obtained using product rule

$$\frac{d(\bar{\mathbf{r}}_k^T\hat{\mathbf{e}}_1)}{dh} = \bar{\mathbf{r}}_k^T\frac{d\hat{\mathbf{e}}_1}{dh} + \frac{d\bar{\mathbf{r}}_k^T}{dh}\hat{\mathbf{e}}_1 \tag{B.5}$$

and by following the same rule of production, the derivative of the $\bar{\mathbf{r}}_k(\hat{\mathbf{e}}_1 + \bar{\mathbf{r}}_1)^T$ is

$$\frac{d(\bar{\mathbf{r}}_k(\hat{\mathbf{e}}_1 + \bar{\mathbf{r}}_1))}{dh} = \bar{\mathbf{r}}_k(\frac{d\hat{\mathbf{e}}_1}{dh} + \frac{d\bar{\mathbf{r}}_1}{dh})^T + \frac{d\bar{\mathbf{r}}_k}{dh}(\hat{\mathbf{e}}_1 + \bar{\mathbf{r}}_1)^T \tag{B.6}$$

The sensitivity of $\mathbf{L}(\bar{\mathbf{r}}_2)$ can be obtained by taking the derivative of Eq. (4.64) with respect to parameter h

$$\frac{d\mathbf{L}_2(\bar{\mathbf{r}}_k)}{dh} = \frac{1}{2}\frac{d\mathbf{S}(\bar{\mathbf{r}}_k)}{dh} - \frac{1}{4}\left(\bar{\mathbf{r}}_k^T\hat{\mathbf{e}}_1\frac{d\mathbf{S}(\bar{\mathbf{r}}_1)}{dh} + \frac{d(\bar{\mathbf{r}}_k^T\hat{\mathbf{e}}_1)}{dh}\mathbf{S}(\bar{\mathbf{r}}_1) + \mathbf{S}(\bar{\mathbf{r}}_k)\frac{d(\hat{\mathbf{e}}_1(\hat{\mathbf{e}}_1 + \bar{\mathbf{r}}_1)^T)}{dh}\right) - \frac{1}{4}\left(\frac{d\mathbf{S}(\bar{\mathbf{r}}_k)}{dh}\hat{\mathbf{e}}_1(\hat{\mathbf{e}}_1 + \bar{\mathbf{r}}_1)^T\right) \tag{B.7}$$

$$\frac{d\mathbf{S}(\bar{\mathbf{r}}_k)}{dh} = \begin{bmatrix} 0 & -\frac{dr_{k3}}{dh} & \frac{dr_{k2}}{dh} \\ \frac{dr_{k3}}{dh} & 0 & -\frac{dr_{k1}}{dh} \\ -\frac{dr_{k2}}{dh} & \frac{dr_{k1}}{dh} & 0 \end{bmatrix} \tag{B.8}$$

The derivative $\frac{d\mathbf{S}(\bar{\mathbf{r}}_1)}{dh}$ can be obtained by substituting $k = 1$ in Eq. (B.8).

$$\frac{d(\hat{\mathbf{e}}_1(\hat{\mathbf{e}}_1 + \bar{\mathbf{r}}_1))^T}{dh} = \hat{\mathbf{e}}_1\left(\frac{d\hat{\mathbf{e}}_1}{dh} + \frac{d\bar{\mathbf{r}}_1}{dh}\right)^T + \frac{d\hat{\mathbf{e}}_1}{dh}(\hat{\mathbf{e}}_1 + \bar{\mathbf{r}}_1)^T \tag{B.9}$$

B.1 derivative of $\mathbf{h}$ matrix

$$\frac{d\mathbf{h}_{I1}}{dh}^T = \left[\begin{array}{cccc} \mathbf{0}^T & \left(\frac{d\mathbf{S}(\mathbf{n}_{I_2})}{dh}\hat{\mathbf{e}}_3 + \mathbf{S}(\mathbf{n}_{I_2})\frac{d\hat{\mathbf{e}}_3}{dh} - \frac{d\mathbf{S}(\mathbf{n}_{I_3})}{dh}\hat{\mathbf{e}}_2 - \mathbf{S}(\mathbf{n}_{I_3})\frac{d\hat{\mathbf{e}}_2}{dh}\right)^T & \mathbf{0}^T & \mathbf{0}^T \end{array} \right] \tag{B.10}$$

$$\frac{d\mathbf{h}_{I2}}{dh}^T = \left[\begin{array}{cc} \left(\mathbf{A}\frac{d\mathbf{n}_{I_3}}{dh} + \frac{d\mathbf{A}}{dh}\mathbf{n}_{I_3}\right)^T & \left(\frac{d\mathbf{S}(\mathbf{n}_{I_1})}{dh}\hat{\mathbf{e}}_3 + \mathbf{S}(\mathbf{n}_{I_1})\frac{d\hat{\mathbf{e}}_3}{dh} - \mathbf{S}(\mathbf{n}_{I_3})\frac{d\hat{\mathbf{e}}_1}{dh} - \frac{d\mathbf{S}(\mathbf{n}_{I_3})}{dh}\hat{\mathbf{e}}_1\right)^T \\ -\left(\mathbf{A}\frac{d\mathbf{n}_{I_3}}{dh} + \frac{d\mathbf{A}}{dh}\mathbf{n}_{I_3}\right)^T & \mathbf{0}^T \end{array} \right] \tag{B.11}$$

$$\frac{d\mathbf{h}_{I3}}{dh}^T = \left[\begin{array}{cc} \left(\mathbf{A}\frac{d\mathbf{n}_{I_2}}{dh} + \frac{d\mathbf{A}}{dh}\mathbf{n}_{I_2}\right) & \left(\frac{d\mathbf{S}(\mathbf{n}_{I_1})}{dh}\hat{\mathbf{e}}_2 + \mathbf{S}(\mathbf{n}_{I_1})\frac{d\hat{\mathbf{e}}_2}{dh} - \mathbf{S}(\mathbf{n}_{I_2})\frac{d\hat{\mathbf{e}}_1}{dh} - \frac{d\mathbf{S}(\mathbf{n}_{I_2})}{dh}\hat{\mathbf{e}}_1\right)^T \\ -\left(\mathbf{A}\frac{d\mathbf{n}_{I_2}}{dh} + \frac{d\mathbf{A}}{dh}\mathbf{n}_{I_2}\right)^T & \mathbf{0}^T \end{array} \right] \tag{B.12}$$

$$\frac{d\mathbf{h}_{J1}}{dh}^T = \left[\begin{array}{cccc} \mathbf{0}^T & \mathbf{0}^T & \mathbf{0}^T & \left(\frac{d\mathbf{S}(\mathbf{n}_{J_2})}{dh}\hat{\mathbf{e}}_3 + \mathbf{S}(\mathbf{n}_{J_2})\frac{d\hat{\mathbf{e}}_3}{dh} - \frac{d\mathbf{S}(\mathbf{n}_{J_3})}{dh}\hat{\mathbf{e}}_2 - \mathbf{S}(\mathbf{n}_{J_3})\frac{d\hat{\mathbf{e}}_2}{dh}\right)^T \end{array} \right] \tag{B.13}$$

$$\frac{d\mathbf{h}_{J2}}{dh}^T = \left[\begin{array}{cc} \left(\mathbf{A}\frac{d\mathbf{n}_{J_3}}{dh} + \frac{d\mathbf{A}}{dh}\mathbf{n}_{J_3}\right)^T & \mathbf{0}^T \\ \left(\frac{d\mathbf{S}(\mathbf{n}_{J_1})}{dh}\hat{\mathbf{e}}_3 + \mathbf{S}(\mathbf{n}_{J_1})\frac{d\hat{\mathbf{e}}_3}{dh} - \mathbf{S}(\mathbf{n}_{J_3})\frac{d\hat{\mathbf{e}}_1}{dh} - \frac{d\mathbf{S}(\mathbf{n}_{J_3})}{dh}\hat{\mathbf{e}}_1\right)^T & -\left(\mathbf{A}\frac{d\mathbf{n}_{J_3}}{dh} + \frac{d\mathbf{A}}{dh}\mathbf{n}_{J_3}\right)^T \end{array} \right] \tag{B.14}$$

$$\frac{d\mathbf{h}_{J3}}{dh}^T = \begin{bmatrix} \left(\mathbf{A}\frac{d\mathbf{n}_{J_2}}{dh} + \frac{d\mathbf{A}}{dh}\mathbf{n}_{J_2}\right)^T & \mathbf{0}^T & -\left(\mathbf{A}\frac{d\mathbf{n}_{J_2}}{dh} + \frac{d\mathbf{A}}{dh}\mathbf{n}_{J_2}\right)^T \\ \left(\frac{d\mathbf{S}(\mathbf{n}_{J_1})}{dh}\hat{\mathbf{e}}_2 + \mathbf{S}(\mathbf{n}_{J_1})\frac{d\hat{\mathbf{e}}_2}{dh} - \left(\mathbf{S}(\mathbf{n}_{J_2})\frac{d\hat{\mathbf{e}}_1}{dh} + \frac{d\mathbf{S}(\mathbf{n}_{J_2})}{dh}\hat{\mathbf{e}}_1\right)\right)^T & & \end{bmatrix} \tag{B.15}$$

where the derivatives $d\mathbf{S}(\mathbf{n}_{I_k})/dh$ and $d\mathbf{n}_{I_k}/dh$ can be obtained using Eq. (B.8) and Eq. (4.80), respectively where $k = 1, 2, 3$.